

**KAIC CII RING FLEXIBILITY GOVERNS THE RHYTHM OF THE
CIRCADIAN CLOCK OF CYANOBACTERIA**

A Dissertation

by

NAI-WEI KUO

Submitted to the Office of Graduate Studies of
Texas A&M University
in partial fulfillment of the requirements for the degree of

DOCTOR OF PHILOSOPHY

May 2011

Major Subject: Biochemistry

**KAIC CII RING FLEXIBILITY GOVERNS THE RHYTHM OF THE
CIRCADIAN CLOCK OF CYANOBACTERIA**

A Dissertation

by

NAI-WEI KUO

Submitted to the Office of Graduate Studies of
Texas A&M University
in partial fulfillment of the requirements for the degree of

DOCTOR OF PHILOSOPHY

Approved by:

Co-Chairs of Committee,	Andy LiWang Pingwei Li
Committee Members,	Deborah Bell-Pedersen Frank Raushel
Head of Department,	Gregory Reinhart

May 2011

Major Subject: Biochemistry

ABSTRACT

KaiC CII Ring Flexibility Governs the Rhythm of the Circadian Clock of Cyanobacteria.

(May 2011)

Nai-Wei Kuo, B.S.; M.S., National Tsing Hua University, Taiwan

Co-Chairs of Advisory Committee: Dr. Andy LiWang,
Dr. Pingwei Li

The circadian clock orchestrates metabolism and cell division and imposes important consequences to health and diseases, such as obesity, diabetes, and cancer. It is well established that phosphorylation-dependent circadian rhythms are the result of circadian clock protein interactions, which regulate many intercellular processes according to time of day. The phosphorylation-dependent circadian rhythm undergoes a succession of phases: Phosphorylation Phase → Transition Phase → Dephosphorylation Phase. Each phase induces the next phase. However, the mechanism of each phase and how the phosphorylation and dephosphorylation phases are prevented from interfering with each other remain elusive. In this research, we used a newly developed isotopic labeling strategy in combination with a new type of nuclear magnetic resonance (NMR) experiment to obtain the structural and dynamic information of the cyanobacterial KaiABC oscillator system. This system is uniquely suited for the mechanistic studies: mixing KaiA, KaiB KaiC, and ATP generates a self-sustained ~24 h rhythm of KaiC phosphorylation *in vitro*. Our data strongly suggest that the dynamic states of KaiC underpin the timing mechanism of cyanobacterial oscillator.

DEDICATION

I dedicate this to my parents, Kuo-Chin, Kuo and Yu-Ping, Chiang, my sisters and brother, Mei-Ling, Tzu-Chia, and Hsin-Hung, and my significant other, Chi-Shou. From their endless love and support, I have had strength to pursue my Ph.D. degree.

ACKNOWLEDGEMENTS

I would like to thank my advisor Dr. Andy LiWang for giving me the opportunity to pursue my graduate career and introducing me to this exciting field. With his guidance and mentoring, he inspired me a lot in science. The pursuit of my Ph.D. was a very good learning experience.

I also want to thank my co-chair, Dr. Pingwei Li, my committee members, Dr. Frank Raushel and Dr. Bell-Pedersen, and my previous committee member, Dr. Susan Golden, for giving me useful guidance in every committee meeting.

I deeply appreciate my colleagues, Tyler Chang and Roger Tseng, and previous colleague, Yong-Ick Kim. From them, I learned how to do the integrated teamwork and independent research. They let me know that success comes from hard work, without giving up, even though the project is a challenge. Persistence, perseverance, and faith can conquer every difficulty.

In addition, I would like to thank Dr. Patricia LiWang for her useful advice in research and life. Moreover, people from her group, Bo Zhao, Yongguang Gao, Jie Xue, and Jun Chiun Chang were helpful for scientific discussion.

Finally, I would like to extend my gratitude to my friends who filled my graduate student life and the people who helped me correct the grammar in my dissertation.

TABLE OF CONTENTS

	Page
ABSTRACT	iii
DEDICATION	iv
ACKNOWLEDGEMENTS	v
TABLE OF CONTENTS	vi
LIST OF FIGURES.....	viii
LIST OF TABLES	xi
 CHAPTER	
I INTRODUCTION	1
1.1 Central Oscillator	1
1.2 Protein Dynamics of Supramolecular Complexes by NMR	21
II MECHANISM OF THE PHOSPHORYLATION PHASE	25
2.1 Introduction	25
2.2 Materials and Methods	30
2.3 Results	35
2.4 Discussion	51
III MECHANISM OF THE TRANSITION PHASE.....	58
3.1 Introduction	58
3.2 Materials and Methods	61
3.3 Results	63
3.4 Discussion	70
IV MECHANISM OF THE DEPHOSPHORYLATION PHASE.....	74

CHAPTER	Page
4.1 Introduction	74
4.2 Materials and Methods	77
4.3 Results	79
4.4 Discussion	91
V CONCLUSION AND FUTURE WORK.....	95
REFERENCES.....	100
APPENDIX A	119
APPENDIX B	131
APPENDIX C	133
APPENDIX D	135
APPENDIX E.....	138
APPENDIX F	144
VITA	153

LIST OF FIGURES

FIGURE	Page
1	The common elements in a circadian loop.....3
2	Model of Per/Tim feedback loop.....5
3	The <i>Synechococcus elongatus</i> circadian clock system.....10
4	The X-ray crystal structures of KaiA, KaiB, and KaiC.....13
5	Overall effect of the sequential cAMP binding to the conformation and dynamics of CAP ^N17
6	Timescale of dynamic processes in protein and the experimental methods that can detect fluctuations on each timescale.....19
7	Comprehensive NMR dynamics experiments over timescales.....22
8	Partial commercially available isotopically labeled α -keto acid precursors.....24
9	KaiC phosphorylation order diagram.....25
10	The NMR structure of the KaiA-KaiC A-loop complex docks on the top of KaiC structure and x-ray crystal structures of KaiC.....26
11	ATP is too far from phosphorylation sites.....28
12	Methyl labeling strategy.....32
13	Robot Collector.....33
14	<i>In vitro</i> KaiC phosphorylation oscillation.....38
15	<i>In vitro</i> 24h phosphorylation of KaiC.....40

FIGURE		Page
16	Methyl-TROSY spectra of wt-KaiC, KaiC-SE, KaiC-EE, KaiC-ET, and KaiC-EE487.	42
17	CII ring flexibility depends on the state of phosphorylation at residues S431 and T432 and A-loop position.....	454
18	Overlay of methyl-TROSY spectra of KaiC-EE (black), CI (blue, residues 1-247), and CII-EE (red, residues 249-518).....	47
19	KaiA and CII binding.	48
20	Phosphorylation profiles of KaiC phosphomimics.....	49
21	Inter-A-loop hydrogen bonds.	54
22	Interactions possibly disrupted by A-loop exposure.	56
23	KaiC phosphorylation order diagram.	58
24	Overlay of seven crystal structures of KaiC Phosphoforms	59
25	Negative-stain EM structures of KaiB and KaiC complex.....	59
26	KaiB-KaiC binding experiments.	66
27	KaiB-CII binding experiments.	66
28	KaiB + KaiC binding kinetics.	67
29	Gel filtration chromatography of CII variants.....	68
30	KaiB conformational changes upon KaiC binding.....	69
31	KaiC phosphorylation order diagram.	75
32	X-ray crystal structure of KaiA and KaiB.....	75

FIGURE	Page
33 Gel filtration chromatography showing the KaiABC-EE497 complex formation.....	83
34 Mapping of KaiA binding site for KaiCB complex by ^1H , ^{15}N -HSQC spectra.....	85
35 ^1H , ^{15}N -HSQC showing SasA-N (residues 1-107) specifically binds to CI monomer.....	88
36 CII-CI interactions depend on the state of phosphorylation at residues S431 and T432.....	90
37 Putative binding site on KaiA on KaiB.....	91
38 KaiA and KaiB temporally control the ordered phosphorylation of KaiC.....	95
39 CII ring flexibility governs the circadian rhythm of the cyanobacterial oscillator.....	96

LIST OF TABLES

	Page
Table 1 NMR Sample Condition and Experiment for CHAPTER II.....	36
Table 2 NMR Sample Condition and Experiment for CHAPTER III.....	64
Table 3 NMR Sample Condition and Experiment for CHAPTER IV.....	80

CHAPTER I

INTRODUCTION

1.1 Central Oscillator

Endogenous circadian clocks have been found in diverse organisms, including prokaryotes, and eukaryotes ranging from cyanobacteria (1), fungi (2), plants (3), insects (4), to humans (5). The coordination of physiological activities and behavior of diverse organisms to the external environment by the circadian clock is crucial to reproductive fitness, as demonstrated by cyanobacteria (6), flies (7), and plants (8).

All circadian clocks fulfill three criteria:

1. The ~24 h rhythm is self-sustained under constant environmental conditions (9).
2. The phase of the clock can be reset by external cues, such as light (10).
3. The rhythm is temperature compensated (11). It means the period of the circadian rhythm changes less with temperature variation than most enzymatic reactions.

All circadian clocks include the following three components:

1. Input pathway is to synchronize biological time to external cues.
2. Central oscillator is to generate a ~24 h rhythm and maintain internal time.
3. Output pathway is to transmit the rhythm downstream to clock-controlled effectors.

Environmental cues, such as daylight, are transduced to the central oscillator through input pathways. They induce a phase shift in the rhythm generated by the oscillator, the magnitude of which depends on the phase position of the signal. Output pathways transduce the biochemical rhythm generated by the oscillator into rhythmic expression of clock-controlled genes. Central to the circadian rhythm is at least one oscillator with positive and negative elements that form feedback loops (12). Up to now, genetic and

biochemical studies have helped identify the components of central oscillators in diverse organisms.

In mammals, the circadian clock has long been associated with health and disease problems, such as obesity (13), diabetes (14), and cancer (15). To date, eight core circadian clock genes have been found in mammals. They are *Casein kinase 1 ϵ* (*CK1 ϵ*); *Cryptochrome1* (*Cry1*) and *Chryptochrome2* (*Cry2*); *Period1* (*Per1*), *Period2* (*Per2*), and *Period3* (*Per3*); *Clock* (*Clk*), and *Bmal1*. The molecular clocks in peripheral tissues are associated with metabolism (13) and cell growth (16). For example, *Clock* mutant mice gain more weight upon aging than normal mice, especially in fat mass over a 10 week period (13). In general, *Clock* mutant mice fed either regular or high-fat diet showed an increase in energy intake and body weight. Comparison of somatic growth and solid organ mass revealed no difference. However, the body weight gain on *Clock* mutant mice fed a regular diet was attributed to 65% of lean mass and 35% of fat mass, whereas 25% lean mass and 75% of fat mass for the mutant mice fed a high-fat diet relative to wild-type mice. At an age of 6-7 months, *Clock* mutant mice developed hypercholesterolemia, hypertriglyceridemia, hyperglycemia, and hypoinsulinemia. The aberrant metabolic changes and endocrine hormones secretion were caused by dysfunctional clock gene expression (13).

Prompted by the evidence that the circadian clock affects the metabolism through cellular processes, Marcheva et al. tried to dissect the impact of clock function within the pancreatic islets (14). They found that disruption of *Clk* and *Bmal1* induce hypoinsulinaemia and diabetes. The pancreatic islets secrete insulin to maintain glucose homeostasis during the feeding period, and dysfunctional insulin release is linked with diabetes (17). The self-sustained circadian rhythms of gene expression of the transcription factors *Clk* and *Bmal1* were found to exist in the pancreatic islets. β -cells are a type of cell in the pancreas and its function is to make and release insulin to control the level of glucose in blood. A mutation in the *Clock* gene disrupted the generation of *Clk* and *Bmal1* and leading to impaired glucose tolerance, reduced insulin secretion, and

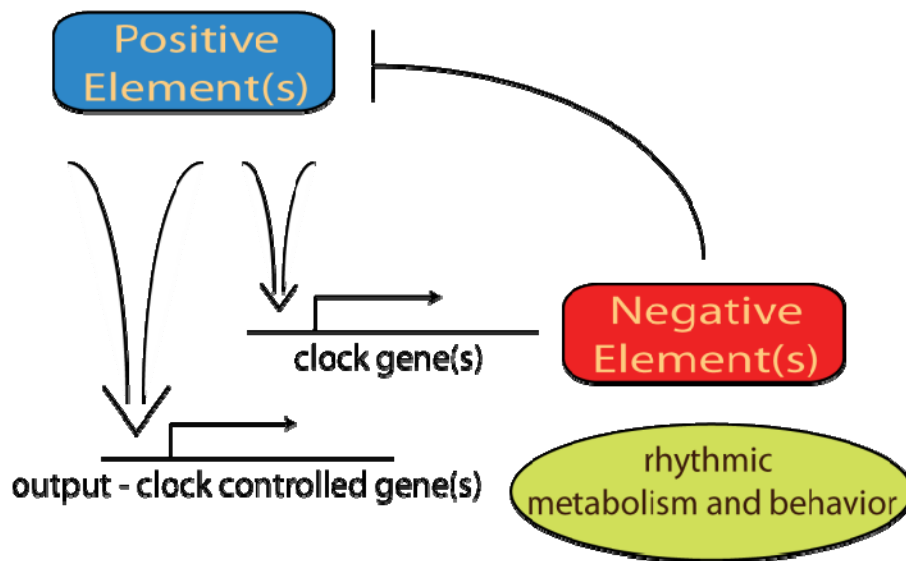


Figure 1 The common elements in a circadian loop. In mammals, positive elements are Clk and Bmal1; in *Drosophila*, positive elements are Clk and Cyc; in *Neurospora*, positive elements are WC1 and WC2. Negative Elements are Per1-3 and Cry in mammals; Per, and Tim in *Drosophila*; FRQ in *Neurospora*. In cyanobacteria, positive element is KaiA and negative elements are KaiB and KaiC. This figure is adopted from (18).

progressive β -cell failure (14). The results showed that ablation of the pancreatic clock can trigger diabetes mellitus.

Furthermore, *Per1* and *Per2*, two clock genes in mice, suppressed tumor growth (16, 19); knockdown of a clock-related gene, *CK1 ϵ* , inhibited the growth of cancer cells (20). Both mPer1 and mPer2 function in tumor suppression by regulating the transcription of the clock-controlled genes, which sensitized cancer cells to radiation-induced apoptosis (16, 19). Furthermore, hPer1 may have direct interactions with a cell-cycle checkpoint pathway (19). Knocking down *CK1 ϵ* , inhibited growth of engineered tumor cells more than in normal cells. Thus, tumor cells are more sensitive than normal cells to the kinase activity of CK1 ϵ . The use of specific kinase inhibitors to CK1 ϵ revealed that Per2 is a substrate of CK1 ϵ and also modulates growth inhibition of tumor cells (20).

The central oscillators of most model organisms apparently follow the transcription translation feedback loop (TTFL) model. Fig. 1 is a simple example of transcription-translation feedback loop (18). The positive elements activate the transcription of the clock genes encoded negative elements; meanwhile, downstream gene expression is also activated by the positive elements. The negative elements inhibit the function of the positive elements. After the degradation of the negative elements in eukaryotes (or dephosphorylation of negative elements in cyanobacteria), the positive elements are derepressed to allow the whole cycle to start anew. In addition to the transcription-translation feedback loop, central oscillators are regulated by post-translational modifications (PTMs), mainly through phosphorylation. Phosphorylation is used to control protein localization, degradation, and the activity of proteins. Phosphorylation exerts its effect by remodeling the protein structure. As we will show here, phosphorylation can also be used to regulate protein flexibility.

Phosphorylation plays a major role in the circadian clock system. Take the *Per/Tim* feedback loop of *Drosophila melanogaster* as an example (Fig. 2) (21). The positive elements clock (*Clk*) and cycle (*Cyc*) form a heterodimer to bind to an E-box from mid day through early night. This *Clk/Cyc* heterodimer activates the transcription of *Period* (*Per*) and *Timeless* (*Tim*), which are negative elements and form a heterodimer to inhibit the transcription of *Clk* and *Cyc*. The *Per* and *Tim* mRNA levels reach a maximum in the night, whereas *Per* and *Tim* proteins do not reach maximal levels until late evening, due to the phosphorylation-dependent destabilization of *Per* by *Dbt* and possibly by *CK2*. *Dbt* and *CK2* phosphorylate *Per* leading to degradation, whereas, *PP2a* can stabilize *Per* by removing the phosphate group (21). *Tim* also stabilizes phosphorylated *Per* in a *Tim:Per:Dbt* complex. This complex is transported to nuclei after *Tim* is phosphorylated by *Sgg*, which occurs in the subjective night. This complex then binds to *Clk/Cyc*, and the *Per/Tim/Clk/Cyc* complex then disengages the E-box to stop transcription of *Per* and *Tim* by subjective night. *Per* and *Clk* are subsequently degraded because of *Dbt*-induced phosphorylation. *Tim* is degraded upon phosphorylation at a tyrosine residue at subjective dawn. After one circadian cycle, the newly-formed *Clk/Cyc* heterodimer will

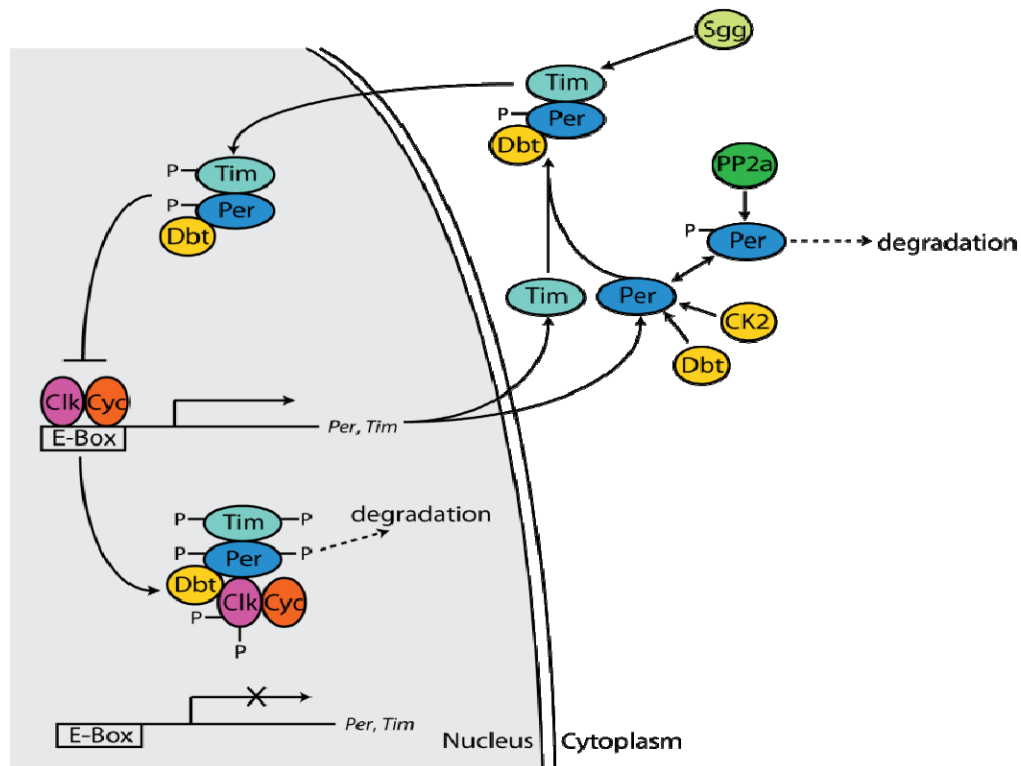


Figure 2 Model of Per/Tim feedback loop. Black line with arrow, sequential steps in the transcription-translation feedback loop; block line, inhibition; dashed line with arrow, protein degradation; P, protein phosphorylation. The figure is adopted from (21).

activate the transcription of Per and Tim to start another cycle. A central feature of the timing mechanism is that phosphorylation of positive and negative elements regulate the delay between activation and repression of transcription to maintain the ~24 h cycle (22).

It has been demonstrated that perturbation of phosphorylation of clock proteins can profoundly affect circadian rhythms. For example, the tau hamster, which has a short free-running period (20 hr), has a mutation in casein kinase I ϵ (CKI ϵ) protein (23), which normally phosphorylates Per2. CKI ϵ [*tau*] reduces the kinase activity on the phosphorylation sites of Per2 that stabilize Per2, whereas phosphorylation sites that destabilize Per2 are not affected or less affected by CKI ϵ [*tau*]. The uneven influence on the different phosphorylation sites may lead to the premature clearance of nuclear Per2

resulting in the short period (24). Moreover, mutation of a CKIε phosphorylation site in human Per2 (Ser662 to Gly) decreases Per2 phosphorylation *in vitro* (25). This T44A mutation of hCKIε decreases its kinase activity on Per2/3 *in vitro* (26). Both mutations have been identified as the causes for Familial Advance Sleep-Phase Syndrome (FASPS) (25-27). The V647G mutation in human Per3, linked to Delayed Sleep-Phase Syndrome (DSPS), is speculated to alter its CKIε dependent phosphorylation (28). The hCKIε S408N mutant, which is commonly found in DSPS individuals, increases its kinase activity by 1.8 fold *in vitro* (29). Although higher organisms have multiple oscillators, more complex TTFLs and PTMs, the basic mechanisms essential for a clock are similar between diverse organisms. For example, in cyanobacteria, at least one oscillator, one transcription-translation feedback loop, and phosphorylation are involved in regulating the clock. Therefore, the timing mechanism of the simple cyanobacterial clock will lead to new insights into the complex clocks of eukaryotes.

Among prokaryotes and eukaryotes, the clock systems of the latter have more complex networks of transcription-translation feedback loops (TTFLs) and post-translational modifications (PTMs). In addition to phosphorylation, mammalian circadian systems have additional PTMs such as acetylation and SUMOylation (30, 31). The Clk/Bmal1 complex activates transcription by acetylation of histone proteins (32, 33). Clk itself is an intrinsic histone acetyltransferase (HAT) (31). Bmal1 enhances Clk HAT activity probably through large conformational changes on Clk. The Clk/Bmal1 heterodimer activates *Per* transcription. However, without acetylation at the *Per1* promoter by Clk, Clk/Bmal1 fails to activate transcription (31). On the other hand, Sumoylation of Bmal1 is induced by Clk (30). Sumoylation affects proteosomal degradation of Bmal1 and also the stability of the Clk/Bmal1 heterodimer (34). In contrast to mammalian systems, in *Drosophila* and *Neurospora*, the only PTM involved in clock regulation is phosphorylation (22). All eukaryotic clock function apparently requires translocation of clock proteins between the cytoplasm and nucleus. These complexities associated with eukaryotic clocks make them difficult systems for mechanistic studies, as their oscillators cannot be separated from the complex milieu of the cell.

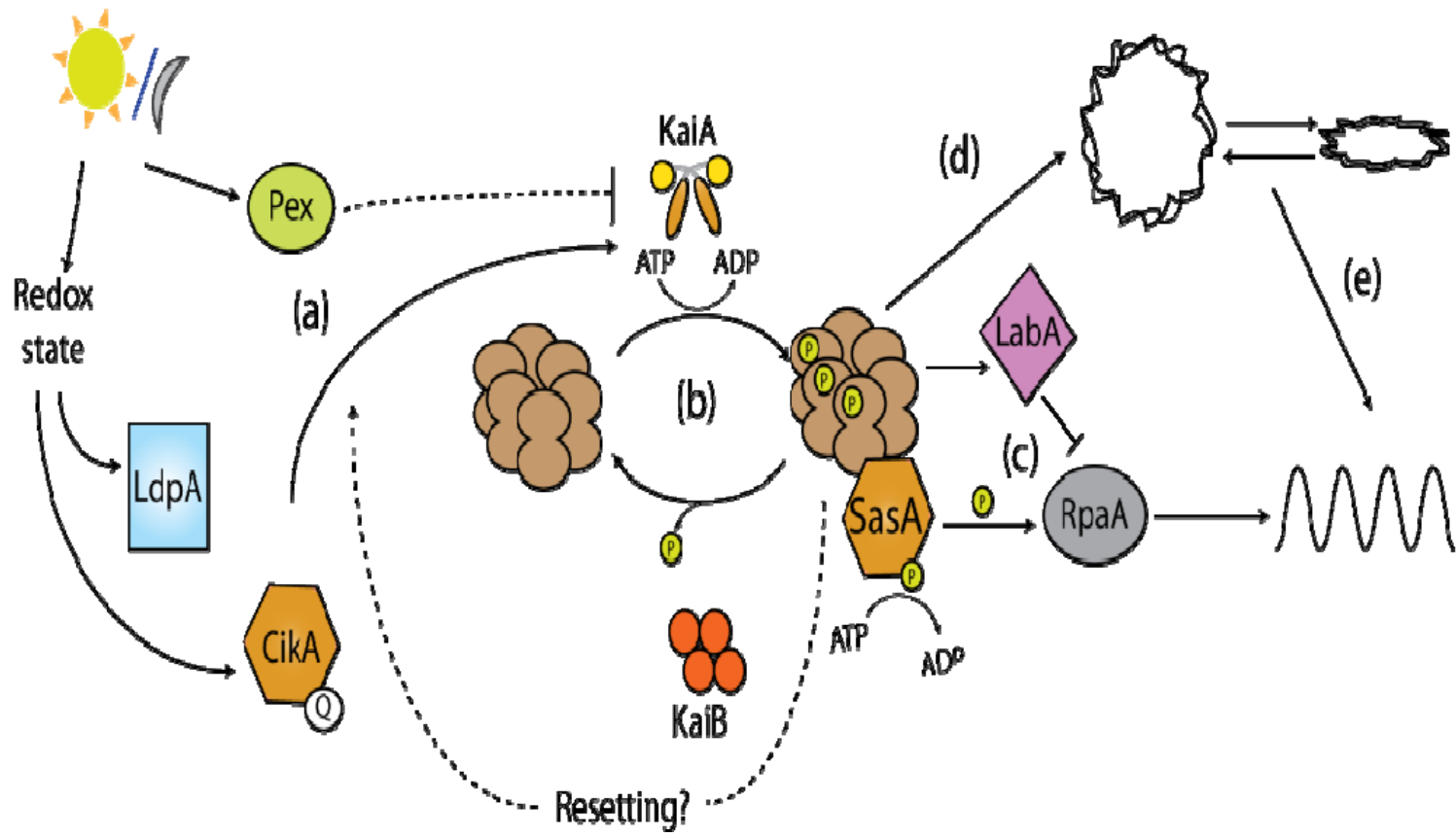
However, the TTFL paradigm for eukaryotic circadian oscillators may be in danger. Recently, robust, temperature compensated circadian rhythms were observed in human red blood cells (RBCs) (35). A novel post-translational biomarker, peroxiredoxin oxidation, was used to confirm the rhythmicity. Red blood cells have no nucleus (or DNA) and thus cannot have a transcription-translation feedback loop. The peroxiredoxins undergo a circadian rhythm in sensing the redox state in RBCs (35). These rhythms must be driven by a non-transcriptional oscillator. This observation is the first one showing that the transcription is not required for self-sustained circadian oscillations in human cells. Peroxiredoxins (PRXs) are a highly conserved family of antioxidant proteins that control the peroxide level in cells (36). They share a common catalytic mechanism in which the Cys residues in the active site are oxidized to sulphenic acid by a peroxide substrate, forming a disulfide bond which is subsequently reduced by thioredoxin to complete one catalytic cycle (36). The dimeric form of PRX was found to be regulated by the redox state in the cell. Therefore, the mechanism of rhythmic PRX-SO_{2/3} formation were explored. RBCs were found to have circadian rhythms of PRX dimerization, hemoglobin tetramer-dimer transitions, and NADH/NADPH ratios (35). Peroxiredoxins dimer formation and NADH/NADPH oscillations were also present in nucleated cells. In *Cry1 Cry2* knock down cells, PRX-SO_{2/3} rhythms persisted, although with longer free-running periods. It indicates that a TTFL probably influences the PRX-SO_{2/3} rhythm. Thus, their finding reveals an interrelationship between TTFLs and PTMs in regulating the circadian rhythm. Overall, it is similar with the model in cyanobacteria where the central oscillator is controlled by both PTM and TTFL. However, the central oscillator of cyanobacteria can be regulated by PTM *in vitro*. Thus, elucidating the mechanism of the KaiABC oscillator will provide important insights into the clocks of eukaryotes.

Cyanobacteria, unicellular photosynthetic prokaryotes, have the simplest known circadian clocks. The most extensively characterized cyanobacterial clock is that of *Synechococcus elongatus* (12, 37). Like all other circadian systems, this one clock has input and output pathways and a central oscillator. There are three well-characterized

components of the clock-input pathway: LdpA (light-dependent period) (38), Pex (period extender) (39), and CikA (circadian input kinase) (40). Light flux affects the cellular redox state through photosynthesis. There is a light-dependent reductive state for growth, and a dark oxidative mode for cell maintenance. LdpA provides a link between light intensity and period length by sensing the redox state of the cell through its iron-sulfur clusters (41) (Fig. 3a). *S. elongatus* mutants that lack the *ldpA* gene no longer follow Aschoff's rule and have free-running periods that are consistent with higher light intensities. Pex plays a role in slowing down the clock (42), probably by repressing expression of *kaiA* by directly binding to its promoter (43). CikA, like LdpA, connects the redox state of the cell with the phase of the circadian rhythm (44). This connection appears to be achieved through direct interactions between quinones and the *pseudo*-receiver domain of CikA (44, 45) (rather than through iron-sulfur clusters). Indeed, in the absence of CikA, *S. elongatus* mutants do not reset the phase of their circadian rhythm in response to dark pulses (46).

All genes in *S. elongatus* are under clock control (46) which means that clock output pathways likely exert genome-wide regulation over gene expression. Indeed, the genome undergoes daily Kai-dependent cycles of compaction and decompaction (47), which should affect rhythmic promoter accessibility (Fig. 3, c, d, and e). A key component of the global output pathway is the protein SasA. Inactivation of SasA abolishes rhythmic expression of all genes except for the *kai* genes (48, 49). However, in *sasA*-null strains chromosome compaction rhythms persist, which suggest that promoter accessibility is not sufficient for rhythmic gene expression and that SasA is required to transmit information from the central oscillator to the gene expression machinery (47). SasA is regulated by the central oscillator through direct interactions between its N-terminal domain and KaiC (48). This interaction induces rhythmic autophosphorylation of a conserved histidine residue in the C-terminal domain of SasA. SasA is a histidine protein kinase and part of a two-component signal transduction system (50). Upon autophosphorylation, SasA transfers the phosphate group to its cognate response regulator, RpaA (49). The phosphorylated form of the response regulator then produces

Figure 3 The *Synechococcus elongatus* circadian clock system. It is schematically shown with interacting (a) input, (b) central oscillator, and (c-e) output components. (a) input pathway. External cue, such as light, is transmitted through Pex, LdpA, and CikA. The quantity of light changes the redox state of cell. LdpA is a redox active-ion-sulfur protein and CikA can sense the redox state and binds to a quinine molecule. Pex protein inhibits *KaiA* expression by direct binding to promoter region. In the absence of any of these three proteins leads to a shorter circadian rhythm. (b) The central oscillator contains three proteins: KaiA, KaiB, and KaiC. KaiA stimulates KaiC phosphorylation and KaiB inhibits KaiA function on KaiC phosphorylation activity. Deficiency at any of these three proteins abolishes the circadian rhythm. (c) SasA binds to N terminus of KaiC. The temporal information is transduced through by KaiC stimulates the autophosphorylation of SasA. Transfer of a phosphoryl group from SasA activates RpaA. LabA serves as a negative regulator modulated by KaiC to repress RpaA function. (d) KaiC oscillator regulates chromosome compaction rhythm and allows transcription machinery to bind to promoter regions. (e) SasA and RapA are not necessary for chromosome compaction but they are necessary for the rhythmic gene expression. The figure is adopted from (37).



an intracellular response, such as regulation of gene expression (50). In fact, disruption of *rpaA* leads to the same arrhythmic transcription phenotype as *sasA* disruption. The SasA-RpaA regulatory system has been linked to ATPase activity from KaiC in controlling downstream cell division (51). The elevated ATPase of KaiC inhibits cell division through SasA-RpaA. Another output pathway protein, LabA, appears to mediate the repressive effects of KaiC on gene transcription (52): in the absence of LabA, KaiC no longer represses its own gene expression.

The central oscillator of the cyanobacterium *S. elongatus* is composed of only three proteins, KaiA, KaiB, and KaiC (53). The phosphorylation rhythm of KaiC, regulated by KaiA and KaiB, correlates to the rhythms of gene expression (54). At first, this oscillator was thought to fit into the TTFL model (53). Indeed, the positive element KaiA enhances transcription of *kaiB* and *kaiC* from a common promoter, whereas KaiC, the negative element, attenuates *kaiBC* expression (53). Yet, early observations suggested that the Kai oscillator might not fit the TTFL paradigm. For example, driving expression of *kaiBC* either from a promoter from *E. coli* (55) or antiphase to its normal rhythm (56) did not disrupt circadian rhythmicity.

Under constant darkness, *S. elongatus*, an obligate photoautotroph, ceases transcription and translation (57). Thus, if the *S. elongatus* clock follows the TTFL model, it should stop under constant darkness, violating a defining criterion that an autonomous circadian rhythm continues to be generated under constant conditions (LL or DD). The Kondo group therefore tested whether circadian rhythms of KaiC phosphorylation persist in *S. elongatus* under constant darkness (or under constant light in the presence of transcriptional or translational inhibitors) (57). Their observation of a robust rhythm of KaiC phosphorylation in the absence of transcriptional and translational activity demonstrated that the central oscillator generates a rhythm only through PTMs (57). Indeed, that same year, the Kondo group showed that a mixture of recombinant KaiA, KaiB, and KaiC proteins purified from *E. coli* and ATP generated a self-sustained and temperature-compensated rhythm of KaiC phosphorylation in a test tube for three days (58). Therefore, this cyanobacterial oscillator, the KaiABC system,

fully viable outside of the complex milieu of the cell, is the most suitable model system for *in vitro* biochemical and structural studies. Our goal here is to establish a comprehensive understanding of the timing mechanism of this simplest of oscillators.

In *S. elongatus* the autonomous rhythm is generated by three proteins, KaiA, KaiB, and KaiC independent of transcriptional and translational processes (58). KaiC is an autokinase and an autophosphatase with two phosphorylation sites, S431 and T432 (54, 59-61). In addition, KaiC has an ATPase activity (53, 62). Both *in vivo* and *in vitro*, KaiA stimulates KaiC autophosphorylation whereas KaiB by itself has no effect on KaiC phosphorylation, but functions by hindering KaiA function, leading to KaiC dephosphorylation (54, 60, 63, 64). Under rhythmic interactions with KaiA and KaiB, KaiC has four different phosphorylation states that are temporally ordered: ST \rightarrow SpT \rightarrow pSpT \rightarrow pST \rightarrow ST (65, 66), where S and T and pS and pT are the unphosphorylated and phosphorylated forms of S431 and T432, respectively. Single mutants or double mutants at these two residues abolish the circadian rhythm, indicating the phosphorylation of these two residues is essential to the clock function (59). *In vivo*, the phosphorylated forms of KaiC are necessary to maintain circadian rhythms of downstream gene expression, but rhythms of KaiC phosphorylation are not (67, 68). Indeed, circadian rhythms of gene expression persist even when KaiC is constitutively phosphorylated (68). However, at low temperatures, rhythmic gene expression requires rhythmic KaiC phosphorylation (68). Thus, these results indicate that multiple pathways are important to maintain accurate and robust circadian rhythms in cyanobacteria *in vivo* (68).

KaiA actively associates with KaiC and stimulates KaiC phosphorylation during the Phosphorylation Phase (54). Then, the high level of KaiC phosphorylation induces the association of KaiB with KaiC and their sequestration of KaiA in a KaiCB(A) complex. This complex induces the Dephosphorylation Phase of KaiC. When KaiC becomes hypophosphorylated, KaiB dissociates from KaiC, thereby reactivating KaiA (69). This model is consistent with the electron microscopy and native gel electrophoresis results (70). Both methods demonstrate that the KaiA:KaiC complex exists at each phase,

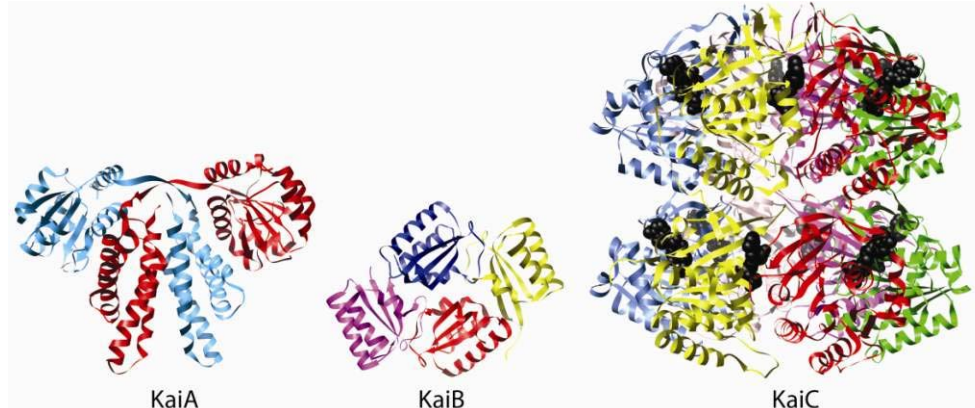


Figure 4 The X-ray crystal structures of KaiA, KaiB, and KaiC. KaiA (PDB ID:1R8J) (71), KaiB (PDB ID: 1WWJ) (72), and KaiC (PDB ID: 1TF7) (73). KaiA, KaiB, and KaiC show as relative size. Each color indicates one subunit. KaiA is a domain-swapped homodimer. KaiB is a homotetramer. KaiC is a homohexamer with two donut-like shape. ATP molecules in KaiC are shown as black spheres.

whereas KaiB:KaiC and KaiCB(A) complexes only exist during the Dephosphorylation Phase (70). Indeed, the four phosphoforms of KaiC, ST, SpT, pSpT, and pST, exist at different ratios at each phase (65, 66, 70). Therefore, temporal Kai protein-protein interactions are correlated with the KaiC phosphorylation cycle, which is characterized by the ratios of different phosphorylation states of KaiC.

To understand the mechanism of KaiC phosphorylation, knowing the structures of the Kai proteins is important. Three-dimensional (3D) high resolution structures of KaiA(64, 71, 74, 75), KaiB(72, 76, 77), and KaiC(73, 78) have been solved by X-ray crystallography (Fig. 4). The potential binding sites among Kai proteins have been studied in molecular and structural detail as well. KaiC is a two-domain homohexamer sharing sequence similarities to the bacterial helicase RecA (Fig. 4) (73, 79). Two domains of KaiC form a doughnut-like shape with twelve ATP molecules bound at the interfaces of both CI (KaiC N-terminal) and CII (KaiC C-terminal) domains. KaiC has a molecular weight of about 360 kDa and a dimension of 100x100 Å (73, 80). Similar to helicases such as RecA, the CI domain, has a weak ATPase activity that oscillates in a

circadian manner with CII autokinase activity (62). Unlike RecA, KaiC has no helicase activity (81). KaiC phosphorylation sites are located in the CII domain (59, 60). CII domain has autokinase and autophosphatase activities (53, 54, 61, 62). The conformation of the CI and CII domains are similar but the ATP binding pockets at the CI and CII domains have significant differences (73). ATP molecules bind more tightly to the CI domain than the CII domain, enabling isolated CI domains to form stable hexamers (80). By comparison, ATP molecules bind weakly to the CII domains (80, 82, 83). Stabilizing interactions between CI residues and the ATP nucleobase moiety are not found between CII residues and adenine (73), which explains the differences in ATP affinities. The X-ray crystal structure of KaiC showed that the distance between the hydroxyl group of T432 and S431 and the γ -phosphorus atom is 6.6 and 8.5 Å, respectively. However, according to an analysis by Mildvan (84), the upper distance limit for phosphoryl transfer between the phosphorus atom and acceptor oxygen is 5.0 Å, which helps explain why KaiC by itself dephosphorylates. This observation also implies that the KaiA:KaiC interaction somehow shortens the distance by at least 1.5 Å, thereby inducing phosphoryl transfer.

S. elongatus KaiA is a domain-swapped homodimer (Fig. 4), where the N-terminal domain of one subunit from residues 1 to 135, KaiA^N, is packed against the C-terminal domain from residues 180 to 283, KaiA^C, of the other subunit (71). KaiA^N adopts the fold of receiver domains (64) but lacks the invariant phospho-accepting aspartate residue of authentic receivers (50). Thus, the structure of KaiA^N is that of a *pseudo*-receiver domain, like the one in CikA (45). KaiA^N has no effect on the phosphorylation activity of KaiC. It is KaiA^C that has the stimulating activity for KaiC (64). Indeed, KaiA^C forms a tight complex with the last thirty C-terminal residues of KaiC (85), which includes a segment that is found looped inside the X-ray structure of KaiC (73). Full-length KaiA enhances KaiC phosphorylation less than KaiA^C does. Thus, KaiA^N may attenuate the KaiA and KaiC interaction by affecting the structure KaiA^C (86). Recent data from our laboratory suggests that KaiA activates KaiC phosphorylation by stabilizing this exposed “A-loop” (86). It is anticipated that displacement of the A-loop reduces the distance

between ATP and T432 by at least 1.5 Å. Phosphorylation is induced by the rearrangement of ATP, S431 and T432 side chains. For the Phosphorylation Phase, in spite of NMR and crystal structures, it is not known how KaiA binding to KaiC activates phosphorylation of KaiC at sites located 20 Å from the KaiA-KaiC binding site.

KaiB hinders KaiA stimulation of KaiC in an unknown manner. The Transition Phase occurs when KaiB dimers form a stable complex with hyperphosphorylated KaiC. According to EM results (87), two KaiB dimers associate with one KaiC hexamer. Once KaiB binds to hyperphosphorylated KaiC, KaiA is recruited to the KaiB:KaiC complex, forming a KaiCB(A) complex in which KaiA is sequestered and unable to stimulate KaiC phosphorylation. Thus, KaiC dephosphorylates within this complex during the Dephosphorylation Phase (69). The formation of KaiCB(A) complexes initiates the Dephosphorylation Phase. When KaiC fully dephosphorylates, KaiB dissociates from the complex, desequestering KaiA. Crystal structures of KaiB show that it exists as a homotetramer with each monomer adopting a fold similar to that of thioredoxin (Fig. 4) (72). It contains a single positively charged cleft flanked by two negatively charged ridges. Site-directed mutagenesis at those positive residues and deletion of the negative residues show that those two regions are important for the proper function of KaiB (72). Although KaiB alone is a tetramer, it binds to KaiC as a dimer on the top of the CII ring (87, 88). Thus, the KaiB:KaiC complex likely changes the structure of KaiB. In the native gel electrophoresis, KaiB does not form a complex with the CI ring of KaiC but forms a complex with the CII ring (87). The KaiB:KaiC interaction is strongest when KaiC is in its pST phosphoform or mutated to the pST phosphomimics S431D or S431E (65, 66). Since residues S431 and T432 are not near surface of KaiC but buried deep within the subunit interfaces, KaiB may not interact directly with them. Several crystal structures of KaiC in different states of phosphorylation are available (89). Remarkably, the structures are virtually identical, including those that do and do not bind KaiB. Thus, they do not inform on how KaiB selectively recognizes the pST and pSpT forms of KaiC. The KaiB:KaiC complex recruits and sequesters KaiA in a KaiCB(A) complex, in which KaiA is unable to stimulate KaiC phosphorylation (65, 66). The KaiCB(A)

complex has been solved by electron microscopy (70). The complex also exists in the absence of KaiC A-loops, the KaiA-binding site, during the Phosphorylation Phase (90). These observations suggest that in the KaiCB(A) complex, KaiA is bound at a site that is different from that during KaiC phosphorylation. However, how KaiB forms a complex with KaiA and KaiC in this dephosphorylating complex is not known. Unfortunately, the EM structure of the KaiCB(A) complex could not resolve the intermolecular interactions among these three proteins.

The binding sites of KaiA or KaiB on KaiC are on the surface of KaiC (70), far away from the phosphorylation sites of KaiC. Therefore, KaiA and KaiB must affect KaiC phosphorylation sites through an allosteric mechanism. It was believed phosphorylation-dependent conformational changes in KaiC played a critical role in the timing mechanism. Indeed, allostery usually is understood as structural changes at the active sites of enzymes induced by ligand binding at distal sites (91, 92). This classic view has been developed for decades, and applies to many biological process, such as catalysis, signal transduction, gene regulation, and metabolism (93-95). The role of protein motions were usually neglected in discussions of allostery. For the past few years, however, the roles of the internal motions of proteins have been shown to play important roles in allosteric mechanisms (96). Thus, the paradigm of allostery is shifting to include dynamics-driven mechanisms. There are an increasing number of examples where instead of a ligand-induced structural change stimulating distal active site activity, the internal motions of the protein mediate allosteric interactions without conformational change (96). In these proteins, long-range communication is regulated by dynamic fluctuations (entropic contribution) without structural changes (enthalpic contribution). In fact, the possibility of this concept was discussed almost three decades ago (97, 98). However, it was not known whether the internal motions could underpin allosteric mechanisms. The Kalodimos group reported the first direct experimental support of this the dynamic allostery hypothesis in 2006 (Fig. 5) (96). The negative cooperative binding of cAMP to catabolite activator protein (CAP) was shown to mediate changes in conformational entropy but not conformational changes (96). CAP is a transcription

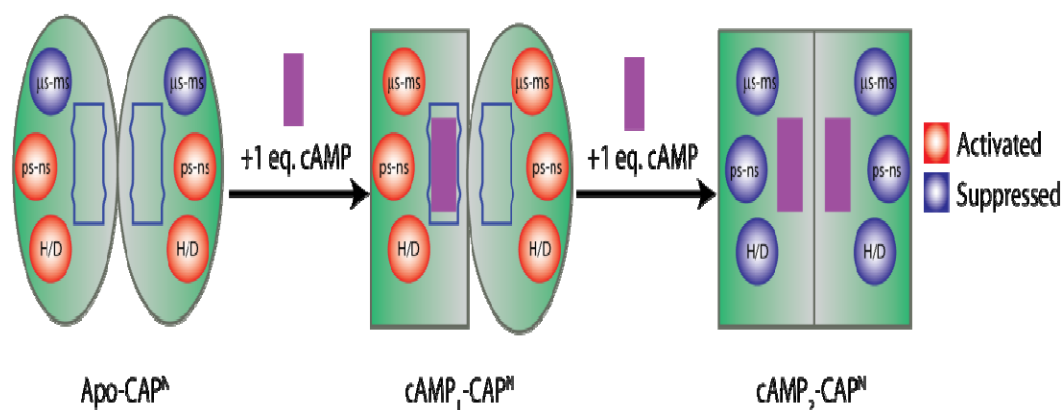


Figure 5 Overall effect of the sequential cAMP binding to the conformation and dynamics of CAP^N. apo-CAP^N showed flexibility at ps-ns and stability (H/D exchange rate). cAMP binding site was flexible shown as wave line. Binding of first cAMP has little effect on ps-ns motion and stability; however, it activated slow motion s-ms. In addition, it changed the structure of liganded subunit but not the unliganded subunit. Binding of second AMP decrease the fast and slow motions and stability (lower H/D exchange rate). The lower favorable entropy along with the second ligand binding compared with first is the source of the negative cooperativity. This figure is adopted from (96).

activator that forms a homodimer (99). Each subunit contains a cAMP binding site at the N terminus, and a DNA binding site at the C terminus. CAP^N is responsible for CAP dimerization (100, 101). Two cAMP molecules bind to the N terminus of CAP with negative cooperativity and increase CAP's affinity for DNA through an allosteric effect (101). Crystallographic studies of other oligomeric systems suggested that the binding of the first ligand may distort the conformation of the other unliganded subunit and resulted in the unfavorable second ligand binding (102, 103). However, failure of getting the crystal structures of unliganded CAP raised the possibility that other mechanisms might affect the negative cooperativity (102, 104, 105). The strong negative cooperativity of CAP^N (106) allowed characterization of the changes in protein structure and dynamics of three distinct states: unliganded state (apo-CAP^N), singly liganded state (intermediate, cAMP₁-CAP^N), and the doubly liganded state (cAMP₂-CAP^N) (96). apo-CAP^N exhibits flexibility on the ps-ns time scale (Fig. 5). Binding of the first cAMP molecule affected

the conformation of the liganded subunit but not second unliganded subunit. Nonetheless, the internal motions of both subunits were dramatically affected, especially, on μs – ms timescale. Binding of the second cAMP molecule had no effect on the other subunit but suppressed both fast and slow motions of almost all residues throughout both subunits (96)(Fig. 5), thereby revealing the basis of the negative cooperativity. Interestingly, there was no evidence of structural changes in this allosteric mechanism. It was therefore concluded that the negative cooperativity of binding of cAMP to CAP^N was entirely through a dynamics-driven mechanism (96).

In the recent years, several examples have demonstrated the importance of protein motions in regulating allosteric interactions (107, 108). Many techniques have been used to detect the protein motions on different time scales, such as fluorescence, ultraviolet and visible spectroscopy, Raman spectroscopy, and infrared spectroscopy (Fig. 6) (107). Nuclear magnetic resonance (NMR) spectroscopy provides both structural information and details on local motions ranging from picoseconds to seconds timescales at multiple sites simultaneously (Fig. 6). Measurement of the dynamic states of proteins by NMR has filled a major gap in understanding that could not be solved by conventional structure-to-function studies. Recent advances in isotopic labeling of proteins and novel NMR experiments have dramatically advanced the applicability of NMR spectroscopy to protein systems of hundreds of kilodaltons (109).

In studying the KaiABC system, there are several problems associated with the status quo of using static structures to understand the mechanism of the cyanobacterial oscillator. For example, there are six X-ray crystal structures of KaiC in different states of phosphorylation, but with virtually identical quaternary structures (89). In fact, the conformations of the long solvent-exposed tails were also identical among the six KaiC phosphoforms, bringing into question whether having the same space group and unit cell dimensions suppressed the effects of phosphorylation on KaiC conformation. Additionally, electron microscopy has produced low-resolution models of KaiCB(A) and KaiB:KaiC complexes, but there is insufficient detail on why, for example, the KaiB:KaiC complex depends on the phosphorylation state of KaiC (87). Indeed, the

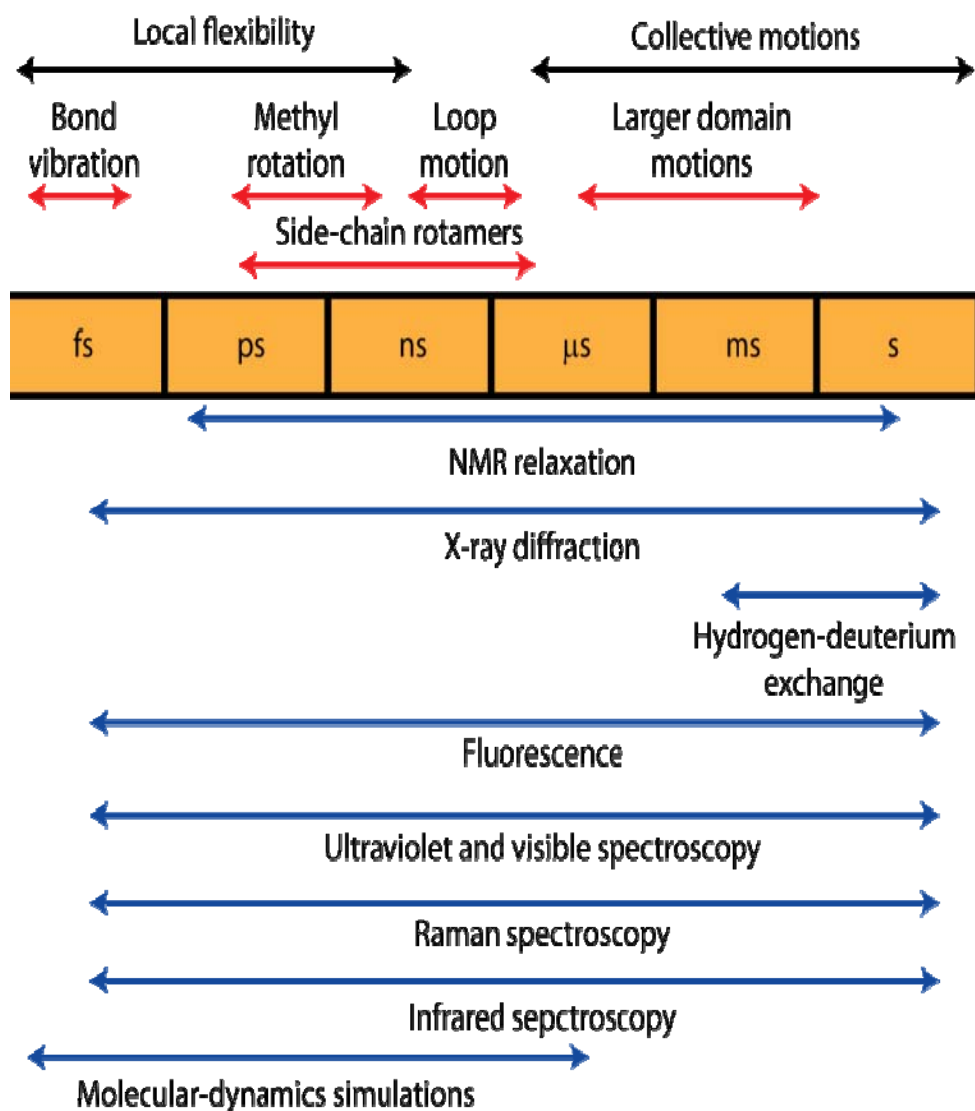


Figure 6 Timescale of dynamic processes in protein and the experimental methods that can detect fluctuations on each timescale. The figure is adopted from (107).

mechanism of KaiA-mediated phosphorylation and KaiB-mediated dephosphorylation of KaiC are still unclear, because it is difficult to reconcile the static Kai structures with their phosphorylation-dependent interactions and biochemistry. The static structures overlook a critical aspect of the oscillator mechanism. Our previous data (86) and modeling by others (110) strongly suggest that intramolecular protein dynamics might

play a central role. We have used a new isotopic labeling strategy and a new type of NMR experiment (111) to investigate the dynamic motions in the KaiABC system. We believe that this approach, which is a significant departure from the status quo in the circadian clock field, will overcome current problems associated with static clock protein structures. The clock proteins which we used for NMR experiments are from the thermophilic cyanobacterium *Thermosynechococcus elongates* BP-1 due to their superior behavior under NMR conditions. For example, KaiA, KaiB, and KaiC from *T. elongates* have higher solubility and thermostability than their *S. elongatus* homologs, which are critical for high quality NMR spectra. High quality spectra of all Kai protein samples were recorded on a Bruker 600 MHz NMR spectrometer equipped with a cryo-probe.

Here, the NMR and biochemical results strongly support that KaiA and KaiB mediate the KaiC phosphorylation cycle through dynamics-driven allosteric mechanism. Our data support a model in which CII ring flexibility is regulated by the KaiC phosphorylation state and interactions of KaiC with KaiA and KaiB. However, dynamic complex formation between KaiA, KaiB, and KaiC in turn regulates the KaiC phosphorylation cycle which leads to changes in the flexibility of KaiC CII ring. Importantly, circadian rhythms of CII ring flexibility separate the Phosphorylation and Dephosphorylation Phases, thereby revealing how these phases do not interfere with each other. Moreover, the flexibility of CII ring is linked to the regulation of ATPase activity. The CI ring of KaiC, to which the N terminus of SasA binds, has an ATPase activity that oscillates with a circadian rhythm. This ATPase activity regulates a cell division checkpoint (51), and thus transduces the KaiABC rhythm along SasA-dependent output pathways. We have evidence that the flexibility of the CII ring regulates CI ATPase activity thereby revealing the source of downstream rhythms.

1.2 Protein Dynamics of Supramolecular Complexes by NMR

Nuclear magnetic resonance (NMR) spectroscopy is a powerful technique to characterize protein structure and dynamics (112, 113). Protein dynamics measured by NMR was first performed nearly 40 years ago (114, 115). Since then, NMR spectroscopy has been widely used to determine protein structures, protein-protein interactions, and the dynamic states of protein. Indeed, that hundreds of spin- $\frac{1}{2}$ nuclei of a protein can be observed simultaneously has deepened understanding of many biological processes. A series of NMR experiments has been developed to monitor protein dynamics across a broad range of time scales, from picoseconds to seconds (Fig. 7) (111). Fig. 7 shows how a spin- $\frac{1}{2}$ nucleus reports conformational exchange between two different states. NMR resonance frequencies of the spin in each state is different. As shown in the figure 7, large spectral changes can be observed when the exchange rate changes. At slow exchange rates, two peaks indicate the two different conformational states. When the exchange rate increases, the peaks become exchange broadened, and will merge to one peak as the exchange rate increases. Under fast exchange, only one sharp peak is observed because the exchange rate is much faster than the difference in chemical shifts between the two states. The corresponding NMR experiments for detection of protein motions on different time scales are listed on the left side of Fig. 7, which shows that the sensitivity of NMR experiments depends on the timescale of protein dynamics.

In the past few years, NMR experiments have been developed to measure the dynamics of supramolecular protein complexes (109). The development of stronger magnets and cryoprobes (116) has dramatically increased the power of the NMR approach to understanding protein function. These advances have been aided by a new isotopic labeling strategy that has pushed the NMR limit on protein size to several kilodaltons (117). Combined with the methyl-TROSY experiment (109), it provides high-resolution structural and dynamic information on supra-protein protein complexes. Moreover, NMR spectroscopy provides information about multiple sites simultaneously.

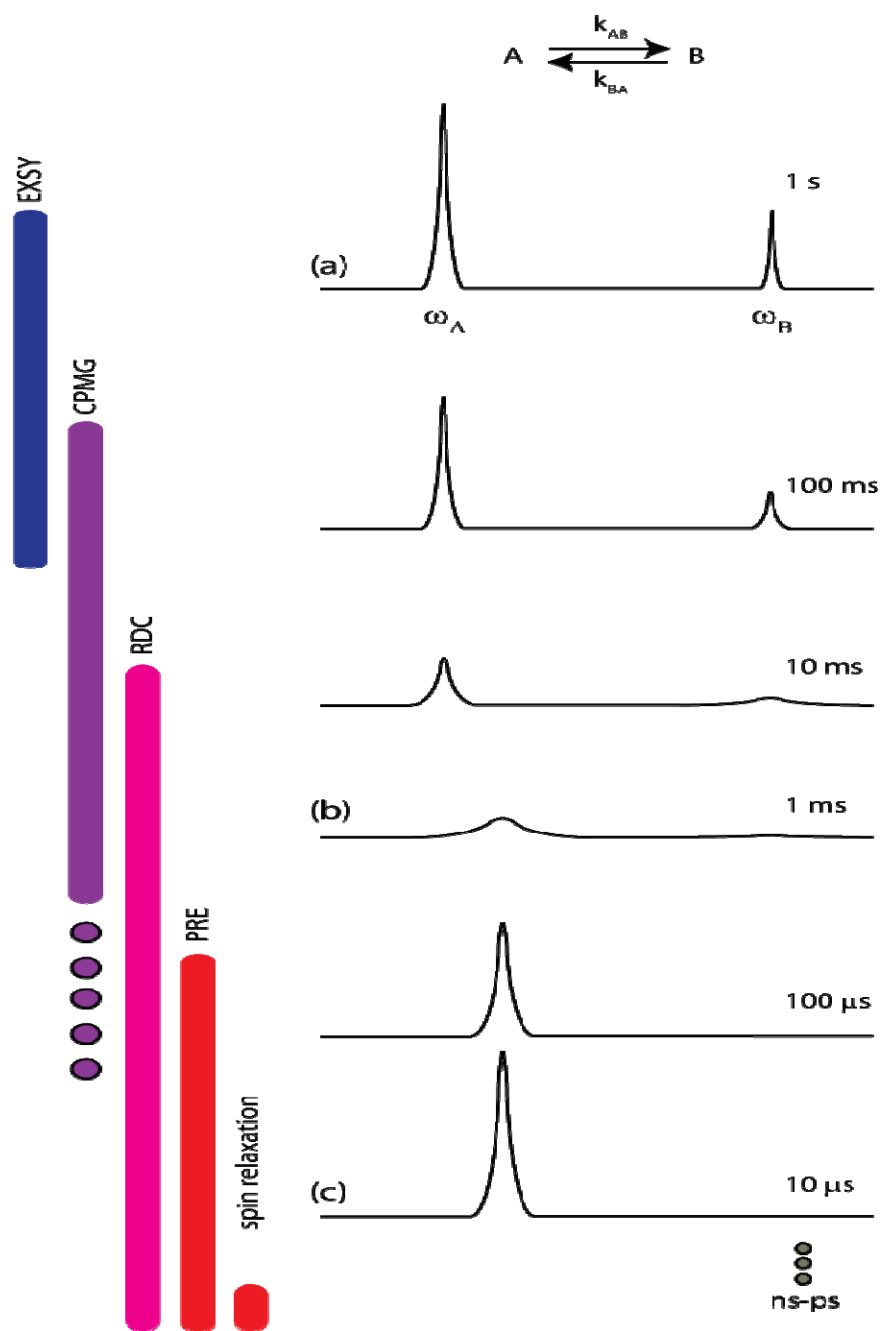


Figure 7 Comprehensive NMR dynamics experiments over timescales. This figure is adopted from (111).

Thus, NMR is a unique and powerful technique for studying protein structure and dynamics. The new isotopic labeling strategy enables specific labeling of methyl group of Ile, Leu, Val, or Met as probes to study protein structure and dynamics in high-molecular-weight system (109). Methyl groups are often located at hydrophobic cores of proteins and many of them tend to be dynamic. Thus, the relaxation rate is relatively slow, resulting in high quality methyl spectra (109, 118). Because methyl groups are sensitive to protein structure and dynamics, they are outstanding probes of protein function (119-122). Since the methyl groups are selectively protonated against a highly deuterated background their sensitivity is maximized, which is critical for supramolecular protein complexes (123). This approach has been used to study protein-ligand interactions (124), fast and slow side-chain dynamic motions (122), dynamics of protein folding (125), and even for the detection of proteins and protein complexes in in-cell NMR experiments (126). Commercially available isotopically labeled α -ketoacids (Fig. 8) serve as amino acid precursors for the incorporation of methyl-labels into the side-chains of valine, leucine, and isoleucine residues of proteins overexpressed in *E. coli* using D₂O-based minimal media (127). Different labeling patterns of these ILV residues can be used for different purposes. For example, proteins from Fig. 8, a and c with linearized ¹³C spin-systems are used for resonance assignments. The same samples can be used to obtain not only chemical shifts for assignments of backbone and ¹³C spins but also ³J_{C γ CO scalar couplings. In another case, the ¹³CH₃/¹²CD₃ labeling scheme from Fig 8, c and f is much better than that from Fig. 8, b and e for methyl-TROSY experiments (127). In order to obtain the isotopically labeled protein, α -ketobutyric acids are added into D₂O-based minimal media 1 h before induction. Methyl-transverse relaxation optimized spectroscopy (methyl-TROSY) experiment is based on the Heteronuclear Multiple Quantum Coherence (HMQC) experiment and exploits enhanced the TROSY effect on ¹³CH₃ (AX₃) spin systems (117). The experiment preserves the slowly relaxing pathways of magnetization (128). A high level of deuteration is critical to maximize the TROSY effect to reduce the external proton relaxation pathways. The original TROSY experiment was applied to A-X systems, such as backbone ¹⁵N-¹H (128)}

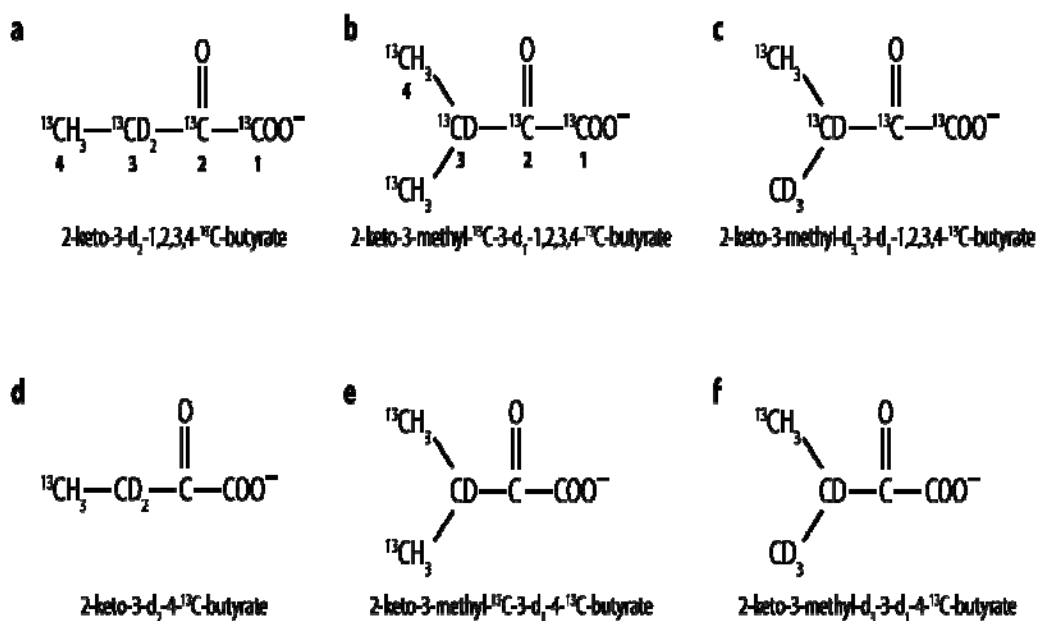


Figure 8 Partial commercially available isotopically labeled α -keto acid precursors. These biosynthesis precursors are used in *E. coli* growth of selectively methyl-labeled proteins. a,d) selectively labeled α -ketobutyrate for isoleucine. b,c,e,f) selectively labeled α -ketoisvalerates for valine and isoleucine. This figure is adopted from (127).

and aromatic ^{13}C - ^1H spin systems (129). The application of the TROSY effect to methyl groups ($^{13}\text{CH}_3$, $^{13}\text{CH}_2\text{D}$, and $^{13}\text{CHD}_3$) was optimized from the HMQC experiment (117, 130). The TROSY effect on $^{13}\text{CH}_3$ spin system is called Methyl-TROSY experiment. Methyl-TROSY is sensitive to the slowly relaxing component of $^{13}\text{CH}_3$ spin systems. This experiment in combination with highly deuterated proteins $^{13}\text{CH}_3$ labeled at the methyl groups of valine, leucine, and isoleucine, increases the methyl-TROSY sensitivity and resolution to systems reaching 700 kDa. Using this approach, deep insights have been recently obtained on several supramolecular protein complexes, such as ClpP protease (305 kDa) (131), and the 20S proteasome (670kDa) (109). Here, we use methyl-TROSY experiment and biochemical studies to understand the role of protein dynamics during the KaiC phosphorylation cycle.

CHAPTER II

MECHANISM OF THE PHOSPHORYLATION PHASE

2.1 Introduction

All circadian oscillators have a Phosphorylation Phase that is critically important to clock function (86). For example, mutation at a phosphorylation site in human Per2, Ser662 to Gly, which decreases Per2 phosphorylation *in vitro* (25), has been identified to be the cause for Familial Advance Sleep-Phase Syndrome (FASPS) (25, 27). Mutation at human Per3, Val647 to Gly, has also been linked to Delayed Sleep-Phase Syndrome (DSPS) (28). In cyanobacteria, the circadian rhythm of KaiC phosphorylation is key to downstream circadian rhythms of gene expression. Mutations at phosphorylation sites of KaiC cause arrhythmicity (59).

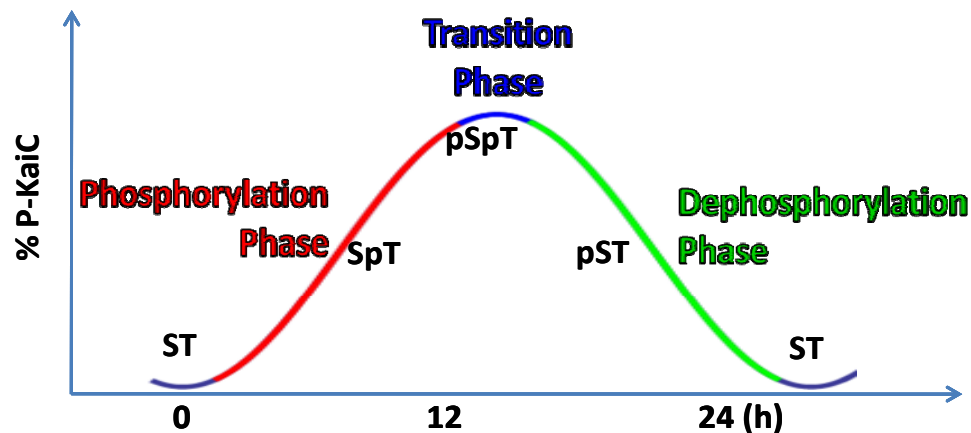


Figure 9 KaiC phosphorylation order diagram. ST: unphosphorylated Serine 431 and unphosphorylated Theronine 432; SpT: unphosphorylated S431 and phosphorylated T432; pSpT: phosphorylated S431 and phosphorylated T432; pST: phosphorylated S431 and unphosphorylated T432. KaiC phosphorylation and dephosphorylated undergoes four different phosphorylated state: ST \rightarrow SpT \rightarrow pSpT \rightarrow pST \rightarrow ST. In our model, the Pphosphorylation Phase is indicated as red part, the Transition Phase showed as blue and the Dephosphorylation Phase is green and whole cycle start anew.

However, the mechanism of the Phosphorylation Phase is not fully understood for any system, creating a major gap in understanding for the field (Fig. 9). For the cyanobacterial oscillator, it has long been known that KaiA induces KaiC phosphorylation (63, 64). Previously, our laboratory found that the exposed and buried positions of the A-loops of KaiC is the switch for phosphorylation and dephosphorylation, respectively (Fig. 10A and B) (86). In addition, we also determined that KaiA binds via its C-terminal domain to KaiC as evidenced by the NMR structure of C-terminal domain of KaiA^C in complex with a KaiC-derived peptide that includes the A-loops (85). Here, the x-ray crystal structure of *S. elongatus* KaiC shows that residues 488-497 (Fig.10A magenta part in KaiC) are buried in a looped conformation (87). We

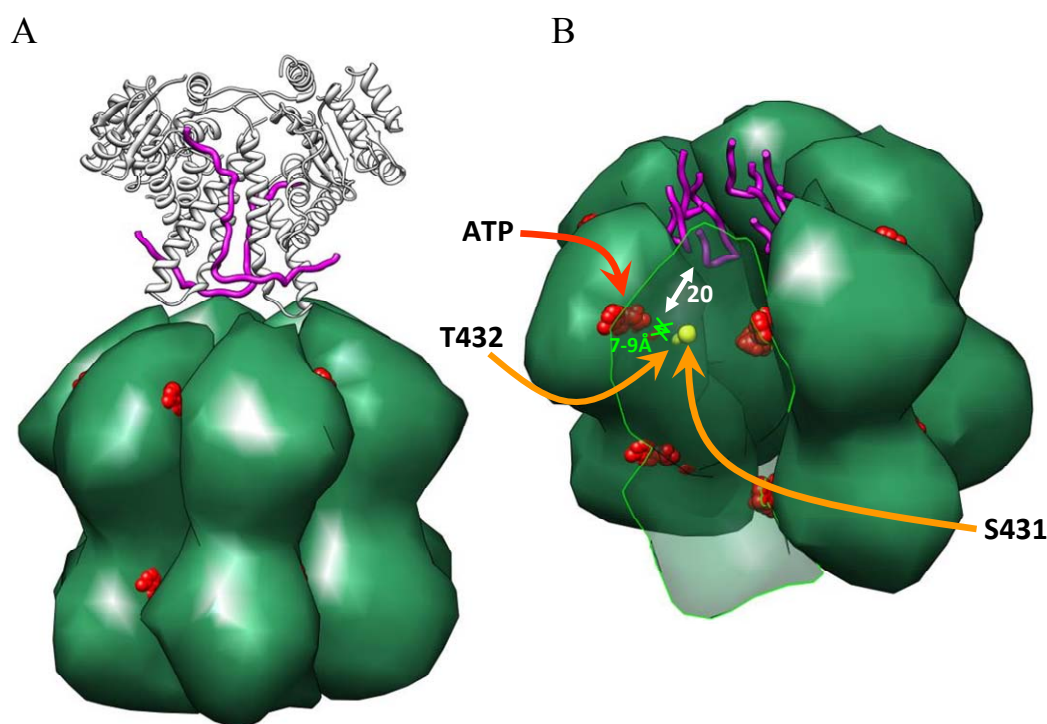


Figure 10 The NMR structure of the KaiA-KaiC A-loop complex docks on the top of KaiC structure and x-ray crystal structures of KaiC. (A) This is a docking model of two independent x-ray crystal structures. The two subunits of the KaiA dimer of the KaiA-KaiC A-loop complex are shown as gray and magenta ribbons(85). (B) The KaiC x-ray crystal structure in the bottom is the same structure shown in (60). (B) The N- and C-terminal domains of five subunits of KaiC (PDB ID : 1tf7) are shown as green surface, whereas the remaining subunit are shown as transparent surface. The A-loops are shown as magenta ribbon ATP molecules are red and S431 and T432 are yellow

refer to the segment as A-loop. Residues 489-519 are referred as “Tail”. Site-directed mutagenesis and negative-stain electron microscopy studies also revealed that KaiA binds exclusively to the CII domain of KaiC (78). These studies suggested that A-loop exposure in the KaiA:KaiC complex induces KaiC phosphorylation. Indeed, mutants of KaiC developed in our lab in which A-loop exposure was mimicked are hyper-phosphorylated (86). Although these discoveries advanced understanding, they could not explain how A-loop position and the active site of KaiC are coupled across 20 Å (Fig. 10B). In the dephosphorylated state of KaiC, the γ -phosphate groups of ATP are 8.5 Å and 6.6 Å away from the hydroxyl oxygens of KaiC phosphorylation sites S431 and T432, respectively (Fig. 11B). However, the upper distance limit for phosphoryl transfer between the phosphorus atom and acceptor oxygen is 5.0 Å, with the oxygen atoms perfectly aligned with the phosphate (84). In other words, when the A-loops are exposed, the distance between the bound ATP molecules and the sites of phosphorylation must decrease by at least 2 Å for phosphoryl transfer (84) to occur. The A-loops in the six crystal structures of KaiC are in the buried conformation, and thus provide little insight into how A-loop position affects the spatial rearrangement or dynamics of the active site(89).

NMR spectroscopy has been invaluable in revealing that dynamics can play key roles in dictating protein functions (108, 132). Increasing number of studies have demonstrated that protein dynamics, rather than structural changes, governs the allosteric mechanism by which protein functions are modulated (108, 132, 133). For example, PDZ3 domain from PSD-95/SAP90 shows a dynamics-driven allosteric effect (108). This PDZ3 domain binds to its natural partner CRIPT protein at C terminus. In heterologous cells, CRIPT causes a redistribution of PSD-95 to microtubules. In brain, CRIPT colocalizes with PSD-95 in the postsynaptic density and can be coimmunoprecipitated with PSD-95 and tubulin (134). The PDZ3 domain from PSD-95/SAP90 contains an additional helix(α 3) at its C terminus. The function of α 3 has been found to mediate the binding affinity for CRIPT protein through dynamic allostery. α 3 is distal from PDZ3 and CRIPT binding site. However, removal of this additional helix decreased by 21 fold the

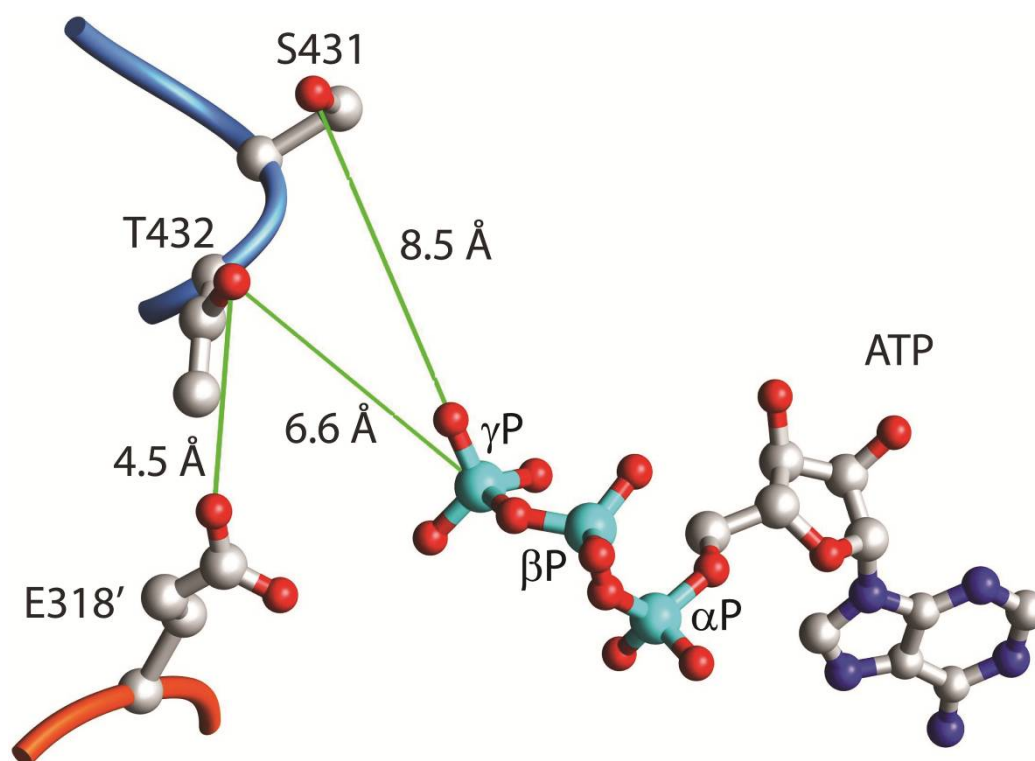


Figure 11 ATP is too far from phosphorylation sites. The sites of phosphorylation of KaiC, S431 and T432, and relevant distances (PDB ID: 1tf7). The prime on E318' from the adjacent subunit. ATP molecules binds to KaiC hexamer in the interface of two subunits at CII domain. The distance between γ P of ATP to hydroxyl group of T432 and S431 are 6.6 and 8.6 Å, respectively. The prime on E318', the putative catalytic glutamate, indicates an adjacent subunit. The upper distance limit between the phosphorus atom and acceptor oxygen for phosphoryl transfer is 5.0 Å, according to an analysis by Dr. Mildvan (84). Thus, the distances between the γ P of ATP and the hydroxyls of S431 and T432 are too far for phosphoryl transfer.

binding affinity for a CRIPT peptide which includes nine C-terminal residues. The structure of PDZ3 domain does not change upon the $\alpha 3$ deletion but dynamics on the ps-ns time scale increases dramatically. This hidden dynamic allostery demonstrated that allostery could arise solely from dynamics changes rather than structural changes. Therefore, we believe that the repositioning of the A-loops may have similar function to that of $\alpha 3$ helix of PDZ3 domain. Our hypothesis for the mechanism of the Phosphorylation Phase is that KaiA stabilizes a state of KaiC in which the CII ring is

flexible, which we propose is critical to KaiC phosphorylation. Here, we will demonstrate that the mechanism of KaiA-mediated KaiC phosphorylation is likely one of dynamic allostery. When the A-loops are buried in the absence of KaiA, ATP molecules are tightly bound in a KaiC hexamer, unable to approach S431 and T432. By comparison, when the A-loops are exposed, either by mutation or by KaiA capture, the CII ring becomes significantly flexible, which we think allows ATP to approach S431 and T432 for phosphoryl group transfer.

To test this hypothesis, we used isotopic labeling and NMR to determine the dynamic state of KaiC. With regard to probing dynamics of supramolecular protein complexes such as those of the Kai proteins (600 kDa), recent advances in isotopic labeling and NMR methodology now make it possible to obtain atomic-resolution details proteins, like 20S proteasome (670 kDa) (109). We prepared U- ^{2}H , ^{15}N], Ile- $[\delta 1 \text{ }^{13}\text{CH}_3]$ -labeled KaiC, U- ^{2}H , ^{15}N], Ile- $[\delta 1 \text{ }^{13}\text{CH}_3]$ -labeled KaiC-SE, U- ^{2}H , ^{15}N], Ile- $[\delta 1 \text{ }^{13}\text{CH}_3]$ -labeled KaiC-EE, and U- ^{2}H , ^{15}N], Ile- $[\delta 1 \text{ }^{13}\text{CH}_3]$ -labeled KaiC-ET to probe KaiC dynamics by recording the methyl-TROSY spectra. X and Y in KaiC-XY represent the amino acyl residues at positions 431 and 432, respectively. Alanyl and glutamyl substitutions at these positions have been shown to mimic the dephosphorylated and phosphorylated states of S431 and T432 (66, 86, 90). A truncation KaiC variant, U- ^{2}H , ^{15}N], Ile- $[\delta 1 \text{ }^{13}\text{CH}_3]$ -labeled KaiC-EE487, which mimics the exposed A-loops state of KaiC-EE, was generated to compare the dynamics change upon A-loop exposure. As the amino acyl substitutions reside in the CII ring, it is reasonable to assume that these spectral differences largely reflect differences in CII ring dynamics. Indeed, SAXS and fluorescence observations by Murayama et al. has suggested that it is the CII ring that undergoes stepwise changes compared with the CI ring (135). Our results revealed that KaiC-EE and KaiC-ET adopt the more rigid conformations than wt-KaiC, which indicated that the CII ring of KaiC is flexible during the Phosphorylation Phase and A-loop exposure can further increases the flexibility of the CII ring. In addition, phospho-T432 has been found to sustain KaiC CII ring flexibility, whereas phospho-S431 reduces the flexibility of the CII ring which also offset phospho-T432 effect. The features can

explain the natural phosphorylation order: ST \rightarrow SpT \rightarrow pSpT. Below, it will be demonstrated that the Phosphorylation Phase is regulated by CII ring flexibility.

2.2 Materials and Methods¹

S. elongates KaiA and KaiB expression and purification. The genes encoding KaiA and KaiB were cloned into the pET32a+ vector (Novagen) between the BamHI and NcoI sites. The resulting plasmids were used to transform *Escherichia coli* BL21(DE3) (Novagen) and the sequences were then confirmed (Gene Technologies Laboratory, Texas A&M University). Transformed *E. coli* cultures were incubated at 37°C until OD₆₀₀ reached about 0.6; at this point, a final concentration of 200 μ M isopropyl β -D-thiogalactopyranoside (IPTG) (Research Product International) was added for overexpression. Cells were harvested after 12 h overexpression at 25°C and pellets were then resuspended in 20 mM Tris-NaOH, 500 mM NaCl, pH 7.0. Cell suspensions were passed twice through a chilled French press cell, and lysates were clarified by centrifugation at 20,000 x g for 60 min at 4°C. Tagged proteins were isolated on a Ni-charged chelating column. Protease and ATPase were removed by anion-exchange chromatography (buffer A: 20 mM Tris Base, 20 mM NaCl, Ph 7.0; buffer B: 20 mM Tris Base, 1M NaCl, Ph 7.0; gradient: 0-80% buffer B over 165 mL column volumes). The tagged proteins were buffer exchanged to enterokinase (EK) cleavage buffer (Novagen) and reactions with 1 unit/ml EK were carried out at room temperature in 30-45 mL proteins. KaiA and KaiB were separated from Thioredoxin-His₆ tag by a second Ni-charged chelating column. All proteins were analyzed for purity by SDS-PAGE and dialyzed against a phosphorylation assay buffer (20 mM Tris Base, 150 mM NaCl, 0.5 mM EDTA, 5mM MgCl₂, 1 mM ATP, pH 8.0). Proteins were concentrated by an Amicon Stirred Ultrafiltration Cell (MILLIPORE) with a YM-10 untrafiltration

¹ Supplementary information of materials and methods are in the Appendixes A-F.

membrane (MILLIPORE) and stored in a -80°C freezer. Coomassie Plus (Pierce) was used as a Bradford Assay reagent for protein concentration determination.

S. elongates KaiC expression and purification. Gene encoding KaiC was cloned into the pGEX-6P-2 vector (GE Healthcare) between the BamHI and XhoI sites, and the resulting plasmids were used to transform *E. coli* DH5 α (Novagen), which produced more soluble recombinant KaiC than did *E. coli* BL21(DE3) (Novagen). Protein purification, analysis and storage were similar as for *S. elongates* KaiA and KaiB and 1 mM ATP was used in all solutions.

T. elongatus KaiA, KaiB, KaiC and KaiC mutants expression and purification. The genes encoding KaiA, KaiB and KaiC from *T. elongatus* were cloned into the pET28a+ vector (Novagen) between the NdeI and HindIII sites. The resulting plasmids were used to transform *Escherichia coli* BL21(DE3), and the sequences were confirmed (DNA Sequencing Facility, University of California, Berkeley). Transformed *E. coli* cultures were incubated at 37°C until OD₆₀₀ reached about 0.6; at this point, a final concentration of 200 μ M isopropyl β -D-thiogalactopyranoside (Research Product International) was added for overexpression. Cells were harvested after 12 h overexpression at 25°C, and pellets were resuspended in 20 mM Tris-NaOH, 500 mM NaCl, pH 7.0. Cell suspensions were passed twice through a chilled French press cell, and lysates were clarified by centrifugation at 20,000 x g for 60 min at 4°C. Tagged proteins were isolated on a Ni-charged column. Proteins were buffer exchanged to 20 M Tris Base, 500 mM NaCl and 20 mM Imidazole and 100 μ l 100 μ M ULP1 protease were added for SUMO-His₆ tag removal. The cleavage reaction was carried out at room temperature 16 h in 15 mL volume. Kai proteins were separated from SUMO-His₆ tag protein by a second Ni-charged column and followed by gel filtration chromatography on a Superdex 200 HiLoad 16/60 prep grade column (GE Healthcare) for KaiC and a Superdex 75 HiLoad 16/60 prep grade column (GE Healthcare) for KaiA and KaiB. Buffers were exchanged to 20 mM Tris Base, 150 mM NaCl, 0.5 mM EDTA, 5mM MgCl₂, 1 mM ATP, pH 7.0 for the phosphorylation assay and 20 mM Tris Base, 50 mM NaCl, 1 mM MgCl₂, 5 mM DTT, 1 mM ATP, pH 7.0 for the binding assay and NMR experiments. Proteins were

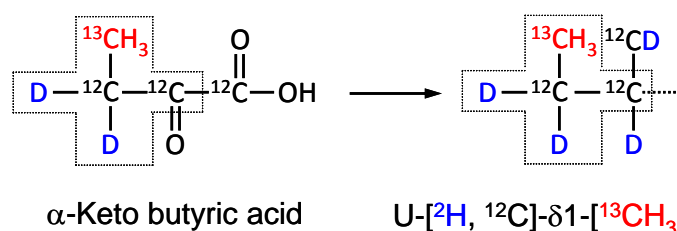


Figure 12 Methyl labeling strategy. Amino acid precursor used to produce proteins with ¹³CH₃-isoleucine (δ 1). Isoleucine (δ 1) methyl group is indicated in red. This figure is adopted from (123).

concentrated by Amicon Stirred Ultrafiltration Cell (MILLIPORE) and stored in a -80°C freezer. KaiA, KaiB, and KaiC did not lose function after repeated cycles of freezing and thawing. One liter LB yields ~ 440 nmol of KaiA, ~ 1728 nmol of KaiB, and ~ 240 nmol of KaiC and KaiC mutants. Coomassie Plus (Pierce) was used as a Bradford Assay reagent for protein concentration determination. For purification of KaiC, all the solutions were prepared with 1 mM ATP.

U-[¹⁵N, ²H], Ile δ 1-[¹³C, ¹H]-KaiC (KaiC, KaiC-SE, KaiC-EE, KaiC-ET, KaiC-EE487) expression and purification. Expression: Follow protocol A-10 and the amino acid precursor adopted scheme is in Fig. 12. Purification: Follow protocol A-11. Note that BioExpress (Cambridge Isotope Laboratories) was used to increase the growth rate of *E. coli*.

ULP1 protease expression and purification. Expression: Follow protocol A-8. Purification: Follow protocol A-12 but stops after the elution step of 1st Ni-NTA column. Note that Ulp1 is not stable in buffers where NaCl is at a concentration lower than 100 mM. For long-term storage, add equal volume of glycerol into the Ulp1 elution sample from Ni-NTA column and store at -80°C. Ulp1 elution sample can be diluted to a final concentration of 200 μ M before adding glycerol. Therefore, the final Ulp1 stock (stored at -80°C) will be 100 μ M in the buffer of 25 mM NaH₂PO₄, 250 mM NaCl, 125 mM imidazole, 50% glycerol, pH 8.0.

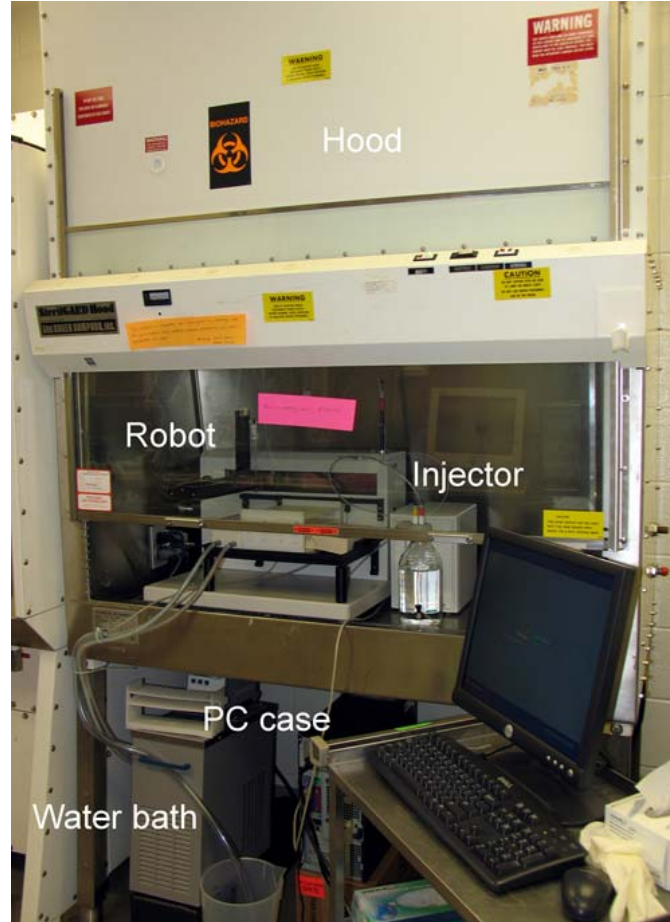


Figure 13 Robot Collector. Set up of Gilson 223 automated liquid handler/injector for collecting the aliquot from the *in vitro* reaction.

In vitro S. elongatus KaiC phosphorylation oscillation. All *S. elongatus* KaiC proteins were preincubated at 30°C for 16 h to allow samples to reach steady state hypophosphorylation before using them in experiments. KaiC proteins were then incubated with KaiA and KaiB in buffer (20 mM Tris, 150 mM NaCl, 0.5 mM EDTA, 5mM MgCl₂, 1 mM ATP, pH 8.0) at 30°C. The final concentrations of KaiA, KaiB, and KaiC were 1.2, 3.5, and 3.5 μM, respectively. Aliquots (37 μl) of the reaction mixtures were collected every 2 h by a Gilson 223 automated liquid handler/injector (Fig. 13). All the reaction was stopped by the addition of 7μl SDS-PAGE gel loading dye (100 mM Tris Base at pH 6.8 with 4% SDS, 0.2% bromophenol blue, 20% glycerol, and 400 mM

β -mercaptoethanol). A sample (7 μ l) for each indicated time point was loaded onto 9 x 10 cm SDS polyacrylamide gels (4% of acrylamide/bisacrylamide for stacking gel, and 6.5% of acrylamide/bisacrylamide for running gel) with 15 wells (10 x 3 x 0.75 mm). The experiments were run at a 60 voltages glycine buffer for 40 minutes and then 140 V for 1 h 50 minutes, with the electrophoresis cell surrounded by ice water. Gels were stained with Coomassie brilliant blue, and the percentage of KaiC that was phosphorylated in each lane was determined by densitometric analysis by using Image J (National Institutes of Health) and PeakFit (SeaSolve Software, Inc.).

T. elongatus KaiC protein kinetics. Recombinant *T. elongatus* KaiA, KaiB, and KaiC proteins were preincubated at 30°C for 16 h to allow samples to reach steady state hypophosphorylation before using them in experiments. KaiC proteins were then incubated with KaiA and KaiB in buffer (20 mM Tris, 150 mM NaCl, 0.5 mM EDTA, 5mM MgCl₂, 1 mM ATP, pH 7.0) at 30°C. The final concentrations of KaiA, KaiB, and KaiC were 1.2, 3.5, and 3.5 μ M, respectively. Aliquots (37 μ l) of the reaction mixtures were collected following the designed time course. The reaction was stopped by the addition of 7 μ l SDS-PAGE gel loading dye (100 mM Tris, 4% SDS, 0.2% bromophenol blue, 20% glycerol, 400 mM β -mercaptoethanol, pH 6.8). A sample (7 μ l) of each reaction was loaded onto 9 x 10 cm SDS polyacrylamide gel (4% of acrylamide/bisacrylamide for stacking gel, 6.5% of acrylamide/bisacrylamide for running gel) with 15 wells (10 x 3 x 0.75 mm).

T. elongatus KaiC variants kinetics. Recombinant *T. elongatus* KaiC proteins were preincubated at 30°C for 16 h to allow samples to reach steady state hypophosphorylation before using them in experiments. KaiC proteins were then incubated with KaiA and KaiB in buffer (20 mM Tris, 150 mM NaCl, 0.5 mM EDTA, 5mM MgCl₂, 1 mM ATP, pH 7.0) at 30°C. The final concentrations of KaiA, and KaiC were 1.2, and 3.5 μ M, respectively. Aliquots (37 μ l) of the reaction mixtures were collected following the designed time course.

Binding Assay. All column binding assays including KaiC-CII alone experiments were carried out using a Superdex 200 10/300 GL gel filtration column (GE Healthcare).

Ferritin (440 kDa), albumin (67 kDa), ovalbumin (43 kDa), and chymotrypsinogen A (25 kDa) were used as molecular mass markers.

KaiC-CII hexamerization. Recombinant CII variants (final concentration: 10 μ M) in 100 μ l binding buffer (20 mM Tris, 50 mM NaCl, 1 mM MgCl₂, 5 mM DTT, 1 mM ATP, pH 7.0) were incubated at 25°C about 0.5 h, and then applied to a Superdex 200 10/300 GL column with a flow rate of 0.8 ml/min.

KaiA and KaiC-CII binding. Recombinant KaiA and KaiC-CII variants were mixed in 1:1 ratio (10 μ M: 10 μ M) in 300 μ l binding buffer (20 mM Tris, 50 mM NaCl, 1 mM MgCl₂, 5 mM DTT, 1 mM ATP, pH 7.0) at 25°C for 0.5 h. Then, the mixture was applied to a Superdex 200 10/300 GL column with a flow rate of 0.8 ml/min.

NMR Sample Preparation and Spectroscopy. NMR sample preparation: Follow protocol C-1. NMR sample information: Please see Table 1. NMR spectroscopy: Follow Protocol C-2.

2.3 Results

Recombinant Kai proteins are functional. To establish that the recombinant Kai proteins are functional in generating the 24h rhythm, the *in vitro* KaiC phosphorylation oscillation with recombinant Kai proteins was carried out in the standard condition (Please see below or materials and methods). Recombinant KaiA, KaiB, and KaiC from *S. elongatus* and ATP were mixed in a sterile microcentrifuge tube and the reaction was incubated at 30°C with final concentrations of 1.2 μ M, 3.5 μ M, 3.5 μ M, and 1 mM, respectively. Aliquots were collected by a Gilson 223 automated liquid handler/injector every two hours for three days. The reactions were stopped by the addition of 7 μ l SDS-PAGE gel loading dye and, then, heating at 60°C for 15 mins. Each aliquot was subjected to 6.5% SDS-PAGE. KaiC displays two bands, with the upper and bottom bands indicating hyperphosphorylated and hypophosphorylated KaiC proteins (Fig. 14B). These gels were processed using image analysis software Image J (National Institutes of

Table 1 NMR Sample Condition and Experiment for CHAPTER II

Sample	Experiment	Sample detail	Experiment detail
KaiC			
U-[¹⁵ N, ² H]-Ile δ 1-[¹³ C, ¹ H]-FLAG-KaiC	Methyl-TROSY	Concentration: 15 μ M Buffer: 20 mM Tris, 50 mM NaCl, 1 mM MgCl ₂ , 5 mM DTT, 1 mM ATP, pH 7.0, 10 μ M DSS, 0.02% NaN ₃ , 99.96% D ₂ O Volume: ~300 μ l Tube: shaped tube	NS=128 40 °C
U-[¹⁵ N, ² H]-Ile δ 1-[¹³ C, ¹ H]-FLAG-KaiC-SE	Methyl-TROSY	Concentration: 8 μ M Buffer: 20 mM Tris, 50 mM NaCl, 1 mM MgCl ₂ , 5 mM DTT, 1 mM ATP, pH 7.0, 10 μ M DSS, 0.02% NaN ₃ , 99.96% D ₂ O Volume: ~300 μ l Tube: shaped tube	NS=256 37 °C
U-[¹⁵ N, ² H]-Ile δ 1-[¹³ C, ¹ H]-FLAG-KaiC-EE	Methyl-TROSY	Concentration: 16 μ M Buffer: 20 mM Tris, 50 mM NaCl, 1 mM MgCl ₂ , 5 mM DTT, 1 mM ATP, pH 7.0, 10 μ M DSS, 0.02% NaN ₃ , 99.96% D ₂ O Volume: ~300 μ l Tube: shaped tube	NS=128 40 °C
U-[¹⁵ N, ² H]-Ile δ 1-[¹³ C, ¹ H]-FLAG-KaiC-ET	Methyl-TROSY	Concentration: 14 μ M Buffer: 20 mM Tris, 50 mM NaCl, 1 mM MgCl ₂ , 5 mM DTT, 1 mM ATP, pH 7.0, 10 μ M DSS, 0.02% NaN ₃ , 99.96% D ₂ O Volume: ~300 μ l Tube: shaped tube	NS=128 40 °C

Table 1 continued

Sample	Experiment	Sample detail	Experiment detail
U-[¹⁵ N, ² H]-Ile δ 1-[¹³ C, ¹ H]-FLAG-KaiC-1-487-EE	Methyl-TROSY	Concentration: 8 μ M Buffer: 20 mM Tris, 50 mM NaCl, 1 mM MgCl ₂ , 5 mM DTT, 1 mM ATP, pH 7.0, 10 μ M DSS, 0.02% NaN ₃ , 99.96% D ₂ O Volume: ~300 μ l Tube: shaped tube	NS=224 37 °C
KaiC-CI			
U-[¹⁵ N, ² H]-Ile δ 1-[¹³ C, ¹ H]-FLAG-KaiC-CI-1-247	Methyl-TROSY	Concentration: 6 μ M Buffer: 20 mM Tris, 50 mM NaCl, 1 mM MgCl ₂ , 5 mM DTT, 1 mM ATP, pH 7.0, 10 μ M DSS, 0.02% NaN ₃ , 99.96% D ₂ O Volume: ~300 μ l Tube: shaped tube	NS=256 40 °C
KaiC-CII-EE			
U-[¹⁵ N, ² H]-Ile δ 1-[¹³ C, ¹ H]-FLAG-KaiC-CII-249-518-EE	Methyl-TROSY	Concentration: 3 μ M Buffer: 20 mM Tris, 50 mM NaCl, 1 mM MgCl ₂ , 5 mM DTT, 1 mM ATP, pH 7.0, 10 μ M DSS, 0.02% NaN ₃ , 99.96% D ₂ O Volume: ~300 μ l Tube: shaped tube	NS=256 25 °C

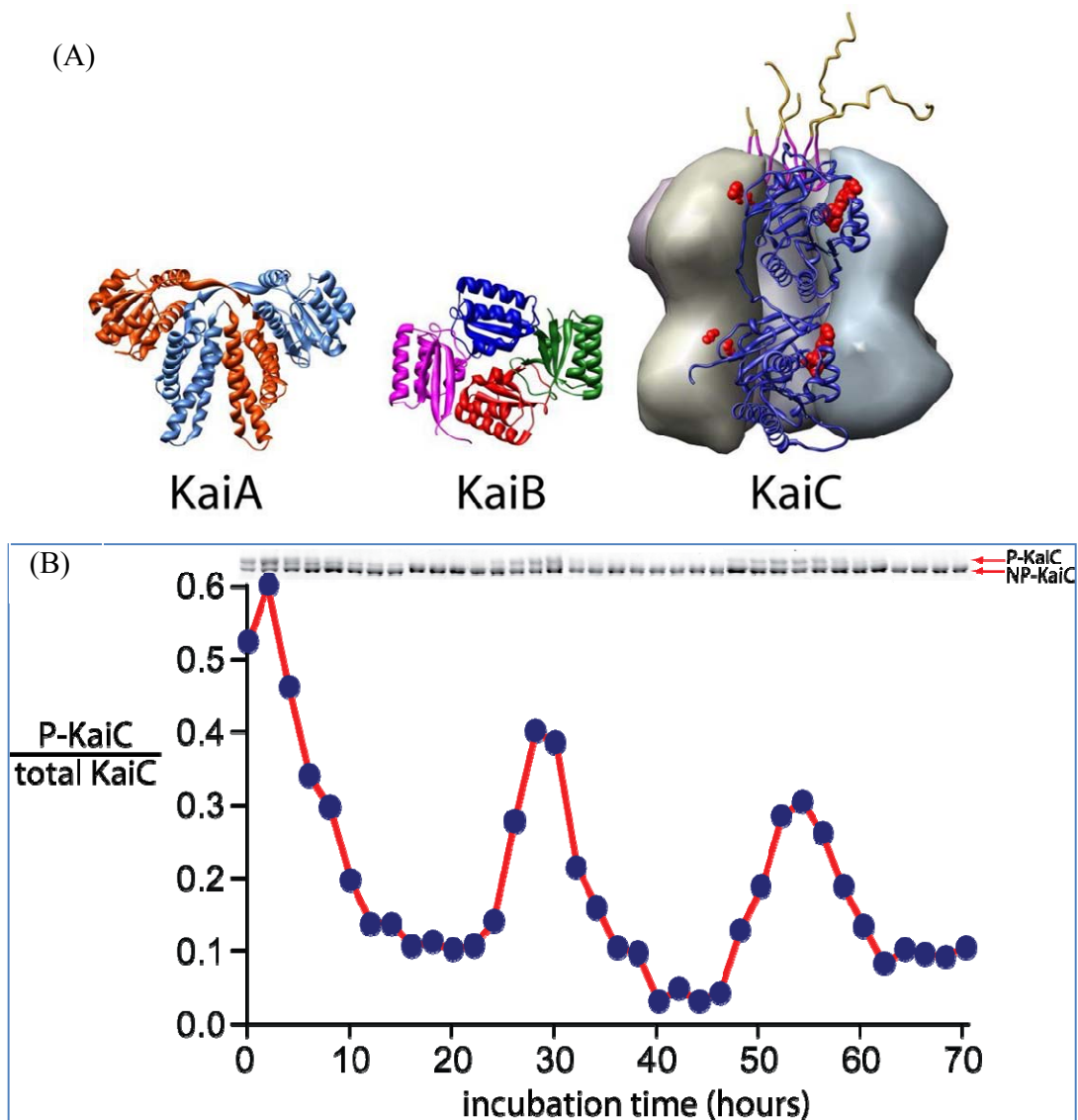


Figure 14 *In vitro* KaiC phosphorylation oscillation. (A) KaiA(71), KaiB(87, 136), and KaiC(60) crystal structures. (B) *In vitro* KaiC phosphorylation oscillation. SDS-PAGE of KaiC phosphorylation (top) and KaiC phosphorylation level (bottom).

Health) and PeakFit (SeaSolve Software, Inc.) for quantification by densitometry. The proportion of phosphorylated KaiC ranged from 30% – 60% during the cycle. The KaiC phosphorylation cycle pattern is similar to that previously reported by the Kondo group

(58). Here, my data strongly indicates that recombinant Kai proteins from our lab are functional and therefore can be used to study the mechanism of the central oscillator.

The Kai proteins we used for NMR experiments are from *T. elongatus* because they are more stable under NMR conditions compared to Kai proteins from *S. elongatus*. Kai proteins from *T. elongatus* have better behavior in terms of expression, stability, and solubility, and they also tolerate higher temperatures. For big proteins such as KaiC, high temperature is critical in many cases for optimal spectral resolution. These properties of *T. elongatus* Kai proteins make them more suitable for experimental study by NMR. Kai proteins from *S. elongatus* and *T. elongatus* share sequence similarities of greater than 80% except for KaiA, which shares about 46% similarity between the two homologs. However, the conserved C-terminal domain of KaiA from the two species (residues 180-283), which binds to KaiC, share 61% similarity. To ensure Kai proteins from *T. elongatus* have the same functionality as Kai proteins from *S. elongatus*, KaiC phosphorylation kinetic assays were carried out under the same condition for 24 h at 30°C. The reaction mixture contained KaiA, KaiB, KaiC, and ATP in final concentrations of 1.2 μM , 3.5 μM , 3.5 μM , and 1 mM, respectively. The KaiC phosphorylation kinetics profile was highly similar to that *S. elongatus*. KaiA stimulates KaiC phosphorylation and KaiC remains in a state of hyperphosphorylation in the absence of KaiB (Fig. 15). However, in the presence of both KaiA and KaiB, KaiC first phosphorylates, and after it reaches the hyperphosphorylation state, starts to dephosphorylate. By comparison, KaiC alone or in the presence of KaiB dephosphorylate over time. The first 24 h KaiC phosphorylation cycle from *T. elongatus* has the same kinetics profile as that of *S. elongatus* KaiC (86). This similarity indicates that Kai proteins from *T. elongatus* behave similarly as Kai proteins from *S. elongatus*. Fluorescence anisotropy results published earlier by our group also support the hypothesis that interactions from *T. elongatus* and *S. elongatus* are similar (86). Thus,

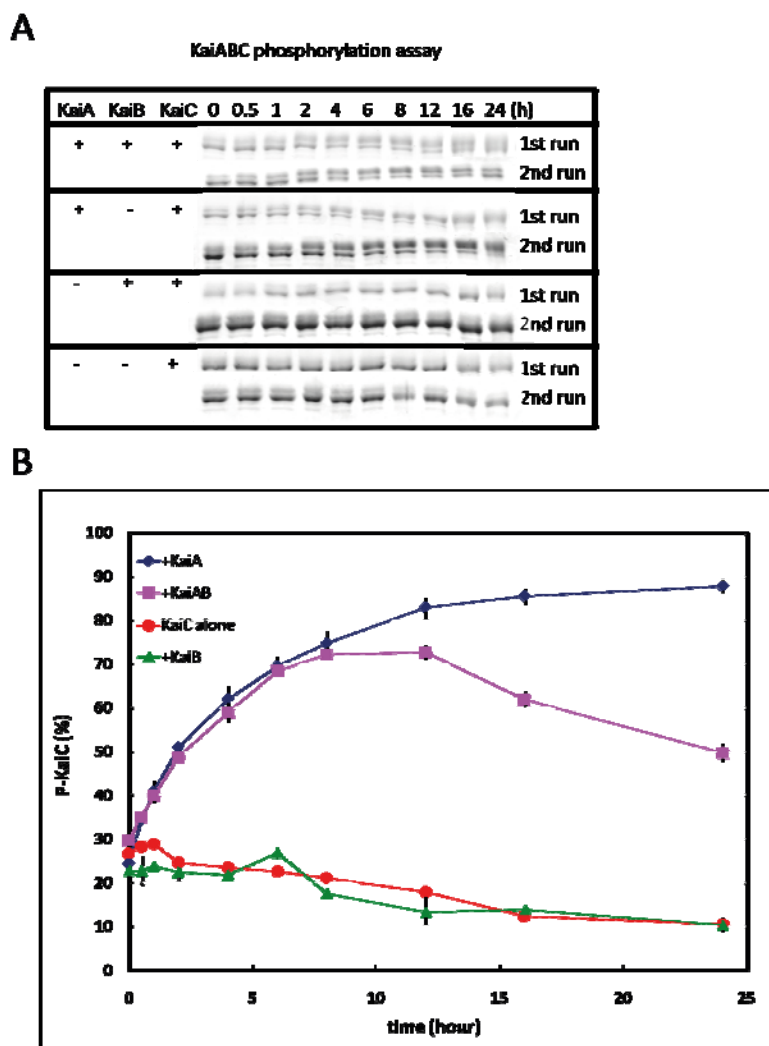


Figure 15 *In vitro* 24h phosphorylation of KaiC. (A) SDS-PAGE gel showing phosphorylation of KaiC in the presence or absence of KaiA and KaiB. (B) Densitometry analysis plotted from (A).

KaiC phosphorylation kinetics data suggest that recombinant Kai proteins from *T. elongatus* can be used to understand the mechanism of the *S. elongatus* oscillator.

A-loop position affects KaiC dynamics. KaiA enhances KaiC phosphorylation, while KaiC alone dephosphorylates. How KaiA enhances KaiC phosphorylation is not clear.

The NMR structure of the KaiA:KaiC peptide complex showed that KaiA binds to KaiC A-loops (Fig. 11A) (85), suggesting that the A-loops in an ensemble of KaiC molecules exist in a dynamic equilibrium between buried and exposed states. KaiA increases KaiC phosphorylation by stabilizing the exposed state of A-loops through direct binding to the A-loops. By contrast, in the crystal structure of phosphorylated and unphosphorylated KaiC (60, 89), the A-loops are buried, and the γ -phosphate group of ATP was 8.5 Å and 6.6 Å from the hydroxyl oxygen of S431 and T432, respectively (Fig. 11). The distance between the A-loops and phosphorylation site is about 20Å (Fig. 10B). The structural information does not explain the specific mechanism by which KaiA enhances KaiC phosphorylation. Prompted by the hidden dynamic allostery mechanism (108), we proposed that A-loops exposure probably significantly affects the dynamics of KaiC and that these dynamics are required for phosphorylation.

Due to the size of the KaiC hexamer (nearly 360 kDa as a hexamer), no significant signal would be generated from traditional NMR experiments. For that reason, we used the methyl-TROSY NMR experiment together with the isotopic labeling methods, which have been shown to be powerful in increasing the sensitivity and resolution of NMR of supra-molecular systems (137, 138). Methyl-TROSY produces spectra with improved resolution and signal to noise and this method pushes up the limitation of protein size by NMR to >700 kDa (109). To probe KaiC dynamics, we prepared the following NMR samples: U-[^2H , ^{15}N], Ile-[$\delta 1$ $^{13}\text{CH}_3$]-labeled wt-KaiC, U-[^2H , ^{15}N], Ile-[$\delta 1$ $^{13}\text{CH}_3$]-labeled KaiC-SE, U-[^2H , ^{15}N], Ile-[$\delta 1$ $^{13}\text{CH}_3$]-labeled KaiC-EE, U-[^2H , ^{15}N], Ile-[$\delta 1$ $^{13}\text{CH}_3$]-labeled KaiC-ET, and U-[^2H , ^{15}N], Ile-[$\delta 1$ $^{13}\text{CH}_3$]-labeled KaiC-EE487. The first four KaiC variants mimic the different phosphoforms of KaiC, and KaiC-EE487 mimics the exposure of the A-loops from KaiC-EE. We used α -ketobutyric acid-4- ^{13}C ,3,3- d_2 sodium salt hydrate, an amino acid precursor, and this chemical only allowed the methyl group at $\delta 1$ of Ile to be labeled. The purification protocols are described in the materials and methods. The concentrations of U-[^2H , ^{15}N], Ile-[$\delta 1$ $^{13}\text{CH}_3$]-labeled

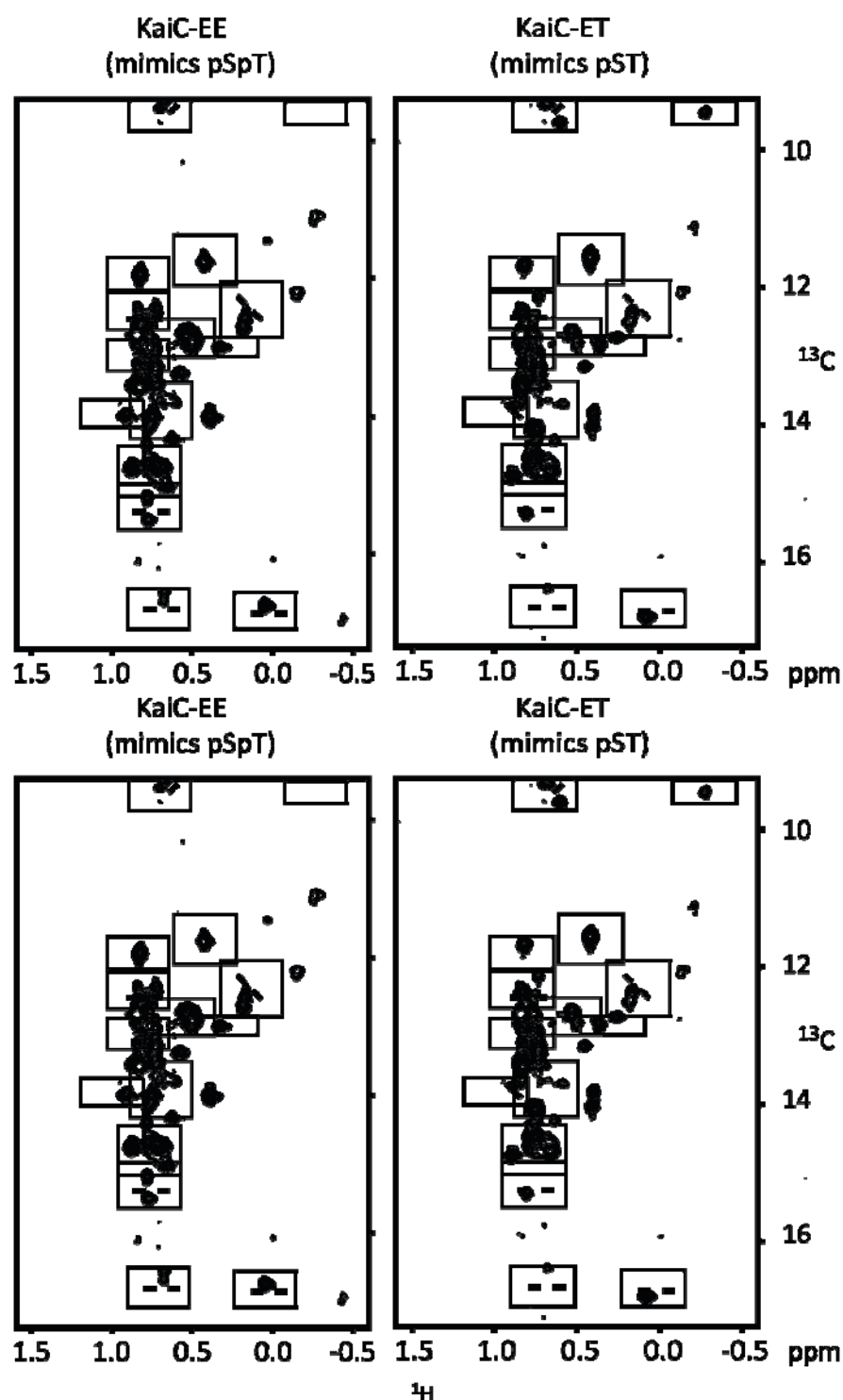


Figure 16 Methyl-TROSY spectra of wt-KaiC, KaiC-SE, KaiC-EE, KaiC-ET, and KaiC-EE487. Fifteen selected peaks are boxed for comparison. Sample conditions and NMR parameters are described in Table 1. Note that the spectra contour levels are plotted at the same relative contour level.

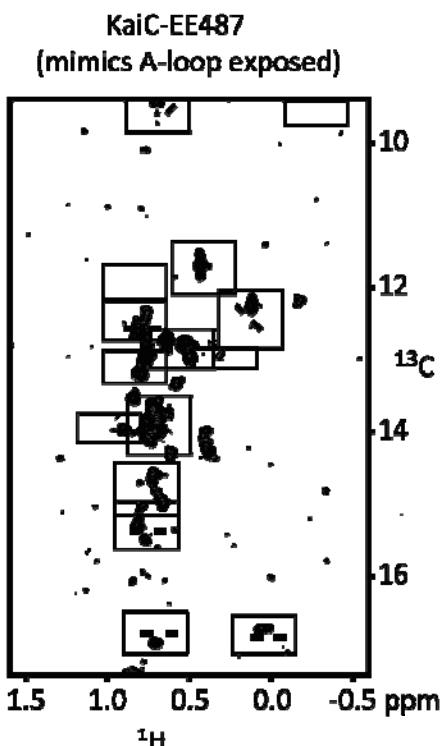


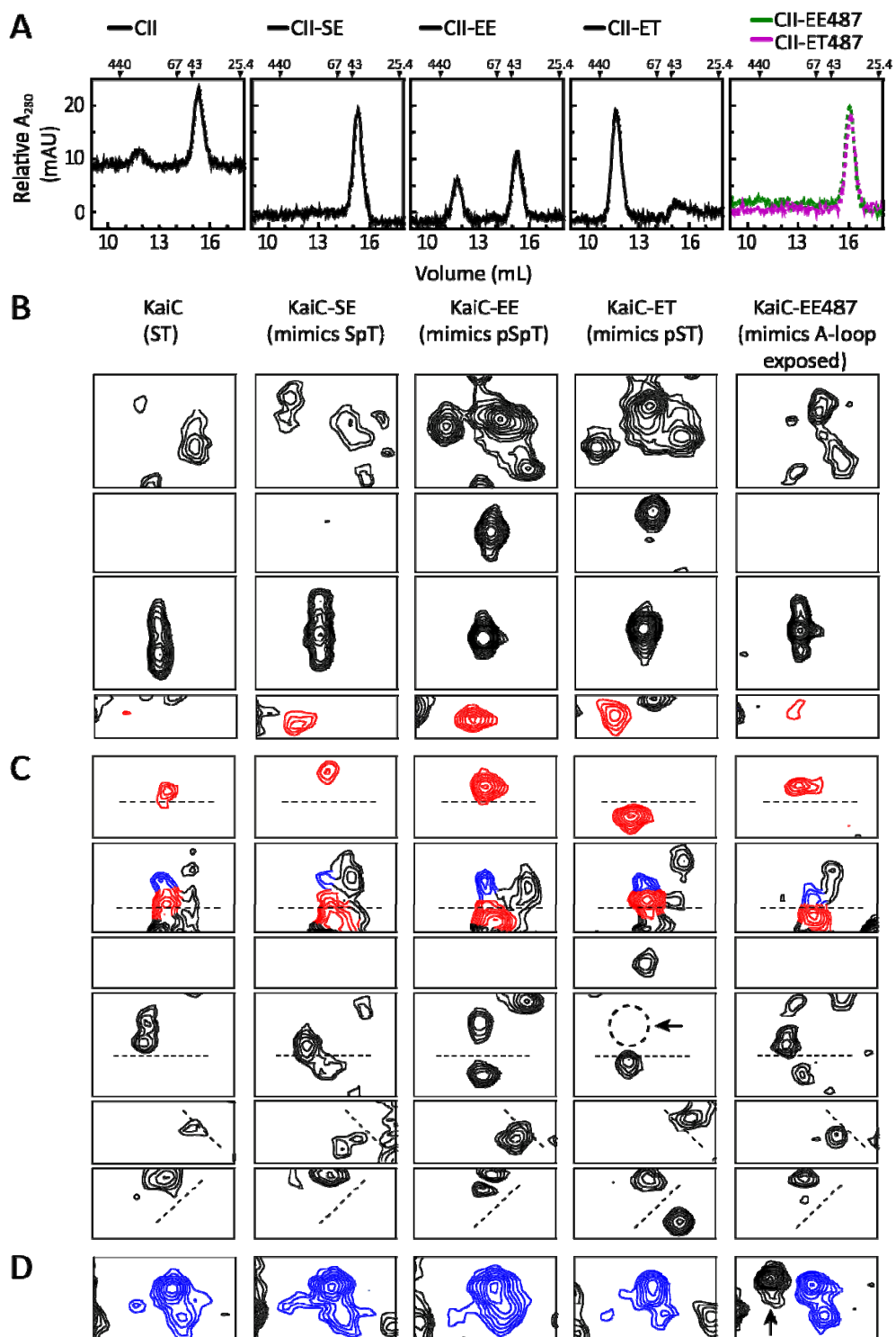
Figure 16 Continued

KaiC, U- ^{2}H , ^{15}N], Ile- $[\delta 1 \text{ } ^{13}\text{CH}_3]$ -labeled KaiC-SE, U- ^{2}H , ^{15}N], Ile- $[\delta 1 \text{ } ^{13}\text{CH}_3]$ -labeled KaiC-EE, U- ^{2}H , ^{15}N], Ile- $[\delta 1 \text{ } ^{13}\text{CH}_3]$ -labeled KaiC-ET, and U- ^{2}H , ^{15}N], Ile- $[\delta 1 \text{ } ^{13}\text{CH}_3]$ -labeled KaiCEE487 are 15, 8, 16, 14, and 8 μM , respectively. Methyl-TROSY spectra were collected at 40°C, except for the KaiC-SE sample, which was collected data at 37°C due to its instability. All spectra were collected on a Bruker 600 MHz Avance III NMR spectrometer equipped with a cryogenically cooled probe-head with the number of scans ranging from 32 to 128. The difference in concentrations and number of scans were considered when the spectra were analyzed. Data are shown in Fig. 16. Overall, the spectra were very similar in term of chemical shift (Fig. 16). Since phosphorylation sites are located on the CII domains, the spectral differences mostly arise from the CII rings. Line shape analysis suggests that phosphorylation at S431 significantly restricts the μs -ms time scale CII ring motions, presumably through enhanced electrostatic interaction between CII domains (89). These spectra were used to assign resonances to the CI and

CII domains of full-length KaiC spectra. Methyl-TROSY line shapes of several resonances, including those assignable to the CII ring, are significantly broader in wt-KaiC and the KaiC-SE than in the KaiC-EE and KaiC-ET (Fig. 17B, panels 1-4). Thus, phospho-S431 restricts μs – ms time scale CII ring motions, presumably through enhanced electrostatic interactions between CII domains (89). KaiC-EE shares spectral signatures with KaiC and KaiC-SE that are absent in KaiC-ET (Fig. 17C, panel 1-4), supporting the notion that phospho-T432 preserves some CII ring flexibility even in the presence of phospho-S431. As shown earlier, KaiC phosphorylation initiates upon selective capture of the A-loops in their exposed position by KaiA (78, 85, 86). For the KaiC and KaiC-SE, the A-loops occasionally sample the exposed position, thereby making themselves available for capture by KaiA. For the rigid KaiC-ET, in contrast, the A-loops are likely trapped in the buried position, contributing to the stability of the CII ring. Indeed, their exposure, as mimicked by their truncation, increases flexibility (Fig. 17, A-D, panel 5). Although the methyl-TROSY spectrum of this KaiC variant is similar to those of the ST and SpT forms, unique spectral features from A-loop exposure (Fig. 17D) probably reflect the conformational and dynamic changes critical to the induction of KaiC phosphorylation. Since KaiC487 is constitutively hyperphosphorylated (86), this data strongly supports the idea that KaiC phosphorylation requires a flexible CII ring that is stabilized by KaiA capture of exposed A-loops.

CII domain dominates the dynamics of KaiC. To confirm that KaiC CII ring flexibility specifically changes during the ordered phosphorylation of KaiC, we decoupled CII variants from CI domains by generating CII domains alone and tested their hexamerization levels using a gel filtration column. The proteins were purified without ATP, and, therefore, they were in the monomeric form during the purified process. ATP was added to a final concentration of 1 mM into the concentrated protein samples before the samples were stored at -80°C . 100 μl of CII variants at a concentration of 10 μM were incubated at 25°C for 30mins before analysis of hexameric formation by a Superdex 200 10/300 GL gel filtration column with a flow rate of 0.8 mL/min. CII-EE and CII-ET show 37% and 94% hexamer, respectively

Figure 17 CII ring flexibility depends on the state of phosphorylation at residues S431 and T432 and A-loop position. A) Gel filtration profiles of isolated CII domains of wt-CII (panel 1) and phosphomimics of SpT-CII (panel 2), pSpT-CII (panel 3), pST-CII (panel 4), and pSpT-CII487 and pST-CII487 (panel 5). The hexameric form of the CI and CII domains eluted at ~11.6 mL, whereas the monomeric form eluted at ~15.4 mL. In panel A5 the constructs were truncated just prior to the A-loops at residue 488, and eluted as monomers at 16 mL. B) – D) Selected regions from methyl-TROSY (117) (139) spectra of U-D, Ile-[1^{13}CH_3] labeled wt-KaiC (panel 1) and phosphomimics of KaiC-SpT (panel 2), KaiC-pSpT (panel 3), KaiC-pST (panel 4), and KaiC-pSpT487 (panel 5). All panels were plotted at the same relative contour level. Gel-filtration experiments (not shown) indicate that these KaiC mutants did not aggregate. Red and blue contours indicate peaks assigned to Ile residues of the CII and CI domains of KaiC, respectively, whereas black contours indicate unassigned peaks. Please see Fig. 2-8, 2-10 and appendixes for details on these assignments and experiments.



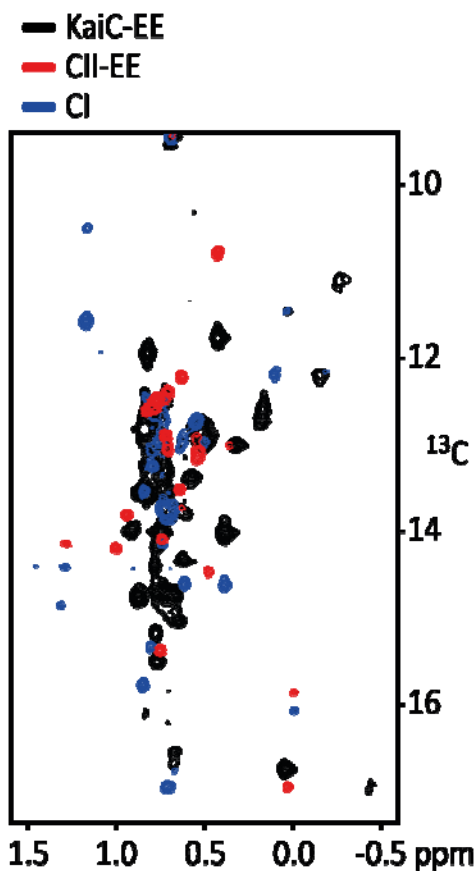


Figure 18 Overlay of methyl-TROSY spectra of KaiC-EE (black), CI (blue, residues 1-247), and CII-EE (red, residues 249-518). Sample conditions and NMR parameters are described in Table 1. These spectra were used to assign resonances to the CI and CII domains of full-length KaiC spectra.

(Fig. 17A). In comparison, CII and CII-SE show only 14% and 0% hexamer, respectively. The trend of hexamerization level confirms that phosphorylation of Ser431 reduces the CII ring flexibility and the induced rigidity results in the formation of hexamers. On the other hand, CII-EE has 63% monomer but CII-ET only has 6% monomer. It suggests that phospho-T432 offsets the rigidity induced by phospho-S431. However, CII-EE487 and CII-ET487 have 100% monomer indicates that the exposed A-loops decrease the rigidity more than the rigidity induced by phospho-S431. Collectively, these gel filtration results corroborate the NMR results of KaiC variants that the formation of hexamer corresponds to the rigidity of the CII ring.

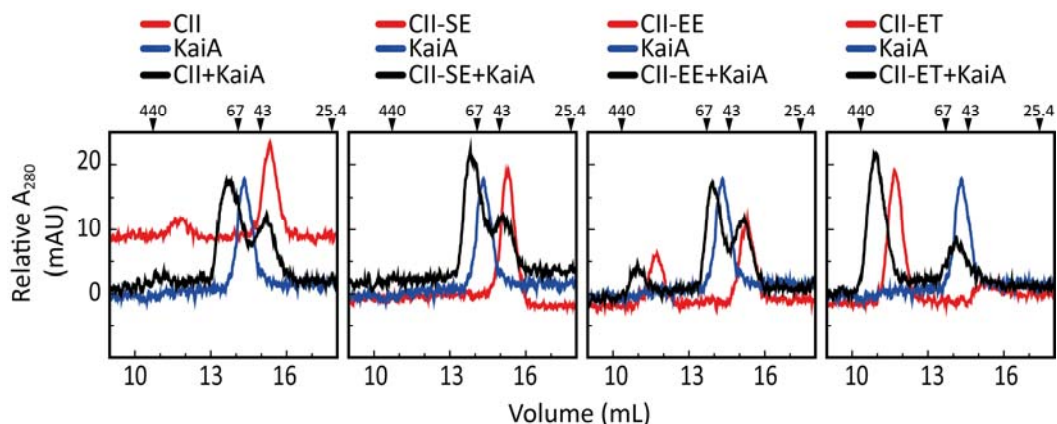


Figure 19 KaiA and CII binding. Gel-filtration profiles of mixtures of KaiB with CII (panel 1) and with phosphomimics of KaiC-SpT (panel 2), KaiC-pSpT (panel 3), and KaiC-pST (panel 4). The elution profiles of KaiB in each panel were from a single run.

KaiA binding is not affected by the oligomeric state of CII domain. We also wondered if KaiA binds to the CII domain variants. This is to test if KaiA binding with A-loops is altered by the change of the flexibility of the CII ring and the oligomeric state of the CII ring. Thus, we prepared the same CII ring variants and they were mixed with KaiA in 1:1 monomeric ratio at a concentration of 10 μM at 25°C for 30 mins in the presence of 1 mM ATP. KaiC phosphorylation profile shows that KaiA enhances KaiC phosphorylation after 30 mins (Fig. 15). In addition, the binding between *S. elongatus* KaiA and unphosphorylated or phosphorylated KaiC is strong, The K_d is 3nM for KaiC-EE and 32 nM for KaiC-AA (90). Therefore, if KaiA binds to CII rings, we should be able to see it in 30 mins incubation. The binding reactions were analyzed by using a Superdex 200 10/300 GL gel filtration column with a flow rate of 0.8 mL/min. Fig. 18 showed KaiA-induced peak shifts for all CII variants mixed with KaiA. KaiA binds to all the monomeric wt-CII, SE-CII, and EE-CII and the hexameric EE-CII and ET-CII (Fig. 19). However, KaiA binding affinity to hexameric KaiC variants is higher than monomeric KaiC variants, as seen from the free monomeric CII peak by gel filtration. Indeed, the binding between KaiA and KaiC phosphomimics are stronger than KaiA

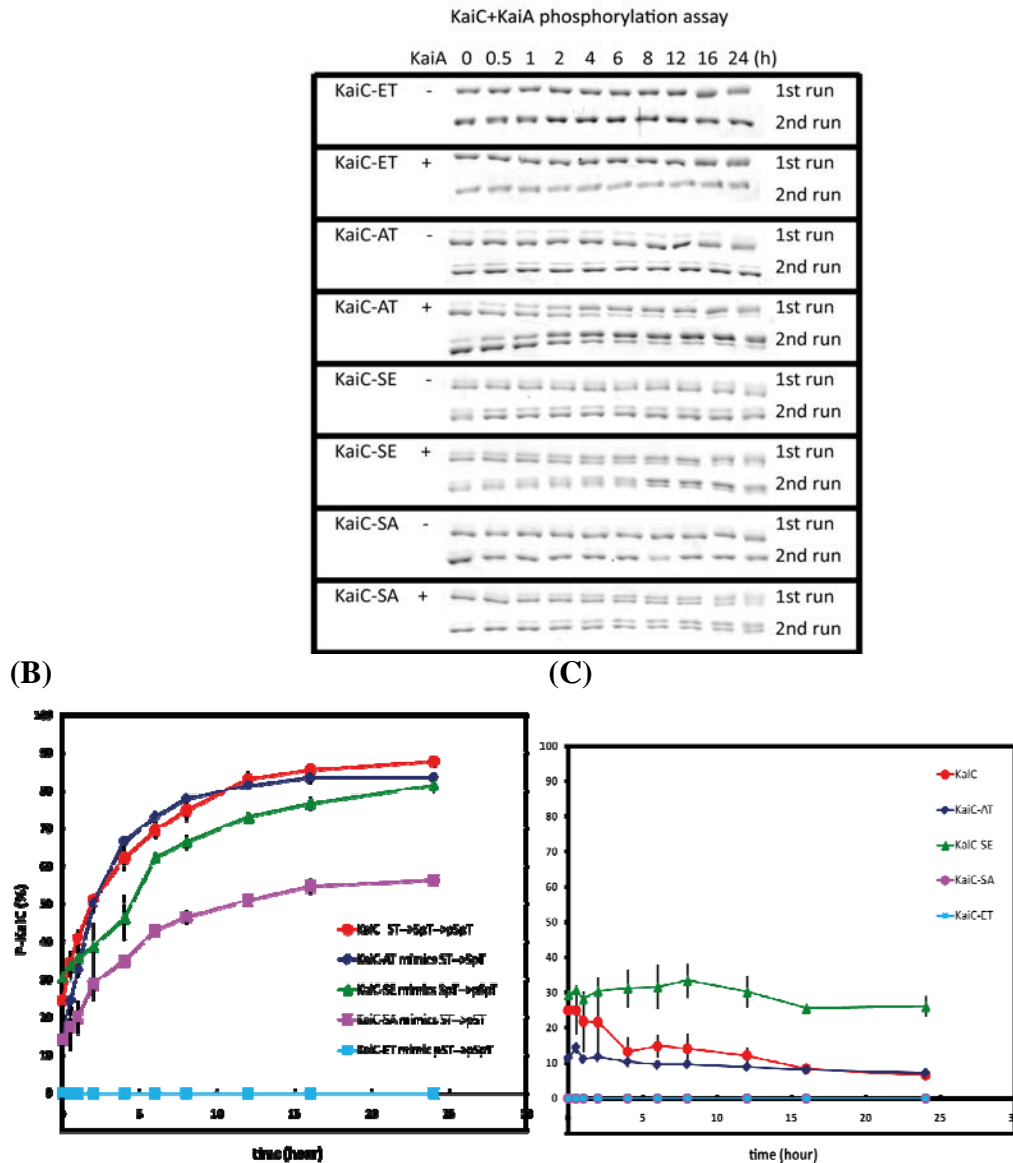


Figure 20 Phosphorylation profiles of KaiC phosphomimics. (A) SDS-PAGE gel showing phosphorylation kinetics of KaiC, KaiC-AT, KaiC-SE, KaiC-SA, and KaiC-ET in the presence or absence of KaiA. (B) Gel densitometry analysis of KaiC in the presence of KaiA. (C) Gel densitometry analysis of KaiC in the absence of KaiA. See Materials and Methods for experimental conditions.

with the A-loops + tail peptides of KaiC (KaiC^{AL+tail}) (90). *S. elongatus* KaiA binding affinity to KaiC^{AL+tail} is 170 μ M (86). The difference in binding affinities between

hexameric and monomeric KaiC variants is probably from differences in the local concentrations of available A-loops. The distribution of A-loops from monomeric KaiC is similar to the distribution of KaiC^{AL+tail} in solution. Thus, the results suggest that KaiA binds to KaiC regardless of flexibility of the CII ring, but the binding affinity is different regarding to oligomeric state of KaiC. Indeed, KaiA has been found to bind to KaiC during the whole phosphorylation cycle (66, 70). The fact that Hayashi et al. (82) showed that KaiA enhances CII phosphorylation about 5% compared with full-length KaiC is probably due to the hexamerization of CII is only 14% based on our observation. Overall, these results indicate that KaiA binding to KaiC is not regulated by the flexibility of the CII ring but hexamerization of KaiC is necessary for the KaiA-induced KaiC phosphorylation.

Dynamics determine the sequential order of phosphorylation. The fact that the CII ring is flexible during the Phosphorylation Phase prompted us to test if CII ring flexibility and rigidity determines the phosphorylation order of Ser431 and Thr432: ST→SpT→pSpT. To understand the role of dynamics in sequential phosphorylation, we prepared KaiC, KaiC-SE, KaiC-SA, KaiC-AT, and KaiC-ET and compared their phosphorylation levels in the presence and absence of KaiA (Fig. 20). All the KaiC variants had been preincubated at 30°C for 16h in order to reach a hypophosphorylated state. The concentration of KaiC variants, KaiA, and ATP were 3.5 μM, 1.2 μM, and 1 mM, respectively. The reactions were prepared in two groups: one is with KaiA and the other is without KaiA. All reactions were incubated at 30°C for another 24h after a 16h preincubation. The aliquots were collected following the time course shown in the Fig.20. In the presence of KaiA, wt-KaiC, KaiC-AT, KaiC-SE, and KaiC-SA gets to 88%, 84%, 81%, and 56% phosphorylation level, respectively. The high phosphorylation levels of KaiC-SE and KaiC-AT indicate that T432 tends to get phosphorylation and its phosphorylation can promote phosphorylation of S431. In contrast, KaiC-SA gets phosphorylation only to 56% in the presence of KaiA. This phenomenon can be explained by the flexibility of the CII ring. The flexibility of the CII ring enhances phosphorylation, whereas the rigidity induced by phospho-S431 promotes

dephosphorylation. In KaiC-SA, phospho-S431 induces rigidity, which inhibits further phosphorylation and results in only 56% pST. In KaiC-ET, no phosphorylation occurred in the presence of KaiA, suggesting that the rigidity induced by phospho-S431 inhibits phosphorylation at T432. On the other hand, in the absence of KaiA, wt-KaiC, KaiC-AT, KaiC-SE, and KaiC-SA all show no phosphorylation increments. It indicates that phospho-T432 is able to sustain the flexibility of the CII ring but the overall flexibility is not enough for KaiC-SE to phosphorylate spontaneously which strongly underlies the importance of KaiA. Although we do not have methyl-TROSY data for KaiC-AT, we believe that KaiC-AT exhibits a flexibility of the CII ring similar to those of hypophosphorylated wt-KaiC, KaiC-SE, and KaiC-AE. Overall, the data strongly suggests that T432 necessarily phosphorylates first so that the CII ring remains flexible enough for A-loop exposure during progressive autophosphorylation of S431 residues and results in the sequential order as ST \rightarrow SpT \rightarrow pSpT.

2.4 Discussion

Exposed A-loops and phospho-T432 are important for the KaiC Phosphorylation Phase. KaiA binds to KaiC on the A-loops to stimulate phosphorylation of KaiC at S431 and T432 (85) (59). Even though no exposed A-loops in full-length KaiC structures have been reported, the hypothesis that A-loop exposure enhances KaiC phosphorylation has been supported by KaiC A-loop truncation experiments (86). KaiC497, which the tail is removed and mimics the buried A-loop state, and KaiC487, which the A-loops and tails are removed, both do not bind to KaiA but stay in the hypophosphorylated state and hyperphosphorylated state, respectively (86). The conclusion that A-loop position affects phosphorylation level is further supported by the phosphorylated level of different length truncations of the A-loops: KaiC496, KaiC495, and KaiC494 show increased phosphorylation levels compared with KaiC497 (86). Nonetheless, overlay of A-loops in the X-ray crystal structures of several different phosphomimics of KaiC are virtually identical at the quaternary level (89). The only phosphorylation-dependent structural

differences on overall KaiC structure are localized around the sites of phosphorylation, which are buried deep in the crevasses between domains of the CII ring.

We have proposed that the A-loops of KaiC exist in equilibrium between exposed and buried states and KaiA stabilizes the exposed state to induce phosphorylation of KaiC (86). Previously, our group showed that KaiC-DT is hypophosphorylated but KaiC-DT487 (A-loops removed) is constitutively hyperphosphorylated, which suggests that A-loops are dominantly buried during the Dephosphorylation Phase. Although all the observations support our proposal, the mechanism by which the state of A-loops is regulated was not clear. Our study here strongly suggests that the flexibility of the CII ring is the key to regulate A-loops position. To prove the exposed state is dictated by the flexibility of the CII ring, we needed to rule out the possibility that the exposed state of A-loops might be pulled out by KaiA. The possibility is not likely because of two points: first, KaiA:KaiC complex has been found existing over the whole phosphorylation cycle (69, 70); second, we did not observe the increasing phosphorylation of KaiC-ET in the presence of KaiA (Fig. 20). If A-loops were pulled out every time when bound to KaiA, we should see the increasing phosphorylation level when KaiC-ET is mixed with KaiA. In fact, KaiA binds to hexameric CII-ET (Fig. 19) which could support KaiA binds to KaiC-ET but no phosphorylation occurs on KaiC-ET (Fig. 20). It indicates that KaiA does not pull out the A-loops of KaiC. Therefore, more likely, KaiA functions as stabilizing the exposed A-loops, and the exposed or buried state is controlled by KaiC itself. Then, the next question would be how KaiC regulates A-loop position. Removal of A-loops from KaiC, like KaiC487 and KaiC-DT487, always increases phosphorylation level; it indicates that the exposed A-loops are favored in phosphorylating KaiC. Therefore, the exposed A-loops are favored in the Phosphorylation Phase and disfavored in the Dephosphorylation Phase. If so, it is rational to speculate that A-loop position is under control by KaiC phosphorylation. However, only subtle structural differences are observed between different phosphorylation states of KaiC, and thus they cannot explain why A-loops prefer the exposed state in the Phosphorylation Phase. Nonetheless, our data clearly shows that the

phosphorylation state of KaiC regulates the CII ring flexibility and, in turn, the flexibility of the CII ring controls A-loop position. Our data reveal that phospho-T432 and phospho-S431 have opposite effects on dynamics that could separate the phosphorylation cycle into two dynamic phases, and A-loop position is regulated by the flexibility of the CII ring.

The NMR data show that phospho-T432 does not reduce the flexibility of the CII ring and the exposed A-loops enhance the flexibility of the CII ring as well. Even KaiC and KaiC-SE exhibit flexibility, but the additional flexibility from KaiA from stabilizing the exposed position of the A-loops is necessary for KaiC $ST \rightarrow SpT \rightarrow pSpT$ phosphorylation and KaiC-SE \rightarrow KaiC-pSE. The results indicate both the exposed A-loops and phospho-T432 are important for KaiC phosphorylation. The model of KaiC phosphorylation in the Phosphorylated Phase is proposed as three steps. First, the flexible CII ring of hypophosphorylated KaiC allows A-loops exposure; the additional flexibility from the exposed A-loops stabilized by KaiA enhances KaiC phosphorylation in the order $ST \rightarrow SpT$. Second, phospho-T432 sustains the flexibility of CII ring, and with the additional flexibility from the exposed A-loops stabilized by KaiA, enhances KaiC phosphorylation in the order $SpT \rightarrow pSpT$. Last, KaiC-pSpT transitions KaiC into the Dephosphorylation Phase. During this Transition Phase, KaiB recognizes the rigid KaiC in the hyperphosphorylated state and binds to it in preparation for the Dephosphorylation Phase. The Transition Phase and the Dephosphorylation Phase will be discussed in CHAPTER III and IV.

Hexamerization caused by phosphorylation. KaiC functions as a hexamer induced by ATP (80). The double doughnut-like rings, CI and CII, share a very similar structure (73) and contain ATPase motifs, including Walker motifs A and B, and a pair of deduced catalytic carboxylate Glu residues (named CatEs) (80). The CI ring has a higher ATP binding affinity than the CII ring and is responsible for the hexamerization, whereas the CII ring is responsible for phosphorylation and stability. Although the CII domains has contribute to hexamerization (80), this is the first report showing that CII phosphorylation correlates to hexamerization of the CII ring in a stepwise mannered

with ATP (Fig. 17A). Previously, mutations at the Walker A motifs of both domains severely suppresses the hexamerization of KaiC, much more so than a mutation only at the CI walker A motif (80). Thus, they concluded that the CII ring also contributes to the hexamerization of KaiC. In addition, our data suggest that full-length KaiC phosphomimics do not inhibit the hexamerization. Therefore, the hexamerization ability of CII phosphomimics shown here not only determines the dynamic difference of the CII ring but also the importance of phosphorylation on hexamerization.

Coupling of the A-loops to the phosphorylation sites. When KaiA stabilizes the exposed A-loops, the A-loops are not fully exposed. In contrast, KaiC487 is constitutively 100% phosphorylated (86). The hyperphosphorylated state of wt-KaiC is more similar to the phosphorylation level of KaiC494 and KaiC 496 (86). Both these two KaiC mutants mimic a partial A-loop exposed state. Clearly, A-loop position is coupled

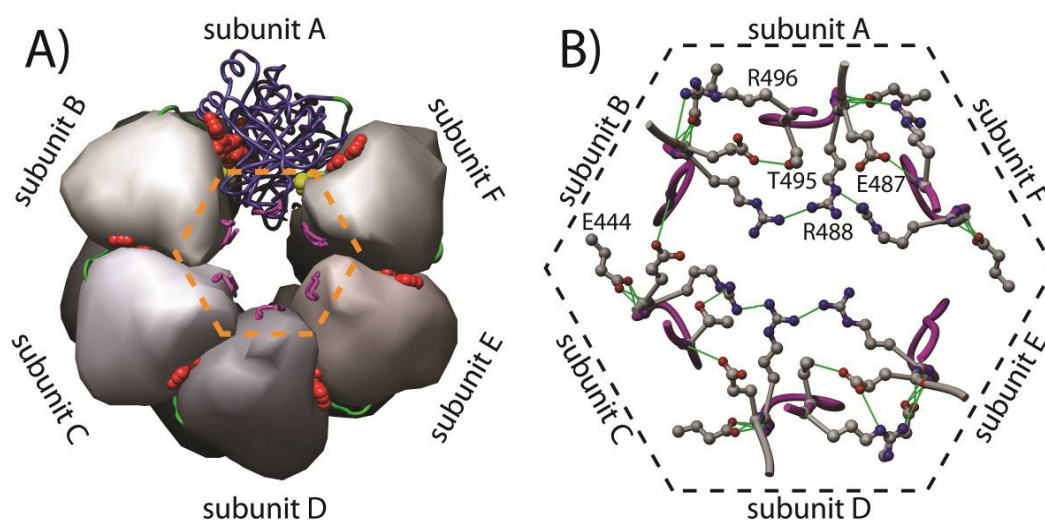


Figure 21 Inter-A-loop hydrogen bonds. Top-down view of KaiC. A) ATPs are red, S431 and T432 are yellow, A-loops are magenta, and the peptide linker between the CI and CII domains is green. Five subunits are shown as surfaces and one subunit is shown as a blue ribbon. B) Expansion of the A-loop region. Putative intersubunit hydrogen bonds involving A-loop residues are shown as green lines. A-loop exposure is expected to disrupt this ring of hydrogen bonds, increasing the dynamics of the CII ring. According to our model, the ATP molecules bound at the interfaces of the CII domains would then be allowed to approach S431 and T432.

to the phosphorylation sites. The distances between the γ P of ATP and the hydroxyls of S431 and T432 are ≥ 1.6 Å beyond the minimal distance for phosphoryl transfer (Fig. 11) (84). Our results support the notion that exposed A-loops affect the flexibility of KaiC by disrupting a hydrogen bond network between CII ring subunits (Fig. 21); leading to disrupted interactions at the phosphorylation sites (Fig. 22). The disruption of interactions at the phosphorylation sites brings ATP, T432, and S431 close for phosphorylation. In the KaiC structure (Fig. 21B), the side-chain of the residues E487 and T495 appears to hydrogen-bonded to each other. The side-chain of the residue R488 also forms a hydrogen bond with the side-chain of R488 from the adjacent subunit, creating a ring of hydrogen bonds. It suggests that hydrogen-bond formation stabilizes the buried position of the A-loops. Indeed, the E487A and T495A substitution resulted in $\sim 100\%$ and 80% phosphorylation of KaiC, respectively (86). In addition, A-loop exposure apparently disrupts interactions at the phosphorylation sites. There are at least three possibilities for how KaiA displacement of the A-loops increases the local flexibility of ATP, S431, and T432 (Fig. 22). A) A-loops exposure could disrupt interactions between D474' and ATP, allowing ATP to move toward S431 and T432. B) Disruption of interactions between the A-loop and E444' is expected to increase the flexibility of P-loop residues (e.g., the highly conserved K294'), which could increase the mobility of the ATP molecule. Indeed, our lab has previously shown that the E444A mutation results in a constitutively hyperphosphorylated KaiC variant (86). C) Others have shown that a G421R substitution lengthens the period to 44 h (73), and the structure of KaiC predicts that G421R disrupts a backbone-backbone hydrogen bond with S491 of the A-loop. Disruption of this hydrogen bond by A-loops exposure is expected to increase the dynamics of S431 and T432, thereby promoting their stochastic approach to the bound ATP molecule. The phosphorylation state of the G421R variant is not known, presently, but our model predicts that it is hyperphosphorylated. Thus, the exposed A-loops likely increase KaiC CII ring flexibility by disruption several interactions between buried A-loops and phosphorylation sites. The disruption of the interactions changes the flexibility of KaiC CII ring to induce autophosphorylation.

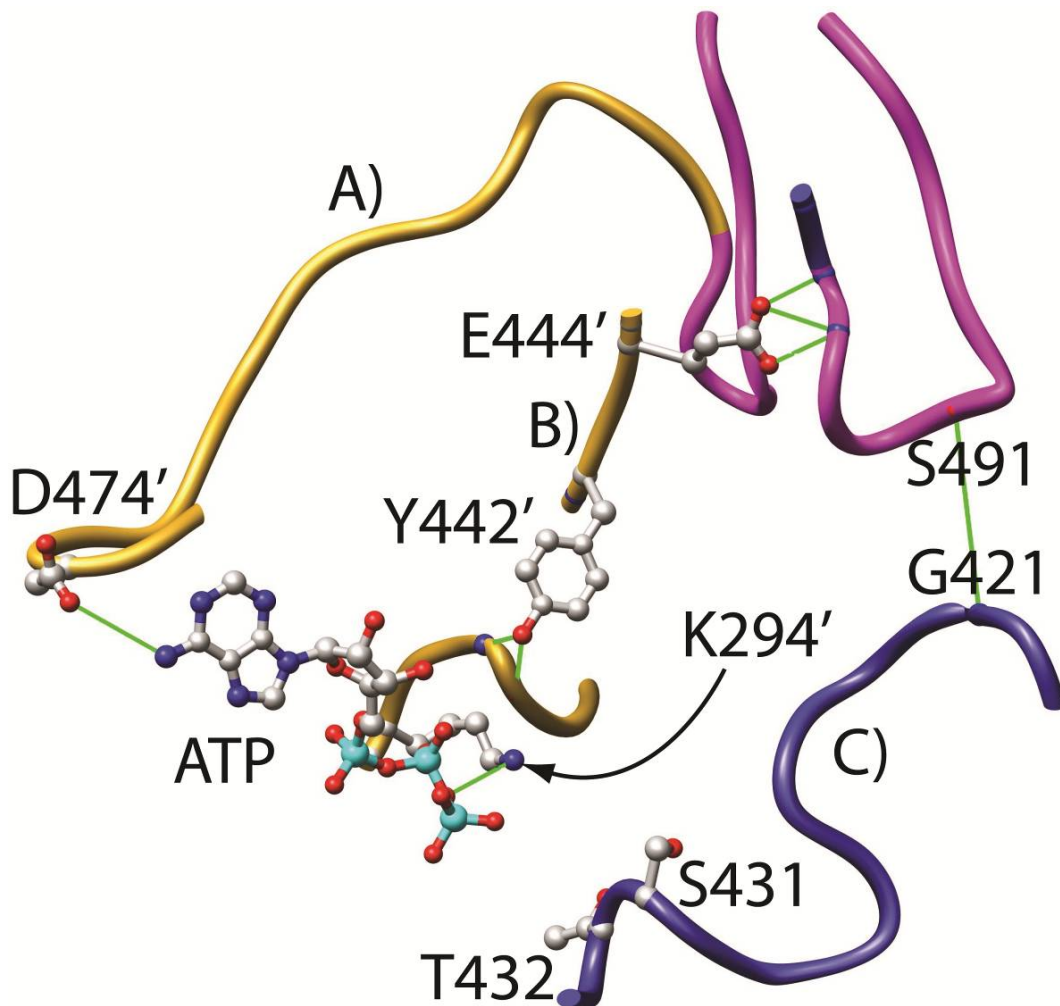


Figure 22 Interactions possibly disrupted by A-loop exposure. Three of the possible ways the KaiA-binding site (A-loop, magenta) and the phosphorylation sites, S431 and T432, of KaiC are coupled. The blue and gold colors are used to indicate different subunits of KaiC. The green lines indicate the locations of putative hydrogen bonds. K294 locates in the P-loop which is responsible for the nucleotide binding.

KaiC dynamics determines the autokinase and autophosphatase activities. KaiC is both an autokinase (61) and an autophosphatase (54). The equilibrium of these two activities is modulated by its phosphorylation, which is regulated by KaiA and KaiB (65, 66). Previously, the A-loops have been suggested to be the switch of autokinase and autophosphatase activities of KaiC depending on their position (exposed or buried). However, we found that the flexibility of the CII ring is the switch of autokinase and

autophosphatase activities. The A-loop position is epistatic to KaiC phosphorylation state in the control of the flexibility of the CII ring. In the Phosphorylation Phase, KaiA stabilizes the exposed A-loops which enhances autokinase activity. However, when KaiC reaches the hyperphosphorylated state, KaiC becomes rigid, resulting in A-loops burial, which inhibits autokinase activity. Once S431 becomes phosphorylated, the A-loops favor the buried state, reducing CII ring flexibility. The autophosphatase activity becomes dominant and KaiC dephosphorylates. Overall, therefore, the autokinase activity is dominant when KaiC is flexible and the autophosphatase activity is dominant when KaiC is rigid. It is clear that the autokinase and autophosphatase activity must be regulated by the flexibility of the CII ring. KaiC is also an ATPase (80). This dynamic state of the CII ring also regulates its ATPase activity. Importantly, the ATPase activity has been linked to the output pathway (51) and this part will be discussed in more detail in CHAPTER IV.

CHAPTER III

MECHANISM OF THE TRANSITION PHASE

3.1 Introduction

All circadian oscillator systems, including those of humans, can be described as a succession of phases (Fig. 23). Therefore, understanding oscillator mechanism amounts to understanding the transitions between phases. In the case of the KaiABC oscillator, The Transition Phase is marked by the formation of the KaiB:KaiC complex, as a result of phosphorylation at residue S431(65, 66). Yet, the transition mechanism is not known. Although there are low resolution electron microscopy (EM) models of this complex (87), they do not inform on why KaiB binds to KaiC only upon S431 phosphorylation. The EM data shows that KaiC, in a hyperphosphorylated state, forms a complex with KaiB or both KaiA and KaiB (87). KaiB forms a complex on the top of KaiC CII ring (Fig. 24). However, KaiC structures in different states of phosphorylation, including

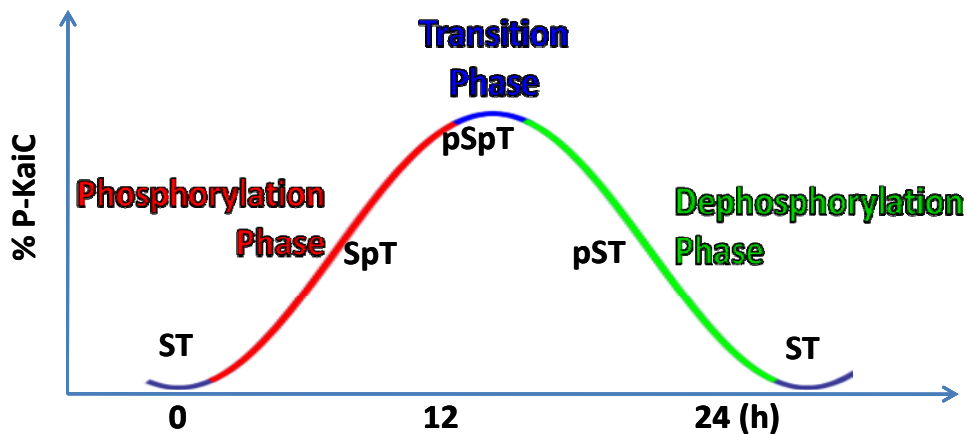


Figure 23 KaiC phosphorylation order diagram. In our model, the Phosphorylation Phase is indicated as red part, the Transition Phase showed as blue and the Dephosphorylation Phase is green and, then, the whole cycle start anew.

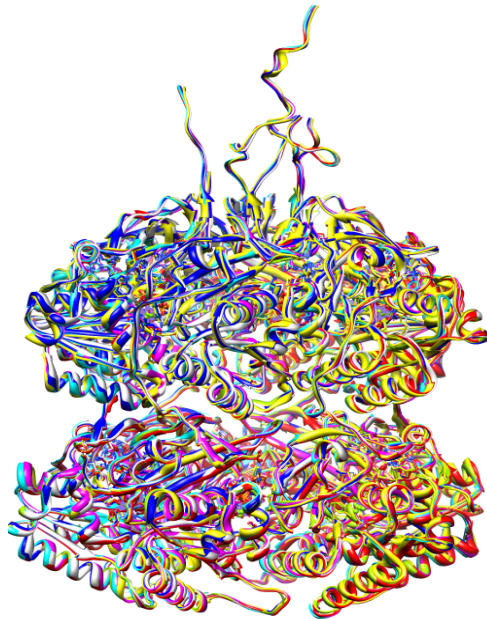


Figure 24 Overlay of seven crystal structures of KaiC phosphoforms. (PDB ID: 3K0A, 3K0C, 3DVL, 3K0E, 3JZM, 3K0F, and 3K09) (89).

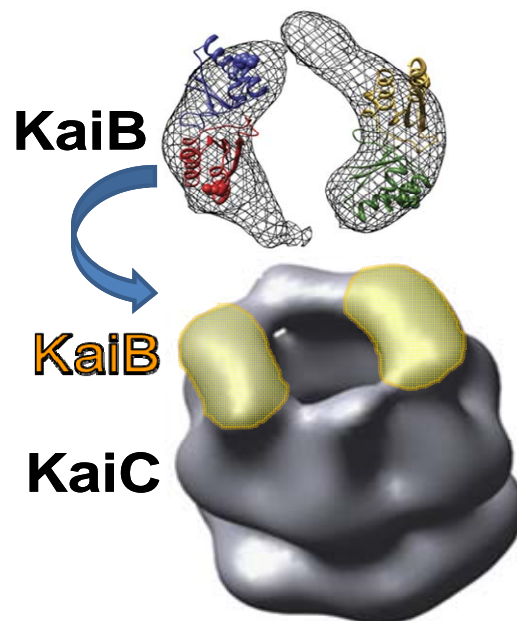


Figure 25 Negative-stain EM structures of KaiB and KaiC complex. (top) Two KaiB dimers (residues 8-94) from the X-ray crystal structure of *ThKaiB* are shown within the third layer of density of the KaiBC structure from (bottom). (bottom) Three-dimensional reconstruction of the KaiBC complex based on 7415 particle images processed without imposed symmetry (87).

those do and do not bind KaiB, are virtually identical (Fig. 25) (89). Furthermore, it is unknown how the KaiB:KaiC interaction during this phase creates a new site to which KaiA will bind in the next phase (90). Thus, my goal here is to elucidate the Transition Phase, which is marked by the formation of a stable KaiB:KaiC complex. Based on the observations that CII ring flexibility is reduced when S431 becomes phosphorylated, we propose that the flexibility of the CII ring plays a central role in the KaiB:KaiC complex formation. There are several protein systems in which protein dynamics has been demonstrated to play a key role in allosteric regulation of protein function (108, 132, 133). For example, cAMP activation of a catabolite activator protein (CAP) mutant for DNA binding is through dynamic allostery. In this CAP mutant, cAMP fails to switch the DNA binding domains to the active conformation, as happens with wt-CAP, but activates the mutant to bind DNA with high affinity and specificity through a large concomitant increase in protein dynamics (i.e., entropy) (132). This example inspired us to think that the formation of the KaiB:KaiC complex might be very similar. One mutation in CAP regulates DNA binding by changing the dynamic states of CAP without inducing structural changes. According to our notion, phospho-S431 may enhance KaiB binding to KaiC by changing the dynamic state of KaiC instead of inducing structural changes. This idea, if true, would explain why X-ray crystal structures of different phosphorylated KaiC proteins are virtually identical. Our hypothesis is that the rigid state of KaiC as induced by phospho-S431 induces KaiB to form a stable complex with it as a dimer, thereby exposing a surface of KaiB previously hidden in its tetrameric state.

To test this hypothesis, first we used gel filtration chromatography to verify the binding between KaiB and the different phosphomimics of KaiC, which are KaiC-ST, KaiC-SE, KaiC-EE, and KaiC-ET. We found KaiB binds to KaiC-EE and KaiC-ET and this is consistent with previous observations (69, 70) that KaiB binds to KaiC in the Dephosphorylation Phase in which KaiC are mostly in the pSpT and pST states. In addition, we have known from CHAPTER I that CI ring provides the hexamerization ability to CII ring formation, therefore, we are interested in if the CII ring could provide

enough rigidity for itself on the binding with KaiB, thus, we prepared wt-CII, CII-SE, CII-EE, and CII-ET and, then, mixed with KaiB to test the binding. Moreover, we want to test if KaiB change its structure upon binding to KaiC since it has been suggested to bind to KaiC in a dimeric form different from its free tetrameric form (87). Thus, we prepared U- ^{15}N , ^2H , ^{12}C],Ile- $[\delta 1 \text{ }^{13}\text{CH}_3]$ -labeled KaiB and U- ^{15}N , ^2H , ^{12}C],Ile- $[\delta 1 \text{ }^{13}\text{CH}_3]$ -labeled KaiC-EE and titrated them with unlabeled KaiC-EE and KaiB, respectively. Methyl-TROSY spectra showed that the formation of the KaiB:KaiC complex depends on sufficiently reduced the flexibility of the CII ring resulting from phosphorylation at residue S431. Nonetheless, KaiB does not form a complex with isolated CII-EE hexamers or CII-ET hexamers. It suggests that the CII ring by itself may not provide enough rigidity for KaiB recognition and, additionally, KaiB recognizes the rigidity of KaiC rather than phospho-S431. The NMR results revealed that KaiB undergoes a large conformation change upon KaiC binding, whereas the structure of KaiC does not change upon KaiB binding.

3.2 Materials and Methods²

T. elongatus KaiB, KaiC and KaiC mutants expression and purification. The genes encoding KaiB and KaiC from *T. elongatus* were cloned into the pET28a+ vector (Novagen) between the NdeI and HindIII sites. The resulting plasmids were used to transform *Escherichia coli* BL21(DE3), and the sequences were confirmed (DNA Sequencing Facility, University of California, Berkeley). Transformed *E. coli* cultures were incubated at 37°C until OD₆₀₀ reached about 0.6; at this point, a final concentration of 200 μM isopropyl β-D-thiogalactopyranoside (Research Product International) was added for overexpression. Cells were harvested after 12 h overexpression at 25°C, and pellets were resuspended in 20 mM Tris-NaOH, 500 mM NaCl, pH 7.0. Cell suspensions were passed twice through a chilled French press cell, and lysates were clarified by

² Supplementary information of materials and methods are in the Appendixes A-F.

centrifugation at 20,000 x g for 60 min at 4°C. Tagged proteins were isolated on a Ni-charged column. Proteins were buffer exchanged to 20 M Tris Base, 500 mM NaCl and 20 mM Imidazole and 100 µl 100 µM ULP1 protease were added for SUMO-His₆ tag removal. The cleavage reaction was carried out at 4°C for 16 h in 15 mL volume. Kai proteins were separated from SUMO-His₆ tag protein by a second Ni-charged column and followed by gel filtration chromatography on a Superdex 200 HiLoad 16/60 prep grade column (GE Healthcare) for KaiC and a Superdex 75 HiLoad 16/60 prep grade column (GE Healthcare) for KaiC-CII variants and KaiB. Buffers were exchanged to 20 mM Tris Base, 50 mM NaCl, 1 mM MgCl₂, 5 mM DTT, 1 mM ATP, pH 7.0 for the binding assay and NMR experiments. Proteins were concentrated by Amicon Stirred Ultrafiltration Cell (MILLIPORE) and stored in a -80°C freezer. KaiA, KaiB, and KaiC did not lose function after repeated cycles of freezing and thawing. One liter LB yields ~ 1728 nmol of KaiB, and ~ 240 nmol of KaiC and KaiC mutants. Coomassie Plus (Pierce) was used as a Bradford Assay reagent for protein concentration determination. For purification of KaiC, all the solutions were prepared with 1 mM ATP.

U-[¹⁵N, ²H], Ileδ1-[¹³C,¹H]-labeled proteins (KaiB and KaiC-EE) expression and purification. Expression: Follow protocol A-10. Purification: Follow protocol A-11. Note that BioExpress (Cambridge Isotope Laboratories) was used to increase the growth rate of *E. coli*.

ULP1 protease expression and purification. Expression: Follow protocol A-8. Purification: Follow protocol A-12 but stops after the elution step of 1st Ni-NTA column. Note that Ulp1 is not stable in buffers where NaCl is at a concentration lower than 100 mM. For long-term storage, add equal volume of glycerol into the Ulp1 elution sample from Ni-NTA column and store at -80°C. Ulp1 elution sample can be diluted to a final concentration of 200 µM before adding glycerol. Therefore, the final Ulp1 stock (stored

at -80°C) will be 100 μ M in the buffer of 25 mM NaH₂PO₄, 250 mM NaCl, 125 mM imidazole, 50% glycerol, pH 8.0.

Binding Assay. All column binding assays including KaiC-CII alone experiments were carried out using a Superdex 200 10/300 GL gel filtration column (GE Healthcare). Ferritin (440 kDa), albumin (67 kDa), ovalbumin (43 kDa), and chymotrypsinogen A (25 kDa) were used as molecular mass standards.

KaiC and KaiB binding. Recombinant KaiC and KaiB were mixed in 1:1 ratio (10 μ M: 10 μ M) in 300 μ l binding buffer (20 mM Tris, 50 mM NaCl, 1 mM MgCl₂, 5 mM DTT, 1 mM ATP, pH 7.0) at 25°C for 17 h.

KaiC-CII variants and KaiB binding. Recombinant KaiC-CII variants and KaiB were mixed in 1:1 ratio (10 μ M: 10 μ M) in 100 μ l binding buffer (20 mM Tris, 50 mM NaCl, 1 mM MgCl₂, 5 mM DTT, 1 mM ATP, pH 7.0) at 25°C for 17 h.

Kinetics of KaiC-EE vs KaiC-ET. Recombinant KaiC and KaiB were mixed in 1:3 ratio (10 μ M: 30 μ M) in 100 μ l binding buffer (20 mM Tris, 50 mM NaCl, 1 mM MgCl₂, 5 mM DTT, 1 mM ATP, pH 7.0) at 25°C.

NMR Sample Preparation and Spectroscopy. NMR sample preparation: Follow protocol C-1. NMR sample information: Please see Table 2. NMR spectroscopy: Follow Protocol C-2.

3.3 Results

KaiB recognizes the rigid state of phospho-S431-KaiC. KaiB antagonizes KaiA stimulation of KaiC phosphorylation but only after KaiC reaches a hyperphosphorylated state (63) (140). KaiB forms a complex with hyperphosphorylated KaiC, marking the transition from the Phosphorylation to Dephosphorylation Phase. We have shown that KaiC exhibits two major dynamic states, depending on its state of phosphorylation. To test if these dynamic features are the key to induce KaiB recognition on KaiC, we prepared KaiC, KaiC-SE, KaiC-EE, and KaiC-ET and mixed them with KaiB in a 1:1 monomeric ratio. The concentrations of KaiC variants and KaiB were 10 μ M each in

Table 2 NMR Sample Condition and Experiment for CHAPTER III

Sample	Experiment	Sample detail	Experiment detail
KaiB			
U-[¹⁵ N, ² H]-Ile δ 1-[¹³ C, ¹ H]-AMA-KaiB	Methyl-TROSY	Concentration: 20 μ M Buffer: 20 mM Tris, 50 mM NaCl, 1 mM MgCl ₂ , 5 mM DTT, 1 mM ATP, pH 7.0, 10 μ M DSS, 0.02% NaN ₃ , 99.96% D ₂ O Volume: ~300 μ l Tube: shaped tube	NS=20 40 °C
KaiC			
U-[¹⁵ N, ² H]-Ile δ 1-[¹³ C, ¹ H]-FLAG-KaiC-EE	Methyl-TROSY	Concentration: 16 μ M Buffer: 20 mM Tris, 50 mM NaCl, 1 mM MgCl ₂ , 5 mM DTT, 1 mM ATP, pH 7.0, 10 μ M DSS, 0.02% NaN ₃ , 99.96% D ₂ O Volume: ~300 μ l Tube: shaped tube	NS=128 40 °C

300 μ l. The reactions were incubated at 25°C for 17h. The final reactions were analyzed by Superdex 200 10/300 GL gel filtration chromatography, with a flow rate of 0.8 mL/min. As shown in CHAPTER I, the CII ring of KaiC is flexible during the Phosphorylation Phase and rigid during the Dephosphorylation Phase. We found that KaiB binds to KaiC-EE and KaiC-ET, which are representative of KaiC in the Dephosphorylation Phase, but not KaiC-ST and KaiC-SE (Fig. 26). The data are consistent with earlier observations that the KaiB:KaiC complex is found during the Dephosphorylation Phase but not the Phosphorylation Phase (69, 70). To test whether KaiB recognizes the rigidity of KaiC or phospho-S431 directly, we prepared KaiC-EE487, which has been shown to be flexible, and, mixed it with KaiB in 1:1 monomeric reaction at a concentration of 10 μ M in 300 μ l at 25°C for 17h with 1 mM ATP. The final reactions were analyzed by Superdex 200 10/300 GL gel filtration column with a flow rate of 0.8 mL/min. We found that KaiB does not bind to KaiC-EE487 (Fig. 26). The result suggests that KaiB recognizes the rigidity of KaiC but not phospho-S431 directly. Indeed, KaiB has been shown to interact with KaiC on the top of the CII ring (70) and not at the phosphorylation site, which is buried inside the interface between two KaiC subunits (60).

Next, we were interested in the binding between KaiB and CII ring variants. KaiC hexamerization depends on ATP (80). The CI domains contributes to the hexamerization of KaiC significantly more than the CII domains (80, 82). The CI ring serve as a platform, whereas the CII ring is the functional center (82). In CHAPTER I, we showed that the CI ring provides hexamerization ability for CII ring formation. Here, we wondered whether the hexamerization scaffold from CI ring contributes to the rigidity of the CII ring. The binding between KaiB and CII variants would inform on the function of CI ring on CII ring rigidity. We purified CII variants without ATP, and, thus, they were in the monomeric form during the purification process. The concentration of KaiB

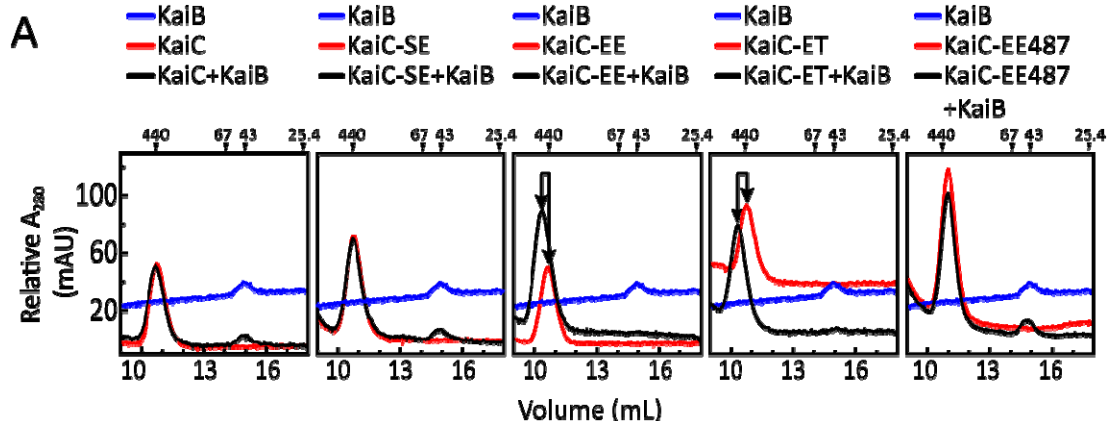


Figure 26 KaiB-KaiC binding experiments. Gel-filtration profiles of mixtures of KaiB with wt-KaiC (panel 1) and with phosphomimics of KaiC-SpT (panel 2), KaiC-pSpT (panel 3), KaiC-pST (panel 4), and KaiC-pSpT487 (panel 5). The elution profiles of KaiB in each panel were from a single run.

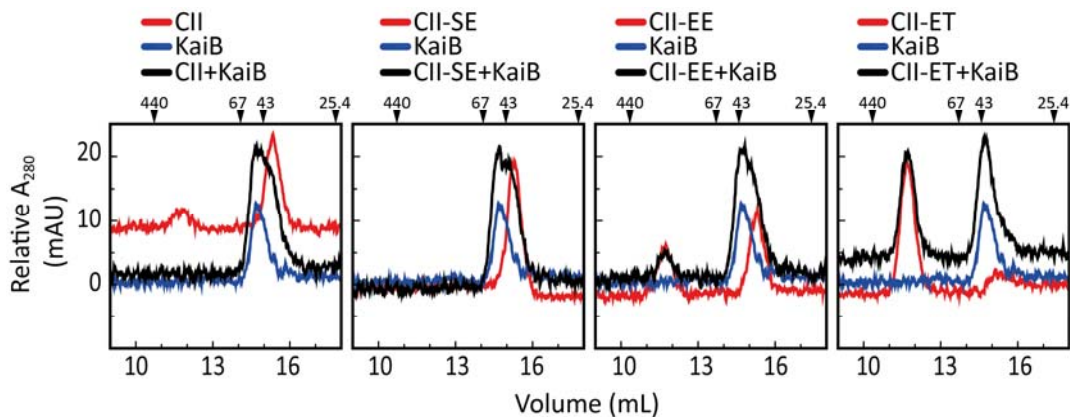


Figure 27 KaiB-CII binding experiments. KaiB and CII variants binding. Gel-filtration profiles of mixtures of KaiA with CII (panel 1) and with phosphomimics of KaiC-SpT (panel 2), KaiC-pSpT (panel 3), and KaiC-pST (panel 4). The elution profiles of KaiB in each panel were from a single run.

and CII variants were mixed in 1:1 monomeric ratio, 10 μ M:10 μ M, in 100 μ l at 25°C for 17h with 1 mM ATP. The reactions were analyzed by a Superdex 200 10/300 GL gel filtration column with a flow rate of 0.8 mL/min. Interestingly, KaiB does not form a

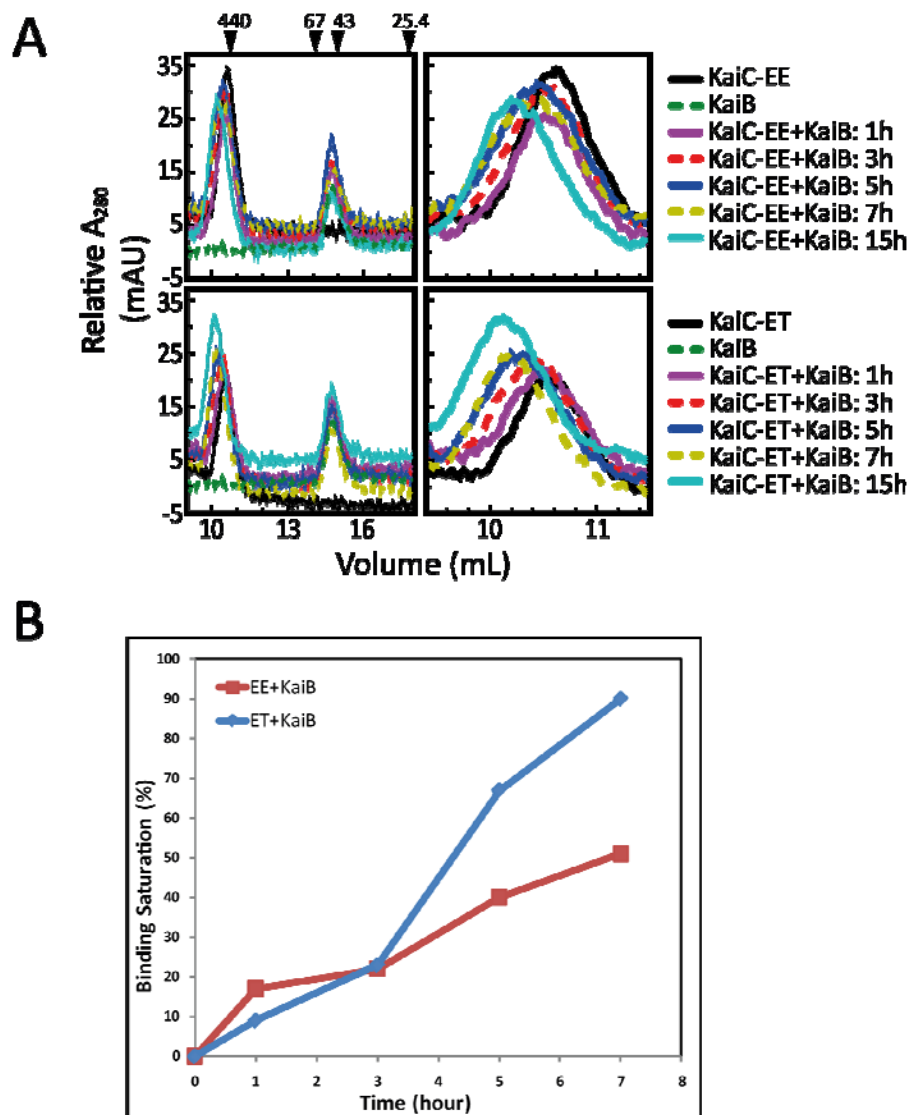


Figure 28 KaiB + KaiC binding kinetics. (A) Time course gel filtration chromatography of KaiB binding to KaiC-EE (first row) and KaiC-ET (bottom row). The chromatograms in the right column are from an expanded region of the chromatograms in the left column. Molecular weight markers in kDa are indicated on top of left panels.

complex with either monomeric wt-CII, CII-SE, CII-EE, and CII-ET or hexameric CII-EE and CII-ET (Fig. 27). The results show that KaiB does not interact with either monomeric CII domains or hexameric CII rings, suggesting that CII ring rigidity induced

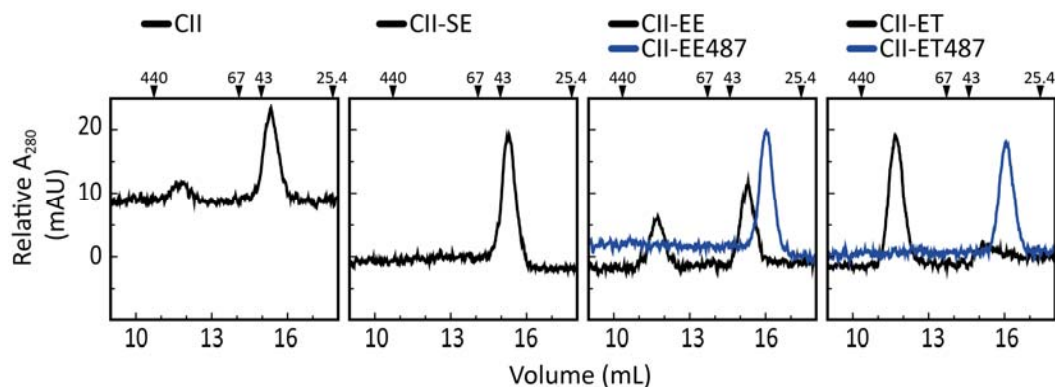


Figure 29 Gel filtration chromatography of CII variants. Hexamerization of CII variants. Gel-filtration profiles of CII (panel 1) and phosphomimics of SpT-KaiC (panel 2), pSpT-KaiC and pSpT-KaiC487 (panel 3), and pST-KaiC and pST-KaiC487 (panel 4). The elution profiles of KaiB in each panel were from a single run.

by phospho-S431 is not sufficient for KaiB recognition, but needs further rigidification provided by the presence of the CI ring.

KaiB binding rate with KaiC mutants. Since we concluded in CHAPTER I that phospho-S431 induces CII ring rigidity and phospho-T432 offsets the rigidity, we were interested whether phospho-T432 decreases the binding kinetics between KaiB and KaiC. We prepared KaiC-EE, and KaiC-ET and mixed them separately with KaiB in 1:1 monomeric ratios. The concentrations of the KaiC variants and KaiB were 10 μ M each in 100 μ l. The reactions were incubated at 25°C and the mixtures were prepared immediately before gel filtration chromatography. We analyzed time points at 0, 1, 3, 5, 7, 15 h. The reactions were analyzed by Superdex 200 10/300 GL gel filtration column with flow rate of 0.8 mL/min at real time. The results show that KaiB binds to KaiC-ET faster than KaiC-EE (Fig. 28), suggesting that the reduced rigidity of KaiC-pSpT relative to KaiC-pST slows the rate of KaiB:KaiC complex formation.

A-loop position affects the rigidity of KaiC. Here, we provide direct evidence that exposed A-loops break the phospho-S431 induced rigidity of the CII ring, corroborating indirect evidence that the rigidity of the CII ring requires that the A-loops are in their buried position. My objective was to elucidate how phosphorylation and A-loop position modulate CII ring flexibility. We compared CII-EE487 and CII-ET487 to CII-EE and

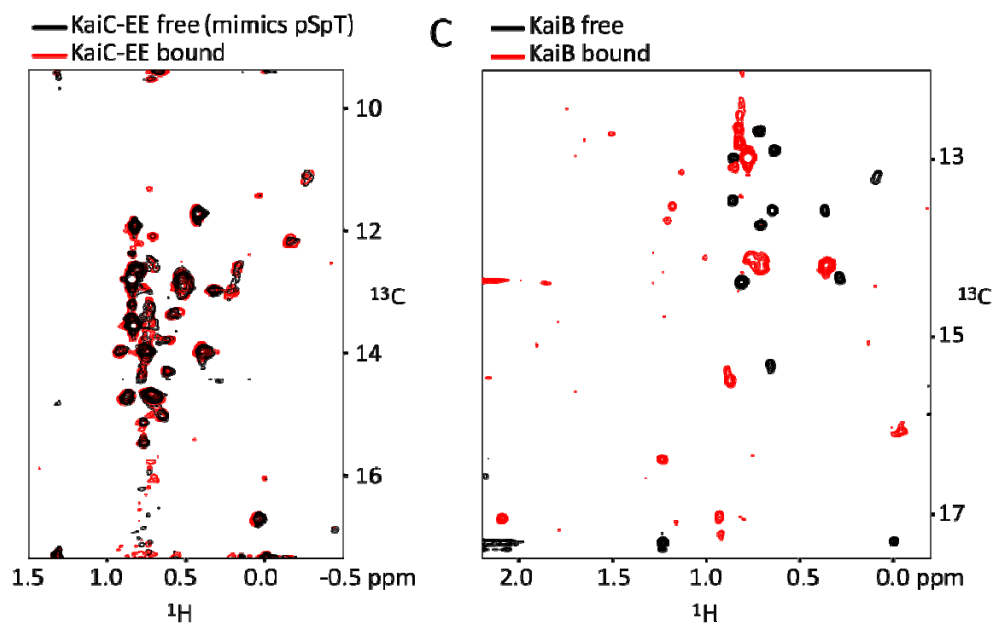


Figure 30 KaiB conformational changes upon KaiC binding. A) Methyl-TROSY spectra of the U-D, Ile- $[\delta 1 \text{ } ^{13}\text{CH}_3]$ labeled KaiC-pSpT phosphomimic free (black contours) and bound (red contours) to unlabeled KaiB. B) Methyl-TROSY spectra of U-D, Ile- $[\delta 1 \text{ } ^{13}\text{CH}_3]$ labeled KaiB free (black contours) and bound (red contours) to the unlabeled KaiC-pSpT phosphomimic.

CII-ET, respectively, by gel filtration chromatography to determine the role of the A-loops CII ring formation. Proteins were purified without ATP, and, therefore, were in the monomeric. We added ATP to a final concentration of 1 mM into the protein samples before storing at -80°C . We prepared CII variants at 10 μM in 100 μl and incubated them 25°C for 30 mins. The reactions were analyzed by a Superdex 200 10/300 GL gel filtration chromatography with a flow rate of 0.8 mL/min. Unlike CII-EE and CII-ET, CII-EE487 and CII-ET487 are 100% monomeric even in the presence of 1 mM ATP (Fig. 29, panel 3 and 4). Phospho-S431 induces the rigidity of CII-EE and CII-ET, as indicated by the hexamerization of CII-EE and CII-ET. However, removal of the A-loops in CII-EE487 and CII-ET487 abolishes the hexamerization. These observations strongly suggest that the A-loops are in their buried position during the Dephosphorylation Phase to preserve CII ring rigidity.

KaiB undergoes a conformational changes upon binding to KaiC. To further understand the interaction between KaiB and KaiC, we made U-[²H,¹⁵N], Ile-[δ1 ¹³CH₃]-labeled KaiC-EE and U-[²H,¹⁵N], Ile-[δ1 ¹³CH₃]-labeled KaiB following the protocols described in the materials and methods section. NMR samples were prepared by mixing either labeled KaiC-EE with unlabeled KaiB or unlabeled KaiC-EE with labeled KaiB at a monomer ratio of 3:2. Unlabeled KaiB and labeled KaiC were mixed in the concentration of 15 μM and 10 μM, respectively. Labeled KaiB and unlabeled KaiC were in 20 μM, and 30 μM, respectively. Both spectra were compared with the free form of U-[²H,¹⁵N], Ile-[δ1 ¹³CH₃]-labeled KaiC-EE and U-[²H,¹⁵N], Ile-[δ1 ¹³CH₃]-labeled KaiB. Methyl-TROSY spectra were obtained at 40°C in a 600 MHz NMR spectrometer with a cryogenically cooled probe-head for 24 h. Fig. 30 shows that KaiB binds to U-[²H,¹⁵N], Ile-[δ1 ¹³CH₃]-labeled EE-KaiC and without inducing chemical shift changes. In contrast, spectra of the free and bound forms of U-[²H,¹⁵N], Ile-[δ1 ¹³CH₃]-labeled KaiB are strikingly different, indicating dramatic conformational changes in KaiB upon binding to KaiC. The number of peaks of KaiB is reduced from 14 to 7. KaiB contains 7 Ile, therefore, the reduced number of peaks suggests that KaiB binds to KaiC as a dimer rather than as the asymmetric KaiB tetramer. Taken together, the results suggest the KaiB undergoes structural changes upon binding, whereas KaiC remains the same. This also suggests that KaiC recruits KaiB through a dynamics-driven mechanism.

3.4 Discussion

Phospho-S431 plays a key role for the Dephosphorylation Phase. Phpho-S431 has been proposed to switch KaiC from an autokinase to an autophosphatase, as well as mediate association among the Kai proteins (65, 69, 70). KaiB specifically recognizes and binds to KaiC when S431 becomes phosphorylated, marking the transition from the Phosphorylation Phase to the Dephosphorylation Phase. KaiB not only forms a complex with KaiC but also recruits KaiA to the KaiB:KaiC complex. The concentrations of

KaiB:KaiC and KaiCB(A) complexes closely follow the abundance of KaiC-pST. Therefore, it has been suggested that phospho-S431 induces a conformational change in KaiC that is recognized by KaiB (65, 69, 70). However, the hypothesis seemingly conflicts with the fact that the phosphoforms of KaiC that do and do not bind KaiB have the same structure. In this study, our data strongly suggest that the selectivity of molecular recognition is based on differences in protein dynamics rather than structures.

KaiB recognizes both KaiC-EE and KaiC-ET but exhibits different binding rates (Fig. 28). The finding that KaiB binds to KaiC-ET faster than KaiC-EE verified our speculation that KaiB's affinity for KaiC depends on the extent of KaiC rigidity. Our model is also supported by the NMR spectra of KaiC-EE and KaiC-ET (Fig. 17). Both spectra indicate greater rigidity relative to KaiC and KaiC-SE, but they also reveal that KaiC-EE is less rigid than KaiC-ET (Fig. 17C). In wild-type KaiABC oscillator reaction, the quantity of KaiB:KaiC complex and KaiCB(A) complex follows a rhythmic abundance of KaiC-pST, even though the accumulation of KaiB:KaiC complex starts earlier than the accumulation KaiCB(A) complex (69, 70). Why does the accumulation of either KaiB:KaiC complex or KaiCB(A) complex not follow the rhythmic abundance of KaiC-pSpT? This question can be answered in two ways: 1) KaiB and KaiC binding is a slow process and, 2) dephosphorylation is a continuous progress. KaiB mainly acts to inhibit KaiA function instead of dephosphorylating KaiC. Indeed, KaiC dephosphorylates. Therefore, while KaiB binds slowly to KaiC-pSpT, dephosphorylation to KaiC-pST is taking place simultaneously. Thus, formation of KaiB:KaiC complexes begins upon appearance of the KaiC-pSpT state. During accumulation of the KaiB:KaiC complex, pSpT-KaiC begins dephosphorylating to KaiC-pST. The KaiB:KaiC complexes recruit KaiA resulting an accumulation of KaiCB(A) complex. When KaiB:KaiC complex binds KaiA, KaiA function is inhibited leading to KaiC dephosphorylation. Once phospho-S431 dephosphorylates, the flexibility of the CII ring increases, causing the KaiCB(A) complex to dissociate, restarting the cycle anew.

The CI ring and buried A-loops contribute to the rigidity of KaiC. In wild-type KaiC, phospho-S431 has been shown to dominate CII ring rigidity (see CHAPTER I).

However, the CI ring and the buried A-loops also affect the rigidity of CII ring (Fig. 27 and 29). Although phospho-S431 induces the hexamerization of the CII ring (Fig. 17A) and the rigidity is not enough for KaiB binding without the CI ring (Fig. 27), and hexamerization of the CII ring is abolished without the buried A-loops (Fig. 29). Even though, in the latter case, full-length KaiC-EE487 is a hexamer, KaiB still does not bind to it (Fig. 26). Therefore, the CI ring and the buried A-loops are both important in regulating the rigidity of the CII ring. Thus, disruption of the CI ring, A-loop exposure, or dephosphorylation at S431 abolishes CII ring rigidity. Since the CI ring affects the rigidity of the CII ring, there is a cross-talk between them. This CII-CI communication may explain why ATPase activity of the CI ring is also affected by the phosphorylation state of the CII ring. Interestingly, a hyperphosphorylated state of KaiC, KaiC489, is able to form a complex with KaiB (90) which is different from our results showing that hyperphosphorylated KaiC487 fails to bind to KaiB. The A-loops + Tail are removed from both mutants except KaiC489 retains the first three residues from the A-loop. The missing A-loop after residue 489 induces KaiC phosphorylation. The difference between KaiB:KaiC487 and KaiB:KaiC489 interactions could be due to the respective absence and presence of residue R488, which forms a ring of hydrogen bonds between adjacent R488 side chains (Fig. 21). We speculate that this ring rigidifies the top of the CII ring enough for KaiB recognition. Notably, KaiB:KaiC489 complex formation was much slower than with KaiC-EE, a hyperphosphorylated KaiC phosphomimic (90). Therefore, a reasonable explanation for the three different binding rates between KaiB and KaiC variants is that the flexibility of CII ring is different in each variant. With the intact full length KaiC, KaiC-EE definitely is more rigid than KaiC489 and KaiC487. In KaiC489, both phospho-S431 and hydrogen bonds network from the remaining A-loop residues provide enough rigidity for KaiB binding. In contrast, KaiC487 has very flexible CII ring, preventing KaiB binding. Overall, the data presented here supports the model that the phosphorylation state of KaiC, A-loop position, and CI-CII communication are key determinants of the flexibility of the CII ring. Moreover, this flexibility dictates rhythmic

associations among the Kai proteins that are critical for the 24h rhythm of the KaiABC oscillator.

CHAPTER IV

MECHANISM OF THE DEPHOSPHORYLATION PHASE

4.1 Introduction

Circadian oscillators can be described as a succession of phases, which must be prohibited from interfering with each other (Fig. 31). The Dephosphorylation Phase occurs by prohibiting KaiA from binding to the A-loops of KaiC, which is critical for KaiC to dephosphorylate (86). Although it is known that KaiB prevents KaiA from stimulating KaiC phosphorylation during this phase (65, 86, 141) and there are low resolution electron microscopy (EM) models of KaiCB(A) complex observed in the Dephosphorylation Phase, the central problem of how it is achieved has not been solved. There are two questions we want to answer in the Dephosphorylation Phase: first, how KaiB interacts with KaiA to inhibit KaiA function; second, what governs the ordered dephosphorylation $pSpT \rightarrow pST \rightarrow ST$. KaiB is a tetramer and KaiA is a dimer (Fig. 32). The weak interaction between KaiA and KaiB is greatly enhanced in the presence of KaiC as studied by yeast two-hybrid system and immunoblotting (142). Indeed, by electron microscopy, KaiA and KaiB were found together only in KaiCB(A) complexes (70). In 2010, the Ishiura group observed direct KaiA and KaiB interactions between MTSSL spin labeled KaiB_{T64C} and KaiA_C (residues 174 to 283) by electron spin resonance (ESR) spectroscopy (143), even though the interaction was too weak for detection by surface plasmon resonance spectroscopy. Thus, in the absence of KaiC, the KaiA-KaiB interaction is very weak. The time constant between MTSL-labeled KaiB_{T64C} and KaiA is 86.2 ± 13.7 (min). ESR experiments suggested that residue T64 of KaiB is located near the KaiA-binding site and one subunit of KaiB_{T64C} binds to one subunit of KaiA_C. However, direct KaiA-KaiB contacts have not been identified, leaving the binding interface poorly delineated (143).

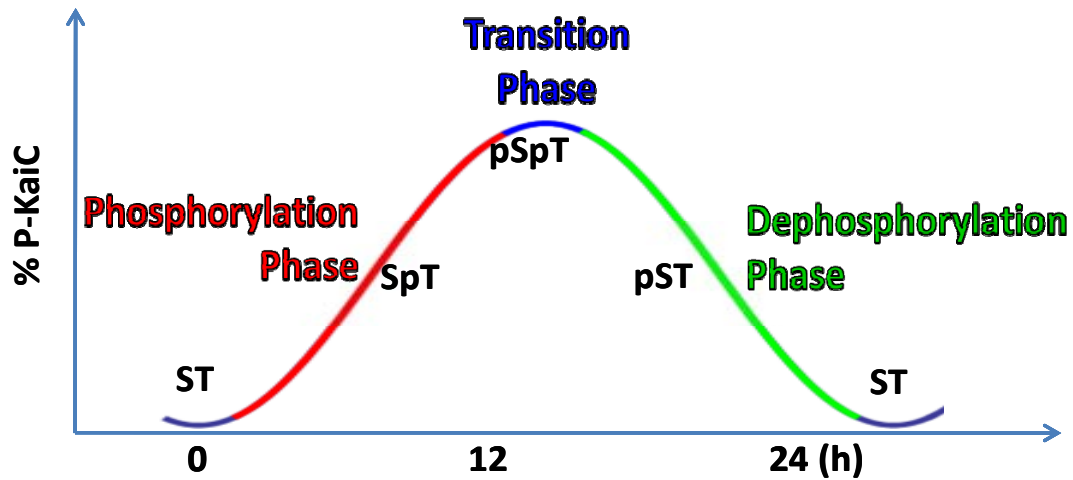


Figure 31 KaiC phosphorylation order diagram. In our model, the Phosphorylation Phase is indicated as red part, the Transition Phase showed as blue and the Dephosphorylation Phase is green and whole cycle start anew.

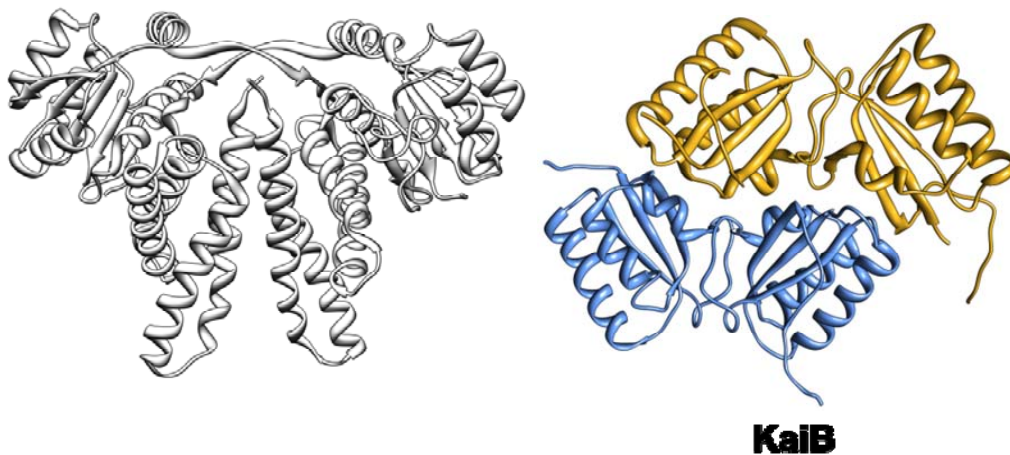


Figure 32 X-ray crystal structure of KaiA and KaiB. (A) X-ray crystal structure of KaiA (71). KaiA showed as a domain-swapped dimer and both subunits are in gray. (B) X-ray crystal structure of KaiB (144). KaiB showed as a tetramer and each color indicates a dimer.

Since KaiC flexibility dictates the ordered pattern of phosphorylation, we also wanted to address whether flexibility also drives the ordered pattern of dephosphorylation, pSpT

→ pST → ST. Therefore, my goal here is to establish the role of dynamics in regulating KaiB-mediated dephosphorylation of KaiC. Success here would also provide insight into how the opposite phases of phosphorylation and dephosphorylation are prevented from interfering each other. KaiA is recruited away from its A-loops binding site on KaiC by KaiB during the Dephosphorylation Phase (90). Without KaiA binding, the A-loops favor their buried position, thereby promoting KaiC dephosphorylation. My hypothesis is that large conformational distortions in KaiB, induced in the KaiCB(A) complex, enhances the interaction between KaiA and KaiB (86). To test this hypothesis, we titrated ¹⁵N-labeled KaiA truncation mutants with KaiB:KaiC-EE497 complex and obtained HSQC spectra. Our results indicated that it is the linker region of KaiA (residues 130 to 180) that binds to the KaiB:KaiC complex during the Dephosphorylation Phase. The large conformational change of KaiB upon binding to KaiC also explains why the direct interaction between KaiA and KaiB in the absence of KaiC is weak. Moreover, the fact that KaiA binds to KaiB:KaiC-EE497, but does not bind to KaiC-EE497 in the absence of KaiB, suggests that KaiA binds directly to KaiB instead of KaiC. Thus, the KaiB:KaiC complex creates a new binding site for inhibiting KaiA function.

In addition to the timing mechanism of Kai-based oscillator is solved, one other important question is how the temporal information is transduced from oscillator to downstream clock-controlled behavior such as genome-wide expression. A yeast-two hybrid screen identified a histidine kinase protein, SasA, which physically interacts with KaiC (48). *In vivo*, KaiA, KaiB, KaiC and SasA interact with each other during (subjective) night and dissociate from each other during (subjective) day (145). Disruption of the *sasA* gene lowers *kaiBC* expression, reduces the amplitude of *kai* gene expression rhythms, shortens the free-running period length, and changes the expression amplitudes and periods of all clock-controlled genes (48). In addition, the *sasA-null* strain does not abolish circadian rhythms completely (48), in contrast to disruption of any *kai* gene (53). Overall, these data identify SasA as a component of a circadian output pathway, acting through direct interactions with KaiC. RpaA, a potential DNA-binding

protein, is the cognate response regulator of SasA, and together they form a two-component signal transduction pathway (49). SasA binds to KaiC mainly in the (subjective) night when KaiC is phosphorylated, which stimulates autophosphorylation of SasA at a conserved histidyl residue. Then, the phosphate group is transferred from SasA to an invariant aspartyl residue located in the receiver domain of RpaA, which supposedly activates the effector domain for DNA binding (49). Thus, the SasA-RpaA two-component regulatory system transmits temporal information from the circadian oscillator to clock-controlled genes (49). The system also governs the gating of cell division, which has been shown to be regulated by the ATPase activity of KaiC. Therefore, understanding the regulation of SasA activity by KaiC will reveal the mechanism of a critical output pathway. We found that SasA specifically binds to the CI ring of KaiC-EE and the flexibility of the CII ring changes during the KaiC phosphorylation cycle, giving rise to ATPase rhythms, mainly in the CI ring. Specifically, the CII ring rhythmically suppresses the ATPase activity of the CI ring when it becomes rigid upon phosphorylation of residue S431. We speculate that rhythmic ATPase activity, therefore, regulates the SasA-RpaA signal transduction pathway.

4.2 Materials and Methods³

T. elongatus Kai proteins and KaiC mutants expression and purification. The genes encoding all Kai proteins from *T. elongatus* were cloned into the pET28a+ vector (Novagen) between the NdeI and HindIII sites. The resulting plasmids were used to transform *Escherichia coli* BL21(DE3), and the sequences were confirmed (DNA Sequencing Facility, University of California, Berkeley). Transformed *E. coli* cultures were incubated at 37°C until OD₆₀₀ reached about 0.6; at this point, a final concentration of 200 μM isopropyl β-D-thiogalactopyranoside (Research Product International) was

³ Supplementary information of materials and methods are in the Appendixes A-F.

added for overexpression. Cells were harvested after 12 h overexpression at 25°C, and pellets were resuspended in 20 mM Tris-NaOH, 500 mM NaCl, pH 7.0. Cell suspensions were passed twice through a chilled French press cell, and lysates were clarified by centrifugation at 20,000 x g for 60 min at 4°C. Tagged proteins were isolated on a Ni-charged column. Proteins were buffer exchanged to 20 M Tris Base, 500 mM NaCl and 20 mM Imidazole and 100 µl 100 µM ULP1 protease were added for SUMO-His₆ tag removal. The cleavage reaction was carried out at 4°C for 16 h in 15 mL volume. Kai proteins were separated from SUMO-His₆ tag protein by a second Ni-charged column and followed by gel filtration chromatography on a Superdex 200 HiLoad 16/60 prep grade column (GE Healthcare) for KaiC and KaiC mutants and a Superdex 75 HiLoad 16/60 prep grade column (GE Healthcare) for KaiC-CII variants, KaiB, KaiA, and SasA-N. Buffers were exchanged to 20 mM Tris Base, 50 mM NaCl, 1 mM MgCl₂, 5 mM DTT, 1 mM ATP, pH 7.0 for the binding assay and NMR experiments. Proteins were concentrated by Amicon Stirred Ultrafiltration Cell (MILLIPORE) and stored in a -80°C freezer. KaiA, KaiB, and KaiC did not lose function after repeated cycles of freezing and thawing. One liter LB yields ~ 440 nmol of KaiA, ~ 1728 nmol of KaiB, and ~ 240 nmol of KaiC and KaiC mutants. Coomassie Plus (Pierce) was used as a Bradford Assay reagent for protein concentration determination. For purification of KaiC, all the solutions were prepared with 1 mM ATP.

Expression of ¹⁵N-labeled proteins. The plasmid encoding the gene of interest was transformed into BL21 (DE3) *E. coli* cells. Cells harboring the plasmid (or such glycerol stocks) were grown in M9 minimal medium (Appendix D) supplemented with appropriate antibiotics at 37°C until an OD₆₀₀ of ~0.6. Note that M9 minimal medium contains ¹⁵N-NH₄Cl and D-glucose as the sole nitrogen and carbon resource, respectively. Protein expression was induced by adding IPTG to a final concentration of 0.2 mM. Protein induction period is about 12 h at 25°C. Expression: Follow protocol on A-9. Purification: Follow protocol on appendix A-12.

ULP1 protease expression and purification. Expression: Follow protocol A-8. Purification: Follow protocol A-12 but stops after the elution step of 1st Ni-NTA column.

Note that Ulp1 is not stable in buffers where NaCl is at a concentration lower than 100 mM. For long-term storage, add equal volume of glycerol into the Ulp1 elution sample from Ni-NTA column and store at -80°C . Ulp1 elution sample can be diluted to a final concentration of 200 μM before adding glycerol. Therefore, the final Ulp1 stock (stored at -80°C) will be 100 μM in the buffer of 25 mM NaH_2PO_4 , 250 mM NaCl, 125 mM imidazole, 50% glycerol, pH 8.0.

Binding Assay. All column binding assays including KaiC-CII alone experiments were carried out using a Superdex 200 10/300 GL gel filtration column (GE Healthcare). Ferritin (440 kDa), albumin (67 kDa), ovalbumin (43 kDa), and chymotrypsinogen A (25 kDa) were used as molecular mass markers.

KaiC-A, KaiB, KaiC-EE, and KaiC-EE497 binding. Recombinant KaiC-EE or KaiC-EE497 and KaiB were mixed in 1:1 ratio (10 μM : 10 μM) in 300 μl binding buffer (20 mM Tris, 50 mM NaCl, 1 mM MgCl_2 , 5 mM DTT, 1 mM ATP, pH 7.0) at 25°C for 17 h. KaiA of the final concentration 10 μM was added into the reaction and incubated for another 6 hours.

KaiC-CII and KaiC-CI binding. Recombinant CII and CI were mixed in a 1:1 molar ratio (final concentration: 10 μM : 10 μM) in 100 μl binding buffer (20 mM Tris, 50 mM NaCl, 1 mM MgCl_2 , 5 mM DTT, 1 mM ATP, pH 7.0) at 25°C about 0.5 h.

NMR Sample Preparation and Spectroscopy. NMR sample preparation: Follow protocol C-1. NMR sample information: Please see Table 3. NMR spectroscopy: Follow Protocol C-2.

4.3 Results

KaiB recruits KaiA away from A-loops to initiate Dephosphorylation Phase. The formation of the KaiCB(A) complex, in which KaiB hinders KaiA from up-regulating the autokinase activity of KaiC, initiates the Dephosphorylation Phase of the phosphorylation cycle of KaiC. How does KaiB antagonize KaiA? Previously, we

Table 3 NMR Sample Condition and Experiment for CHAPTER IV

Sample	Experiment	Sample detail	Experiment detail
KaiA			
N15-labeled KaiA-1-129	[¹ H, ¹⁵ N-HSQC]	Concentration: 40 μM Buffer: 20 mM Tris, 50 mM NaCl, 1 mM MgCl ₂ , 5 mM DTT, 1 mM ATP, pH 7.0, 10 μM DSS, 0.02% NaN ₃ , 95%H ₂ O/5%D ₂ O Volume: ~300 μl Tube: shaped tube	NS=20 40 °C
N15-labeled KaiA-1-129 +FLAG-KaiC-EE-1-497 +AMA-KaiB	[¹ H, ¹⁵ N-HSQC]	Concentration: 40 μM: 60 μM: 40 μM Buffer: 20 mM Tris, 50 mM NaCl, 1 mM MgCl ₂ , 5 mM DTT, 1 mM ATP, pH 7.0, 10 μM DSS, 0.02% NaN ₃ , 95%H ₂ O/5%D ₂ O Volume: ~300 μl Tube: shaped tube	NS=20 40 °C
N15-labeled KaiA-130-283	[¹ H, ¹⁵ N-HSQC]	Concentration: 40 μM Buffer: 20 mM Tris, 50 mM NaCl, 1 mM MgCl ₂ , 5 mM DTT, 1 mM ATP, pH 7.0, 10 μM DSS, 0.02% NaN ₃ , 95%H ₂ O/5%D ₂ O Volume: ~300 μl Tube: shaped tube	NS=20 40 °C
N15-labeled KaiA-130-283 +FLAG-KaiC-EE-1-497 +AMA-KaiB	[¹ H, ¹⁵ N-HSQC]	Concentration: 40 μM: 60 μM: 40 μM Buffer: 20 mM Tris, 50 mM NaCl, 1 mM MgCl ₂ , 5 mM DTT, 1 mM ATP, pH 7.0, 10 μM DSS, 0.02% NaN ₃ , 95%H ₂ O/5%D ₂ O Volume: ~300 μl Tube: shaped tube	NS=20 40 °C

Table 3 continued

Sample	Experiment	Sample detail	Experiment detail
N15-labeled KaiA-180-283	[¹ H, ¹⁵ N-HSQC]	Concentration: 40 μM Buffer: 20 mM Tris, 50 mM NaCl, 1 mM MgCl ₂ , 5 mM DTT, 1 mM ATP, pH 7.0, 10 μM DSS, 0.02% NaN ₃ , 95%H ₂ O/5%D ₂ O Volume: ~300 μl Tube: shaped tube	NS=20 40 °C
N15-labeled KaiA-180-283 +FLAG-KaiC-EE-1-497 +AMA-KaiB	[¹ H, ¹⁵ N-HSQC]	Concentration: 40 μM: 60 μM: 40 μM Buffer: 20 mM Tris, 50 mM NaCl, 1 mM MgCl ₂ , 5 mM DTT, 1 mM ATP, pH 7.0, 10 μM DSS, 0.02% NaN ₃ , 95%H ₂ O/5%D ₂ O Volume: ~300 μl Tube: shaped tube	NS=20 40 °C
SasA			
N15-labeled SasA-1-107	[¹ H, ¹⁵ N-HSQC]	Concentration: 19 μM Buffer: 20 mM Tris, 50 mM NaCl, 1 mM MgCl ₂ , 5 mM DTT, 1 mM ATP, pH 7.0, 10 μM DSS, 0.02% NaN ₃ , 95%H ₂ O/5%D ₂ O Volume: ~300 μl Tube: shaped tube	NS=16 25 °C
N15-labeled SasA-1-107 + FLAG-KaiC-EE	[¹ H, ¹⁵ N-HSQC]	Concentration: 19 μM: 40 μM Buffer: 20 mM Tris, 50 mM NaCl, 1 mM MgCl ₂ , 5 mM DTT, 1 mM ATP, pH 7.0, 10 μM DSS, 0.02% NaN ₃ , 95%H ₂ O/5%D ₂ O Volume: ~300 μl Tube: shaped tube	NS=16 25 °C

Table 3 continued

Sample	Experiment	Sample detail	Experiment detail
N15-labeled SasA-1-107	[¹ H, ¹⁵ N-HSQC]	Concentration: 19 μ M Buffer: 20 mM Tris, 1 mM MgCl ₂ , 1 mM ATP, 5 mM DTT, pH 8.0, 10 μ M DSS, 0.02% NaN ₃ , 95%H ₂ O/5%D ₂ O Volume: ~300 μ l Tube: shaped tube	NS=16 25 °C
N15-labeled SasA-1-107 + KaiC-CII-258-518-S258C-EE-FLAG	[¹ H, ¹⁵ N-HSQC]	Concentration: 19 μ M: 19 μ M Buffer: 20 mM Tris, 1 mM MgCl ₂ , 1 mM ATP, 5 mM DTT, pH 8.0, 10 μ M DSS, 0.02% NaN ₃ , 95%H ₂ O/5%D ₂ O Volume: ~300 μ l Tube: shaped tube	NS=16 25 °C
N15-labeled SasA-1-107	[¹ H, ¹⁵ N-HSQC]	Concentration: 19 μ M Buffer: 1 mM Tris, 18 mM HEPES, 16 mM NaCl, pH 7.0, 10 μ M DSS, 0.02% NaN ₃ , 95%H ₂ O/5%D ₂ O Volume: ~300 μ l Tube: shaped tube	NS=16 25 °C
N15-labeled SasA-1-107 + KaiC-CI-1-247	[¹ H, ¹⁵ N-HSQC]	Concentration: 19 μ M: 12 μ M Buffer: 1 mM Tris, 18 mM HEPES, 16 mM NaCl, pH 7.0, 10 μ M DSS, 0.02% NaN ₃ , 95%H ₂ O/5%D ₂ O Volume: ~300 μ l Tube: shaped tube	NS=16 25 °C

showed that KaiA binds to the A-loops of KaiC. Recently, it was shown that KaiA binds to the KaiB:KaiC complex even with most of the A-loops of KaiC truncated (90). Thus, it seems plausible that the key to answer how KaiA is inactivated by KaiB lies in that KaiA is apparently recruited away from the A-loop binding site to a new binding site formed on the KaiB:KaiC complex. To test this idea, we used KaiC-EE497, which does not bind to KaiA (86). We prepared KaiA, KaiB, KaiC-EE and KaiC-EE497 proteins as described in the materials and methods section. KaiA, KaiB, and KaiC-EE or KaiC-EE497 with mixed in 1:1:1 monomeric ratio with 10 μ M in 300 μ l at 25°C for 17 h in the presence of 1 mM ATP. The reactions were then analyzed by a Superdex 200 10/300 GL gel filtration column with a flow rate of 0.8 mL/min. Fig. 33 shows that KaiA binds

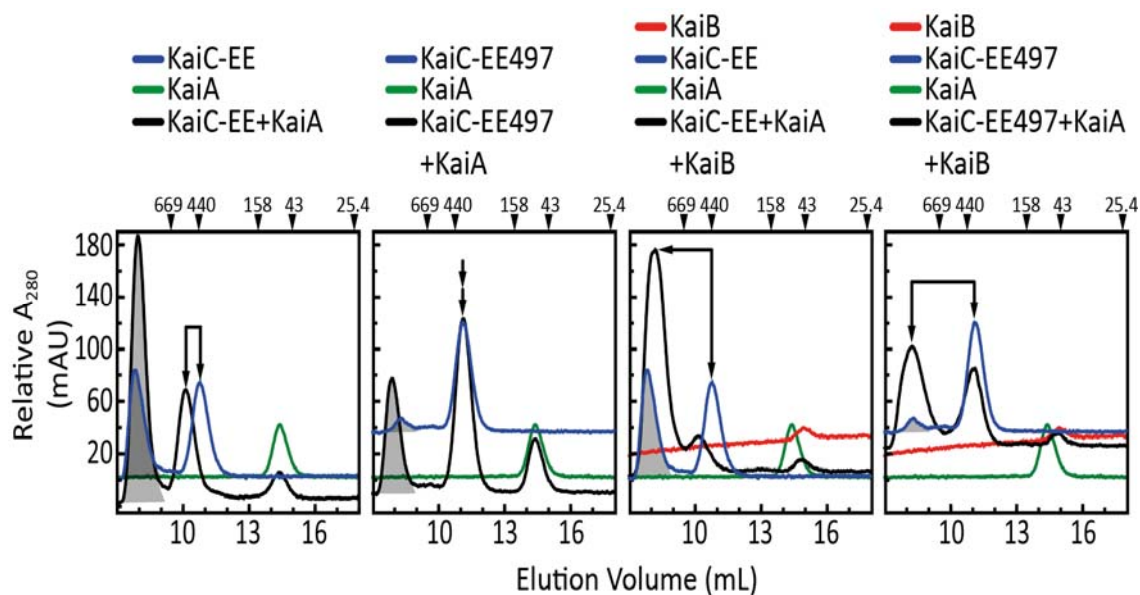


Figure 33 Gel filtration chromatography showing the KaiABC-EE497 complex formation. KaiC-EE full-length serves as a binding control in the presence of KaiA (panel 1) or of KaiA and KaiB (panel 3). The binding between KaiC-EE497, which lacks major part of KaiA binding sites, and KaiA (panel 2) or KaiA and KaiB (panel 4). Arrows in the left two panels indicate free KaiC or KaiC-EE497 (blue peak) and KaiC+KaiA or KaiC-EE497+KaiA (black peak). Arrows in the right two panels indicate free KaiC or KaiC-EE497 (blue peak) and KaiC+KaiA+KaiB or KaiC-EE497+KaiA+KaiB (black peak). Peaks shaded contain no proteins.

to both KaiB:KaiC-EE and KaiB:KaiC-EE497 complexes, but not to KaiC-EE497 in the absence of KaiB. In CHAPTER III, fig. 30 shows that KaiB undergoes a large conformational changes upon KaiC binding. These results suggest that there is a new site on KaiB:KaiC-EE497 for KaiA binding. The newly created binding site is most likely on KaiB as its conformation changes dramatically upon binding to KaiC-EE497 (70). The KaiB:KaiC-EE497 was used by NMR to mapping the binding site on KaiA for the KaiB:KaiC-EE497 complex. To map KaiA and KaiB interacting surface, we made three different ^{15}N -labeled truncation mutants of KaiA, which are ^{15}N -KaiAN129 (N-terminal domain), ^{15}N -KaiA130C (linker region and C-terminal domain), and ^{15}N -KaiA180C (C-terminal domain). These ^{15}N -labeled KaiA proteins were mixed with unlabeled KaiB:KaiC-EE497 in 2:2:3 (monomer) ratio, with the final concentrations of 40, 40, and 60 μM , respectively. The unlabeled KaiB:KaiC-EE497 complex was preincubated at 25 $^{\circ}\text{C}$ for 17 h. Then, ^{15}N -KaiA180C, ^{15}N -KaiA130C, and ^{15}N -KaiAN129 were mixed with unlabeled KaiB:KaiC-EE497 complexes before collecting heteronuclear single quantum coherence (HSQC) spectra at 25 $^{\circ}\text{C}$ for 3.5 h, 5.5 h, and 7.5 h, respectively. HSQC spectra of free ^{15}N -KaiAN129, ^{15}N -KaiA130C, and ^{15}N -KaiA180C collected at 40 $^{\circ}\text{C}$ for 2 h are well-dispersed. We reasoned that if KaiA binds tightly to the KaiB:KaiC-EE497 complex, HSQC signals would broaden beyond detection because the size of the KaiABC complex is > 400 kDa. The HSQC spectra show that there is no binding between either KaiA180C or KaiAN129 to the KaiB:KaiC-EE497 complex (Fig. 34). However, the HSQC peaks from ^{15}N -KaiA130C disappear in the presence of the KaiB:KaiC-EE497 complex (Fig. 34). These spectra collectively indicate that KaiA130C binds to the KaiB:KaiC-EE497 complex via the linker region of KaiA. We conclude that KaiB inhibits KaiA function during the Dephosphorylation Phase by recruiting KaiA away from its original KaiC binding site, the A-loops, through direct interaction with the linker region of KaiA.

Dynamics dominates the Sequential Dephosphorylation Order. KaiC dephosphorylates sequentially as follows: pSpT \rightarrow pST \rightarrow ST. My goal was to determine the basis governing this pattern of dephosphorylation. To test if the rigidity of

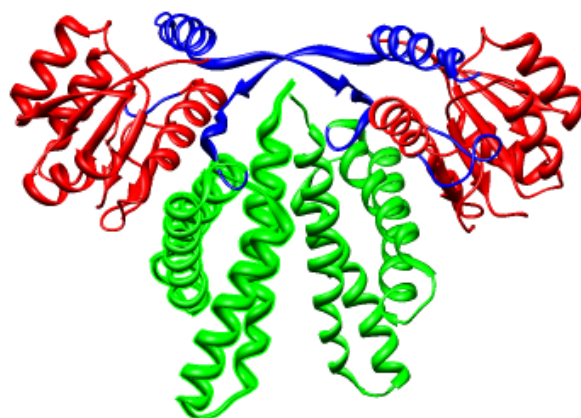


Figure 34 Mapping of KaiA binding site for KaiCB complex by ^1H , ^{15}N -HSQC spectra. Titration of KaiA-N (upper two panels), KaiA-130C (middle two panels), and KaiA-180C (lower two panels) with KaiC-EE497 and KaiB. KaiA-N spans residues 1-129, KaiA-130C spans 130-283, and KaiA-180C includes residues 180-283. The structure of *S. elongatus* KaiA (PDB ID 1r8j) on the right is color coded as follows: red (residues 1-131), blue (132-180; note that residues 137-146 are missing in crystal structure), and green (181-282). The linker of KaiA is colored blue. The molar ratios of KaiA-N, KaiA-180C and KaiA-130C vs KaiC-EE497 and KaiB are all 2:2:3. Note that KaiC-EE497 was used so that KaiA is unable to bind to KaiC in the absence of KaiB. Sample conditions and NMR parameters are described in Table 3.

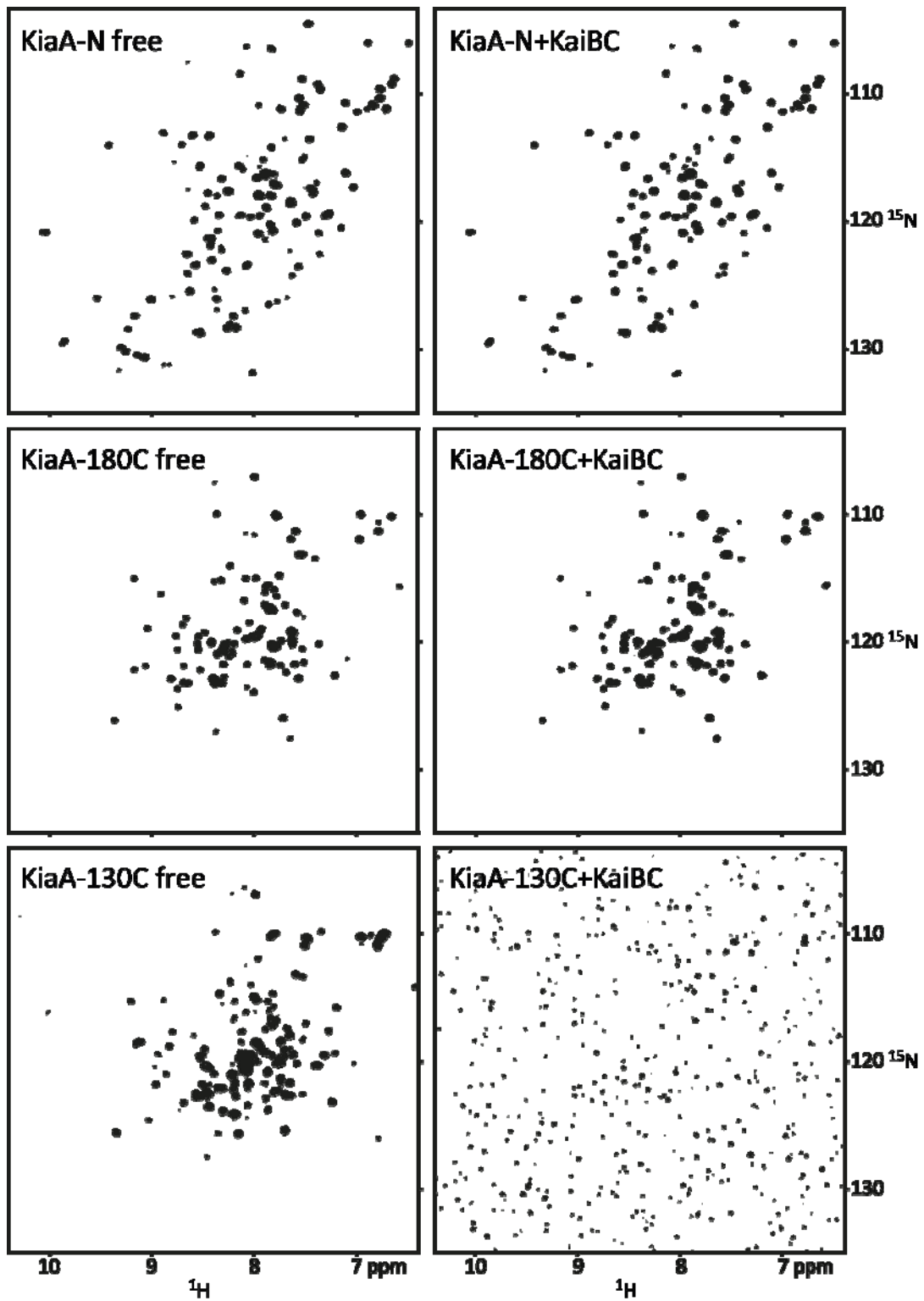


Figure 34 Continued.

the CII ring affects the dephosphorylation order, we prepared KaiC-SE (SpT phosphomimic) and KaiC-ET (pST phosphomimic) reactions in the presence and absence of KaiA and measured the phosphorylation level of KaiC. The purification protocols are as described in the materials and methods. The KaiC variants were preincubated at 30°C for 16 hour to reach a hypophosphorylated state. Reaction mixtures containing 1.2 μ M KaiA, 3.5 μ M KaiC variants and 1 mM ATP were incubated for 24h at 30°C. The aliquots were collected following the time course as shown in Fig. 20. In the presence of KaiA, KaiC-SE phosphorylation increased to 81%, whereas KaiC-ET failed to phosphorylate. In the absence of KaiA, the steady state levels of phosphophorylation were 30% and 0% for KaiC-SE and KaiC-ET, respectively. The results suggest that the rigidity of the CII ring induced by phospho-S431 inhibits the phosphorylation at T432, leading to T432 dephosphorylation first. In contrast, CII ring flexibility sustained by phospho-T432 apparently inhibits dephosphorylation of phospho-S431. Taken together, the data suggest that CII ring flexibility underpins the sequential order of KaiC dephosphorylation.

CII-CI interdomain interactions regulate the SasA-initiated output pathway. The circadian rhythms of gene expression (46, 59), chromosome compaction (47, 81, 146), and cell division gating (51, 147, 148) originate at the Kai oscillator. SasA and RpaA constitute a two-component signal transduction pathway that transduces the oscillator signal downstream (49, 149). SasA is a histidine protein kinase and RpaA is the cognate response regulator. SasA has been shown to interact with KaiC directly (48, 53) but it is not clear to which KaiC domain SasA binds, and how the temporal signal from the oscillator is transduced to output pathways. To identify the domain of KaiC to which SasA binds, we mixed 15 N-labeled SasA-N (N-terminal domain of SasA) with either isolated CI or CII-EE domains. The purification protocols are as described in the materials and methods section. 15 N-SasA-N was mixed with unlabeled KaiC-EE, CII-EE, and CI at 25°C immediately before collecting HSQC spectra. Experimental detail is listed in Table 3. We found that the N-terminal domain of SasA (150) binds to the CI ring but not to the CII ring of KaiC, suggesting that output of the oscillator rhythm is

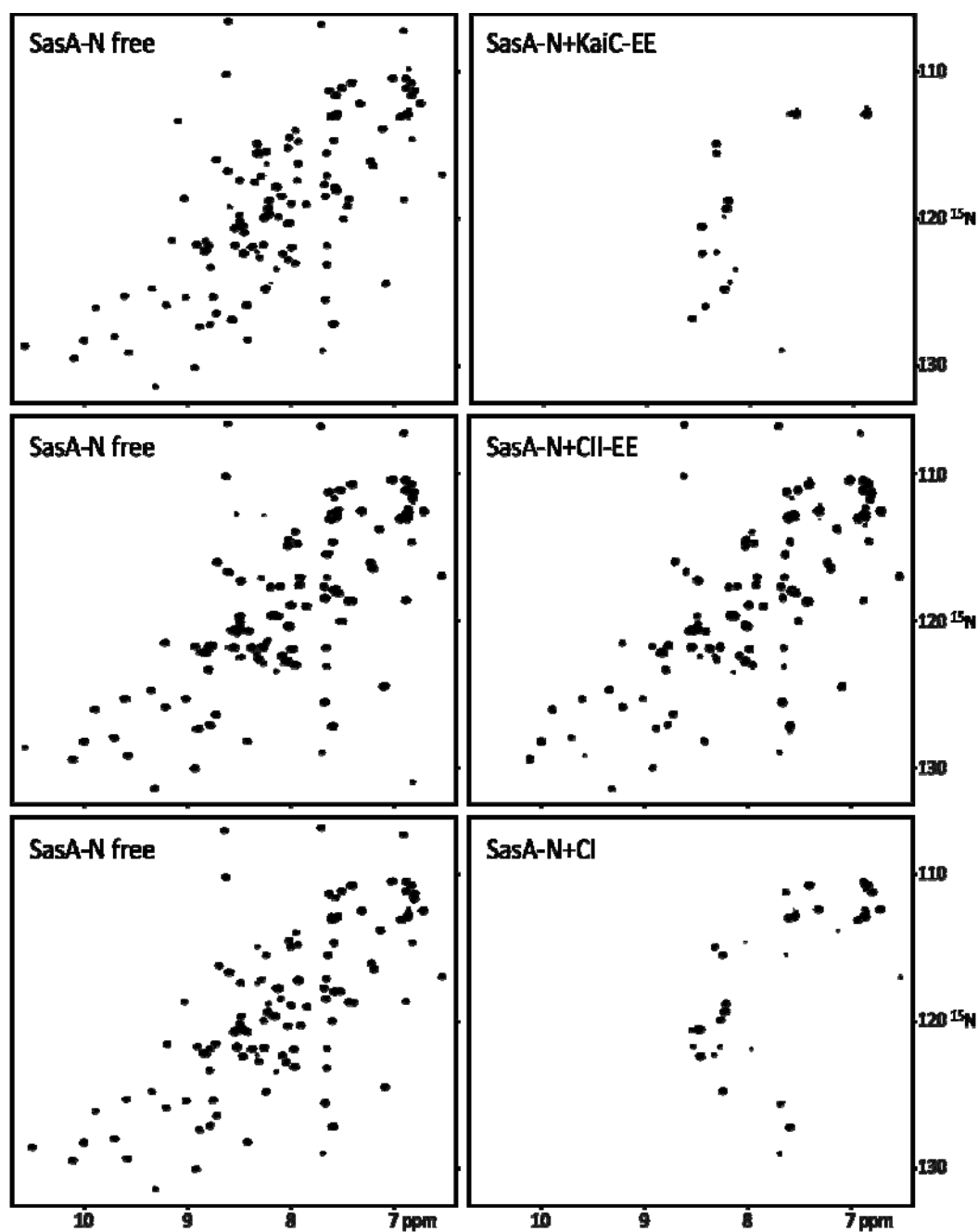


Figure 35 ^1H , ^{15}N -HSQC showing SasA-N (residues 1-107) specifically binds to CI monomer. Titration of SasA-N with KaiC-EE (upper two panels), CII-EE (middle two panels), and CI (lower two panels). Sample conditions and NMR parameters are described in Table 3.

transmitted through the CI ring (Fig. 35). Indeed, the CI ring has an ATPase activity that displays a circadian rhythm (62), and this activity gates cell division using a SasA-dependent pathway (51). Cyanobacterial strains expressing KaiC mutants with high ATPase activities, as with the hyperphosphorylated KaiC487 mutant, results in elongated non-dividing cells (51). In contrast, cyanobacteria expressing KaiC mutants with low ATPase activities, e.g. the KaiC-pSpT phosphomimic (KaiC-DE), undergo normal cycles of cell division. Although both KaiC mutants are hyperphosphorylated, they have different ATPase activities and produce different cell lengths. Thus, the linkage between of ATPase activity and cell length is clear but regulation of the ATPase activity has remained mysterious (51). Our data show that the flexibility of CII ring regulates the ATPase activity of the CI ring. A flexible CII ring enhances CI ATPase activity, whereas a rigid CII ring suppresses CI ATPase activity.

Next, we asked how CII-CI interact to regulate the ATPase of the CI ring. There are two possibilities: 1) through the peptide linkage joining these two rings, or 2) through ring-on-ring stacking. Here, we tested CI-CII ring stacking by mixing isolated CI and CII domains followed by gel filtration chromatography. We prepared CII variants and isolated CI domains as described in the materials and methods section. The reactions were mixed with in a 1:1 monomeric ratio at a concentration of 10 μ M in 100 μ l at 25 $^{\circ}$ C for 0.5 h. The reactions were then analyzed by a Superdex 200 10/300 GL gel filtration column with a flow rate of 0.8 mL/min. As seen in Fig. 36A panel 1-3, the CI ring does not interact with CII, CII-SE, or CII-EE domains. However, interactions were observed with the hexameric CII-ET domain which has the highest hexamerization level among all CII ring variants (Fig. 36A panel 4). Methyl-TROSY spectra of full-length KaiC variants show that peaks assignable to the CI domain have chemical shifts and line shapes that vary depending on the rigidity of the CII ring (Fig. 36B), thereby corroborating the gel filtration data and indicating that CII-CI interactions increase with increasing rigidity of the CII ring (Fig. 36, A and B). These observations suggest a mechanism by which CII ring rigidity suppresses CI ATPase activity, which is through increased ring stacking interactions.

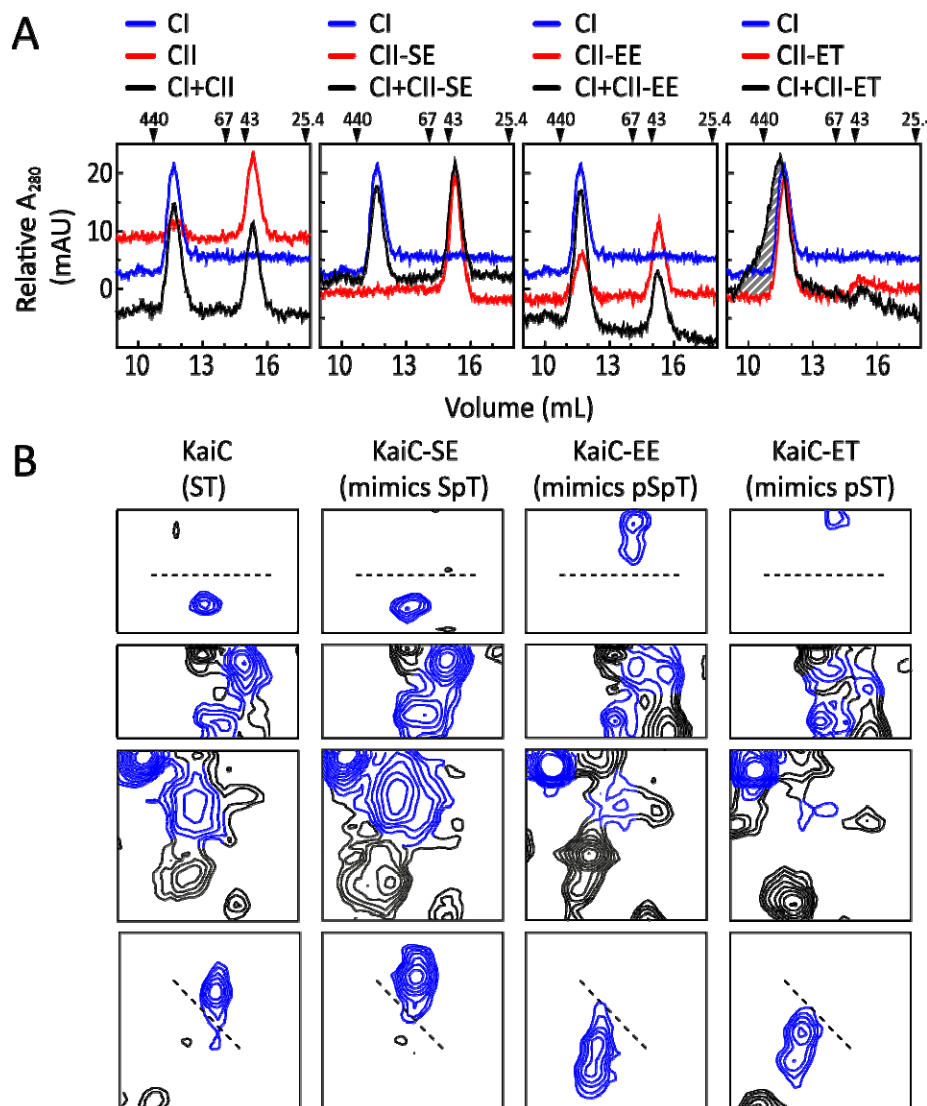


Figure 36 CII-CI interactions depend on the state of phosphorylation at residues S431 and T432. A) Gel-filtration experiments of mixtures of domains of CI with CII (panel 1) and phosphomimics of CII-SpT (panel 2), CII-pSpT (panel 3), and CII-pST (panel 4). The hexameric form of the CI and CII domains eluted at ~11.6 mL, whereas the monomeric form eluted at ~15.4 mL. The shaded region in panel 4 indicates the shift of the CI + pST-CII phosphomimic elution profile relative to those of the domains by themselves. B) Selected regions of methyl-TROSY spectra (139) of U- $[^2\text{H}, ^{15}\text{N}]$, Ile- $[\delta 1 \text{ } ^{13}\text{CH}_3]$ labeled wt-KaiC (panel 1) and the phosphomimics of KaiC-SpT (panel 2), KaiC-pSpT (panel 3), and KaiC-pST (panel 4). All panels were plotted at the same relative contour level. Blue resonances are those assigned to the CI domain, whereas unassigned peaks are black. Please see Table 3 for experimental details.

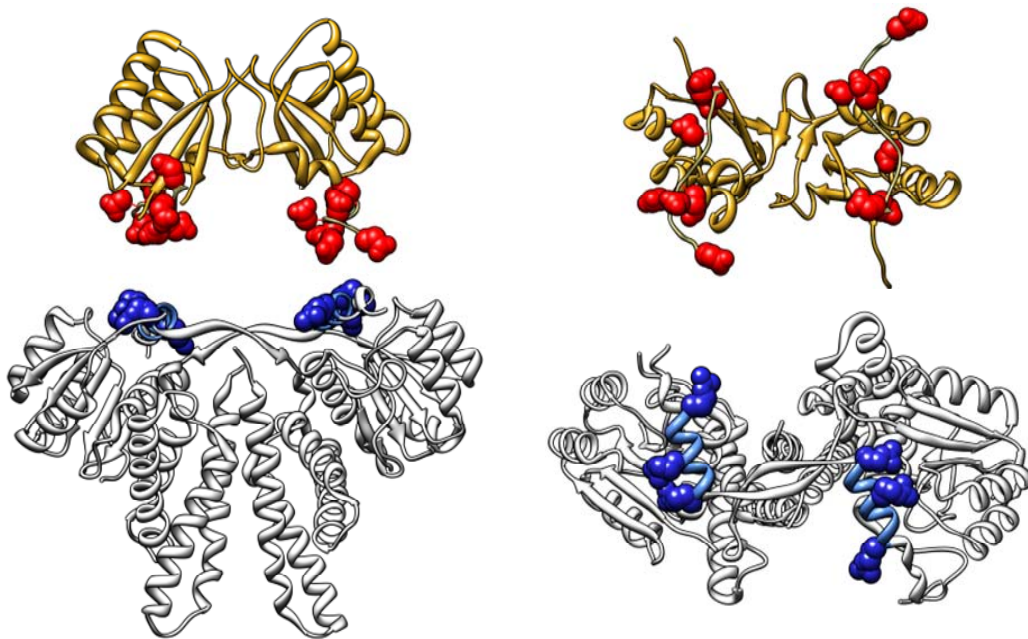


Figure 37 Putative binding site on KaiA on KaiB. KaiB is showed as a dimer form on the top (gold) and putative conserved acidic residues involved in binding surface are showed as red balls. KaiA is showed in dimer form on the bottom (gray) and putative conserved basic residues involved in binding surface are showed as blue balls.

4.4 Discussion

KaiABC complex formation switch *KaiC* from an autokinase to autophosphatase in Dephosphorylation Phase. Qin *et al.* have suggested that the KaiCB(A) complex switches KaiC autokinase to autophosphatase (90). Phospho-S431 is required for the formation of the KaiCB(A) complex. The role of KaiB is to inhibit KaiA function. Formation of the KaiCB(A) complex using the KaiC489 variant shows that the KaiB:KaiC complex creates a new binding site for KaiA, since KaiA's original binding site has been removed in KaiC489. However, how the new binding site is created and where it binds KaiA is not clear. In this study, our results provide new information regarding these questions. KaiA and KaiB have been shown to interact only weakly in

the absence of KaiC (142), and, therefore it was thought that conformational changes either in KaiB or KaiC upon complex formation recruited KaiA away from the A-loops (65, 151). We confirmed by NMR (Fig. 34) that a new binding site is created for KaiA on KaiB:KaiC complex. Our NMR data further shows that the new binding site is created on KaiB (Fig. 30 and 34), which is probably at the interface used to form the tetramer observed in free KaiB. Since KaiC does show any conformational change upon KaiB binding by NMR, it probably does not participate in direct interactions with KaiA during the Dephosphorylation Phase. Strikingly, KaiB undergoes a large conformational change, as indicated by NMR. We speculate that the newly created binding site on KaiB could be from exposing a hidden interface when KaiB binds to KaiC as a dimer. The new binding surface on KaiA has been mapped to the linker region of KaiA (Fig. 34), residues 130 to 180. The linker region contains one loop, two α -helices and one β -sheet. Since KaiB is decorated with charged residues, we suspect that the charged residues on the α -helix, residues 147-163, of KaiA are directly interact with KaiB. The negatively charged C-terminal tail of KaiB is suspected to be the KaiA binding site, as KaiB mutants lacking the tail had arrhythmic free-running rhythms. The negatively charged C-terminal tail of KaiB may interact with the positively charged α -helix on KaiA (Fig. 37). However, we can not rule out the alternative possibility from residues 161 – 174, in the linker region of KaiA. Upon formation of the KaiABC complex, KaiA can no longer bind to the A-loops to stimulate KaiC phosphorylation. At this point, KaiC's autokinase activity is suppressed, allowing its constitutive autophosphatase activity to become the dominant activity (152). When KaiC becomes completely dephosphorylated, the CII ring regains its flexibility, causing the KaiABC complex to dissociate. KaiB sequesters its KaiA binding site by forming tetramers again. KaiA is free to bind to the A-loops again to stimulate KaiC phosphorylation, thereby starting a new cycle.

CI ATPase activity is regulated by the flexibility of the CII ring. It is insightful to speculate on the role of CII ring flexibility in the signal transduction of oscillator signals to downstream events. The ATPase activity of the CI ring of KaiC, which displays a circadian rhythm (62), applies a cell division checkpoint in cyanobacteria (51).

Interestingly, published cell lengths in *S. elongatus* strains expressing KaiC mutants show a strong correlation to our results on CII ring flexibility, with longer lengths corresponding to more flexible CII rings, and shorter lengths corresponding to rigid rings. ATPase levels of *S. elongatus* KaiC (51) also correlate with CII ring flexibility, with flexible rings correlating to higher ATPase levels. This correlation suggests that communication between the CII and CI rings depends on CII ring flexibility. Gel-filtration data showed that isolated CII-ET domains, which form a hexamer, uniquely interact with isolated CI rings (Fig. 36A), allowing us to speculate that a rigid CII ring interacts most strongly with the CI ring, and that it is these ring-on-ring contacts that suppresses CI ATPase activity.

Dong *et al.* (51) have shown that constitutive phosphorylation of KaiC inhibits cell division, however, phosphorylation of KaiC is not essential for cell elongation. Instead, it is the elevated ATPase activity of KaiC that inhibits cell division (51). Two hyperphosphorylated KaiC mutants, KaiC487 and KaiCE444D, cause elongated cells, whereas a hypophosphorylated KaiC mutant, KaiC497, maintains normal cell length. However, a fully phosphorylated KaiC mimic, KaiC-DE, does not inhibit cell division, whereas KaiC-AA does. These two results seemingly conflict with each other, in which two hyperphosphorylated KaiC mutants display opposite cell length phenotypes. Dong *et al.* found that it is an elevated ATPase activity of KaiC that causes elongated cell lengths, whereas low ATPase activities do not. KaiC487 exhibits high ATPase activity and long cells but, in contrast, KaiC-DE exhibits low ATPase activity and normal length cells. It could not be explained, however, why the two hyperphosphorylated mutants, KaiC487 and KaiC-DE, exhibited different cell length phenotypes. Here, our study fills this gap. We showed that it is the flexibility of CII ring that controls CI ATPase activity, and CII ring flexibility, in turn, is regulated by KaiC phosphorylation A-loop position. KaiC487 mimics KaiC with the exposed A-loops, which we have shown to induce flexibility in the CII ring. In contrast, KaiC-DE is in a rigid state. The flexible and rigid states respectively enhance and inhibit CI ATPase activities by weakening and strengthening

CI-CII stacking interactions. Now that we know how KaiC mutants regulate the flexibility of the CII ring, we can predict the cell length accurately.

SasA and RpaA have been found to be epistatic to KaiC in the control of cell division (51). How the temporal signal is transferred from KaiC to SasA-RpaA two component regulatory system has been located to the physical interaction between the CI ring of KaiC and SasA-N by our data (Fig. 35 and 36). Moreover, the CII-CI ring communication has been suggested through chemical linkage (in CHAPTER II and III) and ring-on-ring stacking (Fig. 36). Overall, the results lead to the conclusion that CII ring rhythmic phosphorylation cycle regulates the flexibility of CII ring. The rhythmic flexibility of the CII ring, in turn, governs the cyclic ATPase activity of the CI ring. The rhythmic ATPase activity, then, transfers the temporal signal from KaiC to the SasA-RpaA two component regulatory system ultimately transducing a biochemical rhythm into physiological responses such as cell division.

CHAPTER V

CONCLUSION AND FUTURE WORK

This is the first study to reveal that the timing mechanism of the KaiABC oscillator is underpinned by KaiC CII ring flexibility (Fig. 38 and 39). The flexibility of the CII ring of the KaiC protein governs the sequential pattern of KaiC phosphorylation and dephosphorylation, as well as its interaction with KaiA and KaiB. We show that CII-CI ring-ring stacking in KaiC also depends on the flexibility of the CII ring, which has

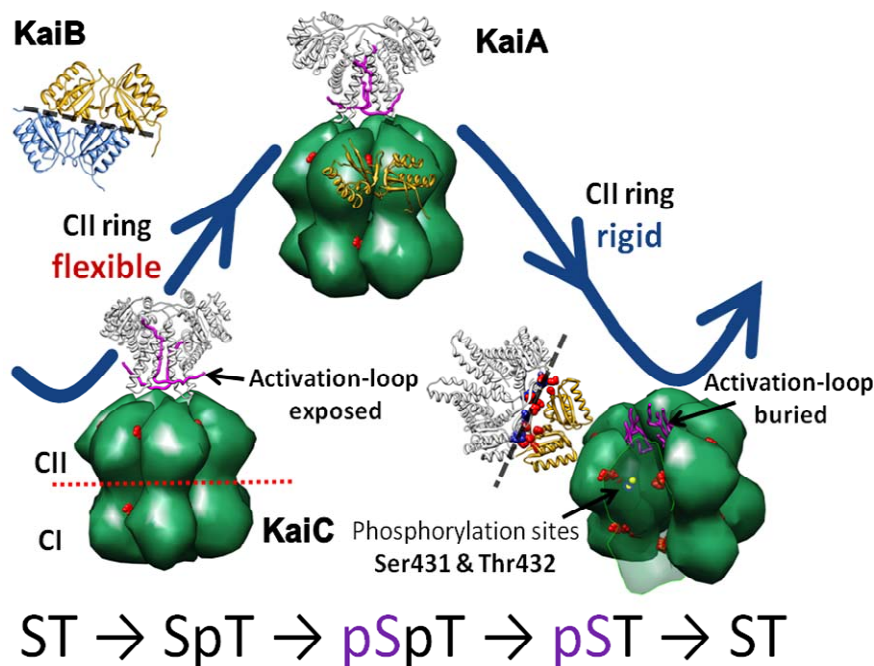


Figure 38 KaiA and KaiB temporally control the ordered phosphorylation of KaiC. In the Phosphorylation Phase, CII ring is flexible. KaiA stabilizes the exposed A-loops and enhances the phosphorylation at T432 and then S431. Once, KaiC gets fully phosphorylated, CII ring becomes rigidity. KaiB binds to the rigid KaiC as a dimer on the top of the CII ring. The KaiB:KaiC complex traps KaiA away from its original binding site. The KaiCB(A) complex inhibits KaiA function and ensure that KaiC dephosphorylates fully.

important implications for regulating cell division. These findings are completely orthogonal to current attempts at understanding oscillator function, which are all from a structural perspective. This study dispels the current notion that functional differences between the phosphoforms of KaiC arise from structural differences. Instead, it arises from the flexibility of the CII ring.

CII ring flexibility is required for the Phosphorylation Phase. The flexibility destabilizes the buried position of the A-loops of KaiC so that they exist in a dynamic equilibrium with an exposed state. KaiA selectively captures the exposed state of the A-loops, which induces KaiC phosphorylation (85). NMR spectra of the A-loop exposed state reveals unique spectral signatures that most likely reflect conformational changes at

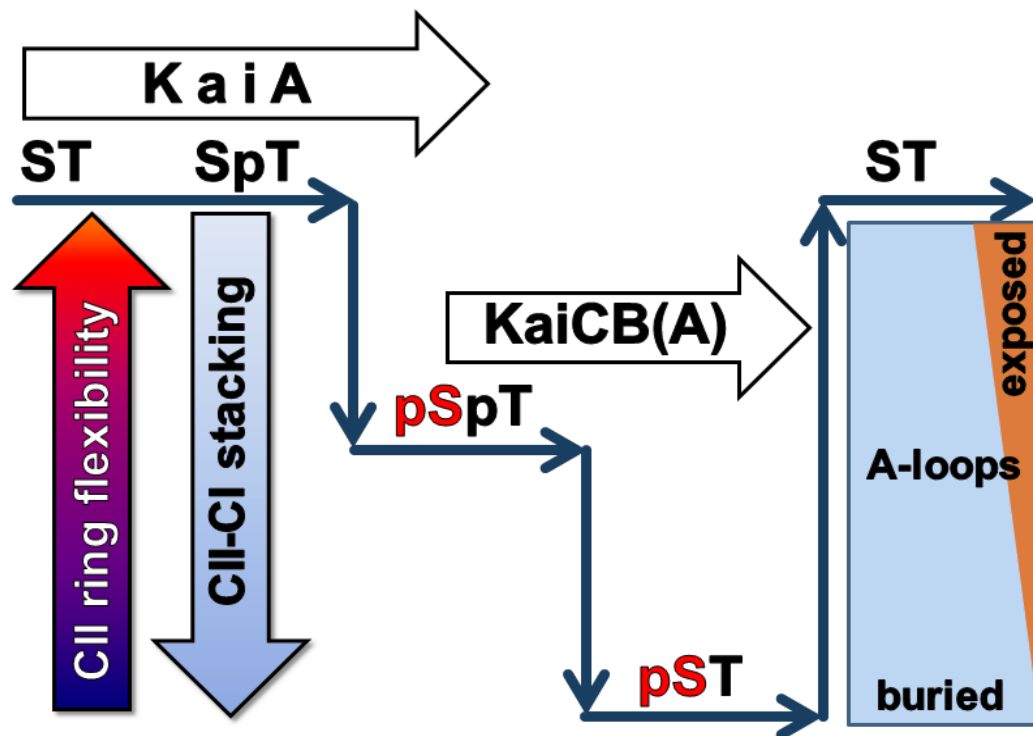


Figure 39 CII ring flexibility governs the circadian rhythm of the cyanobacterial oscillator. The vertical direction indicates the flexibility of the CII ring of KaiC, upon which depends the extent of CII-CI ring-ring stacking and the dynamic equilibrium of the A-loops between their buried and exposed positions (illustrated for free KaiC). The ability of the KaiCB complex to sequester KaiA depends on CII ring rigidity.

the autokinase site required for activation. The ST and SpT phosphoforms are flexible, whereas pSpT is significantly less so. The pST phosphoform in contrast is the least flexible. That phosphorylation of T432 precedes that of S431 can now be understood to be necessary, because pT disallows pS from quenching CII ring flexibility, which is required for A-loop exposure. Hence, the observed pattern of KaiC phosphorylation, ST \rightarrow SpT \rightarrow pSpT (65, 66), can now be explained from the standpoint of CII ring flexibility. The current work has analyzed the NMR spectra on a qualitative level. The next phase of this project is to determine quantitatively the different types of motions in the CII ring under different states of phosphorylation by using NMR experiments sensitive to ps-ns and μ s-ms timescales.

CII ring flexibility dictates the Transition Phase. An ongoing conundrum has been the molecular recognition by KaiB of the pSpT and pST but not of the ST and SpT phosphoforms of KaiC. Indeed, the crystal structures of several different KaiC phosphoforms are virtually identical (89). Our work here reveals that KaiB binding depends on CII ring flexibility, or rather the lack thereof. KaiB binds to pSpT and even more rapidly to pST because of phospho-S431 induced rigidity of the CII ring. The lack of CII ring rigidity during the Phosphorylation Phase explains why KaiB fails to bind prematurely to KaiC. A remaining question is the slow kinetics of KaiB-KaiC binding. As observed here and by others, the formation of a stable KaiB:KaiC complex is on the order of hours. Thus, a future direction for work on the Transition Phase is to elucidate the basis of the slow kinetics of KaiB:KaiC binding. We suspect that the rate determining step is the dissociation of KaiB tetramers into dimers. Another important goal would be to obtain a higher resolution model of the KaiB:KaiC complex than is currently available (87).

CII ring flexibility dictates the Dephosphorylation Phase. The KaiABC complex dephosphorylates as pSpT \rightarrow pST \rightarrow ST (65, 66). Upon reaching the ST state, the complex dissociates, allowing another cycle to start anew. The stability of the KaiCB(A) complex depends critically upon the lack of CII ring flexibility. Hence, phospho-T432 necessarily dephosphorylates before phospho-S431, so that CII ring rigidity can be

maintained until KaiC reaches the ST state. If the order was reversed, pSpT \rightarrow SpT, the KaiABC complex would dissociate prematurely and KaiC would never attain the ST state. An important future goal for this project would be to determine the structure of the KaiCB(A) complex, especially the KaiB:KaiA binding interface.

CII ring flexibility regulates clock output signals. The CI ring has been identified as the source of clock output signals by two lines of evidence. One is that its ATPase activity regulates cell cycle progression (51). The other is that SasA, a clock output protein, binds specifically to the CI ring (145). Regulation of its ATPase activity (62) such that it displays a circadian rhythm indicates that it must somehow communicate with the CII ring, the oscillator part of KaiC. Until now, evidence has been lacking. We revealed here that CI-CII ring-ring interactions are enhanced when the CII ring is rigid and attenuated when the CII ring is flexible (Fig. 36A). Thus, the circadian rhythms of phosphorylation of the CII domain are transmitted to the CI ring through ring-on-ring stacking. Increased stacking inhibits the CI ATPase activity, whereas decreased stacking relieves the inhibition. An exciting extension of this project would be to determine how ring-on-ring stacking affects the structure and dynamics of the CI ring, especially at the ATPase active sites. It would also be illuminating to elucidate how stacking affects the interaction between the CI ring and SasA, and how these interactions regulate the structure and function of SasA.

Inside the KaiABC oscillator, phospho-S431 plays an important role to ensure the 24 h rhythm. KaiCB(A) complex formation is initiated when CII ring rigidity is induced by phospho-S431. The stable KaiCB(A) complex switches KaiC from the Phosphorylation Phase to the Dephosphorylation Phase and from an autokinase to autophosphatase (90). On the other hand, phospho-S431 is also suggested to play a role in the temperature compensation mechanism (135). Specifically, the particular pST phosphoform sustains the 24 h rhythm across the physiological temperature range by regulating the ATPase activity of KaiC (135). According to our data, temperature compensation of the ATPase activity is linked to CII ring flexibility. Our model, in total, predicts that CII ring flexibility/rigidity unifies oscillator and output functions of the Kai system.

In conclusion, we present the surprising finding that the *flexibility* of the CII ring of the KaiC protein governs the sequential pattern of KaiC phosphorylation and dephosphorylation, as well as its interactions with clock proteins KaiA and KaiB. We showed that CII-CI ring-on-ring stacking in KaiC also depends on the flexibility of the CII ring, which has important implications for regulating cell division. By revealing that all known functions of KaiC originate from the flexibility of its CII ring, we present a unifying model. These findings are completely orthogonal to current attempts at understanding oscillator function, which are from a structural perspective. Thus, we think this work will shake up the field of biological timekeeping, and demonstrates that other investigations of this and other clock mechanisms need serious consideration of the different *dynamic states* of clock proteins.

REFERENCES

1. Huang, T. C., Tu, J., Chow, T. J., Chen, T. H. (1990) Circadian Rhythm of the Prokaryote *Synechococcus* sp. RF-1. *Plant Physiology* 92: 531-533.
2. Lee, K., Loros, J. J., Dunlap, J. C. (2000) Interconnected feedback loops in the *Neurospora* circadian system. *Science* 289: 107-110.
3. Bunning, E. (1935) Zur Kenntnis der erblichen tagesperiodizität bei den primärblättern von *Phaseolus multiflorus*. *Jahrb Wiss Bot* 81: 411.
4. Beling, I. (1929) Über das Zeitgedächtnis der Bienen. *Z. Vgl. Physiol* 9: 259.
5. Aschoff, J., Wever, J. (1962) Spontanperiodik des Menschen bei Ausschluss aller Zeitgeber. *Naturwissenschaften* 49: 337.
6. Ouyang, Y., Andersson, C. R., Kondo, T., Golden, S. S., Johnson, C. H. (1998) Resonating circadian clocks enhance fitness in cyanobacteria. *Proc Natl Acad Sci U S A* 95: 8660-8664.
7. Beaver, L. M., Gvakharia, B. O., Vollintine, T. S., Hege, D. M., Stanewsky, R., Giebultowicz, J. M. (2002) Loss of circadian clock function decreases reproductive fitness in males of *Drosophila melanogaster*. *Proc Natl Acad Sci U S A* 99: 2134-2139.
8. Green, R. M., Tingay, S., Wang, Z. Y., Tobin, E. M. (2002) Circadian rhythms confer a higher level of fitness to *Arabidopsis* plants. *Plant Physiology* 129: 576-584.
9. Sweeney, B. (1987) *Rhythmic Phenomena in Plants* (Academic, San Diego).
10. Johnson, C. H., Golden, S. S., Kondo, T. (1998) Adaptive significance of circadian programs in cyanobacteria. *Trends Microbiol* 6: 407-410.

11. Pittendrigh, C. S. (1960) Circadian rhythms and the circadian organization of living systems. *Cold Spring Harb Symp Quant Biol* 25: 159-184.
12. Bell-Pedersen, D., Cassone, V. M., Earnest, D. J., Golden, S. S., Hardin, P. E., Thomas, T. L., Zoran, M. J. (2005) Circadian rhythms from multiple oscillators: Lessons from diverse organisms. *Nat Rev Genet* 6: 544-556.
13. Turek, F. W., Joshu, C., Kohsaka, A., Lin, E., Ivanova, G., McDearmon, E., Laposky, A., Losee-Olson, S., Easton, A., Jensen, D. R., *et al.* (2005) Obesity and metabolic syndrome in circadian Clock mutant mice. *Science* 308: 1043-1045.
14. Marcheva, B., Ramsey, K. M., Buhr, E. D., Kobayashi, Y., Su, H., Ko, C. H., Ivanova, G., Omura, C., Mo, S., Vitaterna, M. H., *et al.* (2010) Disruption of the clock components CLOCK and BMAL1 leads to hypoinsulinaemia and diabetes. *Nature* 466: 627-631.
15. Sahar, S., Sassone-Corsi, P. (2009) Metabolism and cancer: The circadian clock connection. *Nat Rev Cancer* 9: 886-896.
16. Fu, L., Pelicano, H., Liu, J., Huang, P., Lee, C. (2002) The circadian gene Period2 plays an important role in tumor suppression and DNA damage response in vivo. *Cell* 111: 41-50.
17. Polonsky, K. S., Given, B. D., Hirsch, L. J., Tillil, H., Shapiro, E. T., Beebe, C., Frank, B. H., Galloway, J. A., Van Cauter, E. (1988) Abnormal patterns of insulin secretion in non-insulin-dependent diabetes mellitus. *The New England Journal of Medicine* 318: 1231-1239.
18. Dunlap, J. C. (1999) Molecular bases for circadian clocks. *Cell* 96: 271-290.

19. Gery, S., Komatsu, N., Baldjyan, L., Yu, A., Koo, D., Koeffler, H. P. (2006) The circadian gene *per1* plays an important role in cell growth and DNA damage control in human cancer cells. *Mol Cell* 22: 375-382.
20. Yang, W. S., Stockwell, B. R. (2008) Inhibition of casein kinase 1-epsilon induces cancer-cell-selective, PERIOD2-dependent growth arrest. *Genome Biol* 9: R92.
21. Hardin, P. E. (2005) The circadian timekeeping system of *Drosophila*. *Curr Biol* 15: R714-722.
22. Gallego, M., Virshup, D. M. (2007) Post-translational modifications regulate the ticking of the circadian clock. *Nature Reviews* 8: 139-148.
23. Lowrey, P. L., Shimomura, K., Antoch, M. P., Yamazaki, S., Zemenides, P. D., Ralph, M. R., Menaker, M., Takahashi, J. S. (2000) Positional syntenic cloning and functional characterization of the mammalian circadian mutation tau. *Science* 288: 483-492.
24. Vanselow, K., Kramer, A. (2007) Role of phosphorylation in the mammalian circadian clock. *Cold Spring Harb Symp Quant Biol* 72: 167-176.
25. Toh, K. L., Jones, C. R., He, Y., Eide, E. J., Hinz, W. A., Virshup, D. M., Ptacek, L. J., Fu, Y. H. (2001) An hPer2 phosphorylation site mutation in familial advanced sleep phase syndrome. *Science* 291: 1040-1043.
26. Xu, Y., Padiath, Q. S., Shapiro, R. E., Jones, C. R., Wu, S. C., Saigoh, N., Saigoh, K., Ptacek, L. J., Fu, Y. H. (2005) Functional consequences of a CKIdelta mutation causing familial advanced sleep phase syndrome. *Nature* 434: 640-644.
27. Jones, C. R., Campbell, S. S., Zone, S. E., Cooper, F., DeSano, A., Murphy, P. J., Jones, B., Czajkowski, L., Ptacek, L. J. (1999) Familial advanced sleep-phase

- syndrome: A short-period circadian rhythm variant in humans. *Nat Med* 5: 1062-1065.
28. Ebisawa, T., Uchiyama, M., Kajimura, N., Mishima, K., Kamei, Y., Katoh, M., Watanabe, T., Sekimoto, M., Shibui, K., Kim, K., *et al.* (2001) Association of structural polymorphisms in the human period3 gene with delayed sleep phase syndrome. *EMBO Rep* 2: 342-346.
 29. Takano, A., Uchiyama, M., Kajimura, N., Mishima, K., Inoue, Y., Kamei, Y., Kitajima, T., Shibui, K., Katoh, M., Watanabe, T., *et al.* (2004) A missense variation in human casein kinase I epsilon gene that induces functional alteration and shows an inverse association with circadian rhythm sleep disorders. *Neuropsychopharmacology* 29: 1901-1909.
 30. Cardone, L., Hirayama, J., Giordano, F., Tamaru, T., Palvimo, J. J., Sassone-Corsi, P. (2005) Circadian clock control by SUMOylation of BMAL1. *Science* 309: 1390-1394.
 31. Doi, M., Hirayama, J., Sassone-Corsi, P. (2006) Circadian regulator CLOCK is a histone acetyltransferase. *Cell* 125: 497-508.
 32. Etchegaray, J. P., Lee, C., Wade, P. A., Reppert, S. M. (2003) Rhythmic histone acetylation underlies transcription in the mammalian circadian clock. *Nature* 421: 177-182.
 33. Ripperger, J. A., Schibler, U. (2006) Rhythmic CLOCK-BMAL1 binding to multiple E-box motifs drives circadian Dbp transcription and chromatin transitions. *Nature Genetics* 38: 369-374.
 34. Lee, J., Lee, Y., Lee, M. J., Park, E., Kang, S. H., Chung, C. H., Lee, K. H., Kim, K. (2008) Dual modification of BMAL1 by SUMO2/3 and ubiquitin promotes

- circadian activation of the CLOCK/BMAL1 complex. *Molecular and Cellular Biology* 28: 6056-6065.
35. O'Neill, J. S., Reddy, A. B. (2011) Circadian clocks in human red blood cells. *Nature* 469: 498-503.
 36. Hall, A., Karplus, P. A., Poole, L. B. (2009) Typical 2-Cys peroxiredoxins--structures, mechanisms and functions. *The FEBS Journal* 276: 2469-2477.
 37. Mackey, S. R., Golden, S. S. (2007) Winding up the cyanobacterial circadian clock. *Trends Microbiol* 15: 381-388.
 38. Katayama, M., Kondo, T., Xiong, J., Golden, S. S. (2003) ldpA encodes an iron-sulfur protein involved in light-dependent modulation of the circadian period in the cyanobacterium *Synechococcus elongatus* PCC 7942. *J Bacteriol* 185: 1415-1422.
 39. Kutsuna, S., Kondo, T., Aoki, S., Ishiura, M. (1998) A period-extender gene, pex, that extends the period of the circadian clock in the cyanobacterium *Synechococcus* sp. strain PCC 7942. *J Bacteriol* 180: 2167-2174.
 40. Schmitz, O., Katayama, M., Williams, S. B., Kondo, T., Golden, S. S. (2000) CikA, a bacteriophytochrome that resets the cyanobacterial circadian clock. *Science* 289: 765-768.
 41. Ivleva, N. B., Bramlett, M. R., Lindahl, P. A., Golden, S. S. (2005) LdpA: A component of the circadian clock senses redox state of the cell. *Embo J* 24: 1202-1210.
 42. Takai, N., Ikeuchi, S., Manabe, K., Kutsuna, S. (2006) Expression of the circadian clock-related gene pex in cyanobacteria increases in darkness and is required to delay the clock. *J Biol Rhythms* 21: 235-244.

43. Arita, K., Hashimoto, H., Igari, K., Akaboshi, M., Kutsuna, S., Sato, M., Shimizu, T. (2007) Structural and biochemical characterization of a cyanobacterium circadian clock-modifier protein. *J Biol Chem* 282: 1128-1135.
44. Ivleva, N. B., Gao, T., LiWang, A. C., Golden, S. S. (2006) Quinone sensing by the circadian input kinase of the cyanobacterial circadian clock. *Proc Natl Acad Sci U S A* 103: 17468-17473.
45. Gao, T., Zhang, X., Ivleva, N. B., Golden, S. S., LiWang, A. (2007) NMR structure of the pseudo-receiver domain of CikA. *Protein Sci* 16: 465-475.
46. Liu, Y., Tsinoremas, N. F., Johnson, C. H., Lebedeva, N. V., Golden, S. S., Ishiura, M., Kondo, T. (1995) Circadian orchestration of gene expression in cyanobacteria. *Genes Dev* 9: 1469-1478.
47. Smith, R. M., Williams, S. B. (2006) Circadian rhythms in gene transcription imparted by chromosome compaction in the cyanobacterium *Synechococcus elongatus*. *Proc Natl Acad Sci U S A* 103: 8564-8569.
48. Iwasaki, H., Williams, S. B., Kitayama, Y., Ishiura, M., Golden, S. S., Kondo, T. (2000) A kaiC-interacting sensory histidine kinase, SasA, necessary to sustain robust circadian oscillation in cyanobacteria. *Cell* 101: 223-233.
49. Takai, N., Nakajima, M., Oyama, T., Kito, R., Sugita, C., Sugita, M., Kondo, T., Iwasaki, H. (2006) A KaiC-associating SasA-RpaA two-component regulatory system as a major circadian timing mediator in cyanobacteria. *Proc Natl Acad Sci U S A* 103: 12109-12114.
50. Robinson, V. L., Buckler, D. R., Stock, A. M. (2000) A tale of two components: A novel kinase and a regulatory switch. *Nature Structural Biology* 7: 626-633.
51. Dong, G., Yang, Q., Wang, Q., Kim, Y. I., Wood, T. L., Osteryoung, K. W., van Oudenaarden, A., Golden, S. S. (2010) Elevated ATPase activity of KaiC applies

- a circadian checkpoint on cell division in *Synechococcus elongatus*. *Cell* 140: 529-539.
52. Taniguchi, Y., Katayama, M., Ito, R., Takai, N., Kondo, T., Oyama, T. (2007) *labA*: A novel gene required for negative feedback regulation of the cyanobacterial circadian clock protein KaiC. *Genes Dev* 21: 60-70.
 53. Ishiura, M., Kutsuna, S., Aoki, S., Iwasaki, H., Andersson, C. R., Tanabe, A., Golden, S. S., Johnson, C. H., Kondo, T. (1998) Expression of a gene cluster *kaiABC* as a circadian feedback process in cyanobacteria. *Science* 281: 1519-1523.
 54. Xu, Y., Mori, T., Johnson, C. H. (2003) Cyanobacterial circadian clockwork: Roles of KaiA, KaiB and the *kaiBC* promoter in regulating KaiC. *Embo J* 22: 2117-2126.
 55. Nakahira, Y., Katayama, M., Miyashita, H., Kutsuna, S., Iwasaki, H., Oyama, T., Kondo, T. (2004) Global gene repression by KaiC as a master process of prokaryotic circadian system. *Proc Natl Acad Sci U S A* 101: 881-885.
 56. Ditty, J. L., Canales, S. R., Anderson, B. E., Williams, S. B., Golden, S. S. (2005) Stability of the *Synechococcus elongatus* PCC 7942 circadian clock under directed anti-phase expression of the *kai* genes. *Microbiology* 151: 2605-2613.
 57. Tomita, J., Nakajima, M., Kondo, T., Iwasaki, H. (2005) No transcription-translation feedback in circadian rhythm of KaiC phosphorylation. *Science* 307: 251-254.
 58. Nakajima, M., Imai, K., Ito, H., Nishiwaki, T., Murayama, Y., Iwasaki, H., Oyama, T., Kondo, T. (2005) Reconstitution of circadian oscillation of cyanobacterial KaiC phosphorylation in vitro. *Science* 308: 414-415.

59. Nishiwaki, T., Satomi, Y., Nakajima, M., Lee, C., Kiyohara, R., Kageyama, H., Kitayama, Y., Temamoto, M., Yamaguchi, A., Hijikata, A., *et al.* (2004) Role of KaiC phosphorylation in the circadian clock system of *Synechococcus elongatus* PCC 7942. *Proc Natl Acad Sci U S A* 101: 13927-13932.
60. Xu, Y., Mori, T., Pattanayek, R., Pattanayek, S., Egli, M., Johnson, C. H. (2004) Identification of key phosphorylation sites in the circadian clock protein KaiC by crystallographic and mutagenetic analyses. *Proc Natl Acad Sci U S A* 101: 13933-13938.
61. Nishiwaki, T., Iwasaki, H., Ishiura, M., Kondo, T. (2000) Nucleotide binding and autophosphorylation of the clock protein KaiC as a circadian timing process of cyanobacteria. *Proc Natl Acad Sci U S A* 97: 495-499.
62. Terauchi, K., Kitayama, Y., Nishiwaki, T., Miwa, K., Murayama, Y., Oyama, T., Kondo, T. (2007) ATPase activity of KaiC determines the basic timing for circadian clock of cyanobacteria. *Proc Natl Acad Sci U S A* 104: 16377-16381.
63. Iwasaki, H., Nishiwaki, T., Kitayama, Y., Nakajima, M., Kondo, T. (2002) KaiA-stimulated KaiC phosphorylation in circadian timing loops in cyanobacteria. *Proc Natl Acad Sci U S A* 99: 15788-15793.
64. Williams, S. B., Vakonakis, I., Golden, S. S., LiWang, A. C. (2002) Structure and function from the circadian clock protein KaiA of *Synechococcus elongatus*: a potential clock input mechanism. *Proc Natl Acad Sci U S A* 99: 15357-15362.
65. Rust, M. J., Markson, J. S., Lane, W. S., Fisher, D. S., O'Shea, E. K. (2007) Ordered phosphorylation governs oscillation of a three-protein circadian clock. *Science* 318: 809-812.

66. Nishiwaki, T., Satomi, Y., Kitayama, Y., Terauchi, K., Kiyohara, R., Takao, T., Kondo, T. (2007) A sequential program of dual phosphorylation of KaiC as a basis for circadian rhythm in cyanobacteria. *Embo J* 26: 4029-4037.
67. Murayama, Y., Oyama, T., Kondo, T. (2008) Regulation of circadian clock gene expression by phosphorylation states of KaiC in cyanobacteria. *J Bacteriol* 190: 1691-1698.
68. Kitayama, Y., Nishiwaki, T., Terauchi, K., Kondo, T. (2008) Dual KaiC-based oscillations constitute the circadian system of cyanobacteria. *Genes Dev* 22: 1513-1521.
69. Kageyama, H., Nishiwaki, T., Nakajima, M., Iwasaki, H., Oyama, T., Kondo, T. (2006) Cyanobacterial circadian pacemaker: Kai protein complex dynamics in the KaiC phosphorylation cycle in vitro. *Mol Cell* 23: 161-171.
70. Mori, T., Williams, D. R., Byrne, M. O., Qin, X., Egli, M., McHaourab, H. S., Stewart, P. L., Johnson, C. H. (2007) Elucidating the ticking of an in vitro circadian clockwork. *PLoS Biol* 5: e93.
71. Ye, S., Vakonakis, I., Ioerger, T. R., LiWang, A. C., Sacchettini, J. C. (2004) Crystal structure of circadian clock protein KaiA from *Synechococcus elongatus*. *J Biol Chem* 279: 20511-20518.
72. Iwase, R., Imada, K., Hayashi, F., Uzumaki, T., Morishita, M., Onai, K., Furukawa, Y., Namba, K., Ishiura, M. (2005) Functionally important substructures of circadian clock protein KaiB in a unique tetramer complex. *J Biol Chem* 280: 43141-43149.
73. Pattanayek, R., Wang, J., Mori, T., Xu, Y., Johnson, C. H., Egli, M. (2004) Visualizing a circadian clock protein: crystal structure of KaiC and functional insights. *Mol Cell* 15: 375-388.

74. Uzumaki, T., Fujita, M., Nakatsu, T., Hayashi, F., Shibata, H., Itoh, N., Kato, H., Ishiura, M. (2004) Crystal structure of the C-terminal clock-oscillator domain of the cyanobacterial KaiA protein. *Nat Struct Mol Biol* 11: 623-631.
75. Vakonakis, I., Sun, J., Wu, T., Holzenburg, A., Golden, S. S., LiWang, A. C. (2004) NMR structure of the KaiC-interacting C-terminal domain of KaiA, a circadian clock protein: implications for KaiA-KaiC interaction. *Proc Natl Acad Sci U S A* 101: 1479-1484.
76. Garces, R. G., Wu, N., Gillon, W., Pai, E. F. (2004) Anabaena circadian clock proteins KaiA and KaiB reveal a potential common binding site to their partner KaiC. *Embo J* 23: 1688-1698.
77. Hitomi, K., Oyama, T., Han, S., Arvai, A. S., Getzoff, E. D. (2005) Tetrameric architecture of the circadian clock protein KaiB. A novel interface for intermolecular interactions and its impact on the circadian rhythm. *J Biol Chem* 280: 19127-19135.
78. Pattanayek, R., Williams, D. R., Pattanayek, S., Xu, Y., Mori, T., Johnson, C. H., Stewart, P. L., Egli, M. (2006) Analysis of KaiA-KaiC protein interactions in the cyano-bacterial circadian clock using hybrid structural methods. *Embo J* 25: 2017-2028.
79. Leipe, D. D., Aravind, L., Grishin, N. V., Koonin, E. V. (2000) The bacterial replicative helicase DnaB evolved from a RecA duplication. *Genome Research* 10: 5-16.
80. Hayashi, F., Suzuki, H., Iwase, R., Uzumaki, T., Miyake, A., Shen, J. R., Imada, K., Furukawa, Y., Yonekura, K., Namba, K., *et al.* (2003) ATP-induced hexameric ring structure of the cyanobacterial circadian clock protein KaiC. *Genes Cells* 8: 287-296.

81. Woelfle, M. A., Xu, Y., Qin, X., Johnson, C. H. (2007) Circadian rhythms of superhelical status of DNA in cyanobacteria. *Proc Natl Acad Sci U S A* 104: 18819-18824.
82. Hayashi, F., Iwase, R., Uzumaki, T., Ishiura, M. (2006) Hexamerization by the N-terminal domain and intersubunit phosphorylation by the C-terminal domain of cyanobacterial circadian clock protein KaiC. *Biochem Biophys Res Commun* 348: 864-872.
83. Hayashi, F., Itoh, N., Uzumaki, T., Iwase, R., Tsuchiya, Y., Yamakawa, H., Morishita, M., Onai, K., Itoh, S., Ishiura, M. (2004) Roles of two ATPase-motif-containing domains in cyanobacterial circadian clock protein KaiC. *J Biol Chem* 279: 52331-52337.
84. Mildvan, A. S. (1997) Mechanisms of signaling and related enzymes. *Proteins* 29: 401-416.
85. Vakonakis, I., LiWang, A. C. (2004) Structure of the C-terminal domain of the clock protein KaiA in complex with a KaiC-derived peptide: Implications for KaiC regulation. *Proc Natl Acad Sci U S A* 101: 10925-10930.
86. Kim, Y. I., Dong, G., Carruthers, C. W., Jr., Golden, S. S., LiWang, A. (2008) The day/night switch in KaiC, a central oscillator component of the circadian clock of cyanobacteria. *Proc Natl Acad Sci U S A* 105: 12825-12830.
87. Pattanayek, R., Williams, D. R., Pattanayek, S., Mori, T., Johnson, C. H., Stewart, P. L., Egli, M. (2008) Structural model of the circadian clock KaiB-KaiC complex and mechanism for modulation of KaiC phosphorylation. *Embo J* 27: 1767-1778.
88. Johnson, C. H. (2007) Bacterial circadian programs. *Cold Spring Harb Symp Quant Biol* 72: 395-404.

89. Pattanayek, R., Mori, T., Xu, Y., Pattanayek, S., Johnson, C. H., Egli, M. (2009) Structures of KaiC circadian clock mutant proteins: a new phosphorylation site at T426 and mechanisms of kinase, ATPase and phosphatase. *PLoS One* 4: e7529.
90. Qin, X., Byrne, M., Mori, T., Zou, P., Williams, D. R., McHaourab, H., Johnson, C. H. (2010) Intermolecular associations determine the dynamics of the circadian KaiABC oscillator. *Proc Natl Acad Sci U S A* 107: 14805-14810.
91. Monod, J., Wyman, J., Changeux, J. P. (1965) On the nature of allosteric Transitions: A plausible Model. *J Mol Biol* 12: 88-118.
92. Koshland, D. E., Jr., Nemethy, G., Filmer, D. (1966) Comparison of experimental binding data and theoretical models in proteins containing subunits. *Biochemistry* 5: 365-385.
93. Pan, P., Woehl, E., Dunn, M. F. (1997) Protein architecture, dynamics and allostery in tryptophan synthase channeling. *Trends in Biochemical Sciences* 22: 22-27.
94. Birnbaumer, L., Abramowitz, J., Brown, A. M. (1990) Receptor-effector coupling by G proteins. *Biochimica et Biophysica Acta* 1031: 163-224.
95. Ptashne, M., Gann, A. (1998) Imposing specificity by localization: mechanism and evolvability. *Curr Biol* 8: R812-822.
96. Popovych, N., Sun, S., Ebright, R. H., Kalodimos, C. G. (2006) Dynamically driven protein allostery. *Nat Struct Mol Biol* 13: 831-838.
97. Cooper, A., Dryden, D. T. F. (1984) Allostery without conformational change - a plausible model. *Eur. Biophys. J. Biophys. Lett.* 11: 103-109.
98. Wand, A. J. (2001) Dynamic activation of protein function: A view emerging from NMR spectroscopy. *Nature Structural Biology* 8: 926-931.

99. Brown, A. M., Crothers, D. M. (1989) Modulation of the stability of a gene-regulatory protein dimer by DNA and cAMP. *Proc Natl Acad Sci U S A* 86: 7387-7391.
100. Passner, J. M., Schultz, S. C., Steitz, T. A. (2000) Modeling the cAMP-induced allosteric transition using the crystal structure of CAP-cAMP at 2.1 Å resolution. *J Mol Biol* 304: 847-859.
101. Harman, J. G. (2001) Allosteric regulation of the cAMP receptor protein. *Biochimica et Biophysica Acta* 1547: 1-17.
102. Koshland, D. E., Jr. (1996) The structural basis of negative cooperativity: Receptors and enzymes. *Current Opinion in Structural Biology* 6: 757-761.
103. Anderson, A. C., O'Neil, R. H., DeLano, W. L., Stroud, R. M. (1999) The structural mechanism for half-the-sites reactivity in an enzyme, thymidylate synthase, involves a relay of changes between subunits. *Biochemistry* 38: 13829-13836.
104. Leslie, A. G., Wonacott, A. J. (1984) Structural evidence for ligand-induced sequential conformational changes in glyceraldehyde 3-phosphate dehydrogenase. *J Mol Biol* 178: 743-772.
105. Hampele, I. C., D'Arcy, A., Dale, G. E., Kostrewa, D., Nielsen, J., Oefner, C., Page, M. G., Schonfeld, H. J., Stuber, D., Then, R. L. (1997) Structure and function of the dihydropteroate synthase from *Staphylococcus aureus*. *J Mol Biol* 268: 21-30.
106. Heyduk, E., Heyduk, T., Lee, J. C. (1992) Intersubunit communications in *Escherichia coli* cyclic AMP receptor protein: studies of the ligand binding domain. *Biochemistry* 31: 3682-3688.

107. Henzler-Wildman, K., Kern, D. (2007) Dynamic personalities of proteins. *Nature* 450: 964-972.
108. Petit, C. M., Zhang, J., Sapienza, P. J., Fuentes, E. J., Lee, A. L. (2009) Hidden dynamic allostery in a PDZ domain. *Proc Natl Acad Sci U S A* 106: 18249-18254.
109. Sprangers, R., Kay, L. E. (2007) Quantitative dynamics and binding studies of the 20S proteasome by NMR. *Nature* 445: 618-622.
110. van Zon, J. S., Lubensky, D. K., Altena, P. R., Wolde, P. R. (2007) An allosteric model of circadian KaiC phosphorylation. *Proc Natl Acad Sci U S A* 104: 7420-7425.
111. Mittermaier, A. K., Kay, L. E. (2009) Observing biological dynamics at atomic resolution using NMR. *Trends in Biochemical Sciences* 34: 601-611.
112. Tolman, J. R., Ruan, K. (2006) NMR residual dipolar couplings as probes of biomolecular dynamics. *Chemical Reviews* 106: 1720-1736.
113. Palmer, A. G., 3rd (2004) NMR characterization of the dynamics of biomacromolecules. *Chemical Reviews* 104: 3623-3640.
114. Wagner, G., Wuthrich, K (1978) Internal motions in globular proteins. *Trends in Biochemical Sciences* 3: 227-230.
115. Allerhand, A., Doddrell, D., Glushko, V., Cochran, D. W., Wenkert, E., Lawson, P. J., Gurd, F. R. (1971) Conformation and segmental motion of native and denatured ribonuclease A in solution: Application of natural-abundance carbon-13 partially relaxed Fourier transform nuclear magnetic resonance. *Journal of the American Chemical Society* 93: 544-546.

116. Kovacs, H., Moskau, D., Spraul, M. (2005) Cryogenically cooled probes: A leap in NMR technology. *Progress in Nuclear Magnetic Resonance Spectroscopy* 46: 131-155.
117. Tugarinov, V., Hwang, P. M., Ollerenshaw, J. E., Kay, L. E. (2003) Cross-correlated relaxation enhanced ^1H - ^{13}C NMR spectroscopy of methyl groups in very high molecular weight proteins and protein complexes. *Journal of the American Chemical Society* 125: 10420-10428.
118. Gardner, K. H., Rosen, M. K., Kay, L. E. (1997) Global folds of highly deuterated, methyl-protonated proteins by multidimensional NMR. *Biochemistry* 36: 1389-1401.
119. Rosen, M. K., Gardner, K. H., Willis, R. C., Parris, W. E., Pawson, T., Kay, L. E. (1996) Selective methyl group protonation of perdeuterated proteins. *J Mol Biol* 263: 627-636.
120. Mueller, G. A., Choy, W. Y., Yang, D., Forman-Kay, J. D., Venters, R. A., Kay, L. E. (2000) Global folds of proteins with low densities of NOEs using residual dipolar couplings: application to the 370-residue maltodextrin-binding protein. *J Mol Biol* 300: 197-212.
121. Nicholson, L. K., Kay, L. E., Baldisseri, D. M., Arango, J., Young, P. E., Bax, A., Torchia, D. A. (1992) Dynamics of methyl groups in proteins as studied by proton-detected ^{13}C NMR spectroscopy. Application to the leucine residues of staphylococcal nuclease. *Biochemistry* 31: 5253-5263.
122. Mulder, F. A., Mittermaier, A., Hon, B., Dahlquist, F. W., Kay, L. E. (2001) Studying excited states of proteins by NMR spectroscopy. *Nature Structural Biology* 8: 932-935.

123. Sprangers, R., Velyvis, A., Kay, L. E. (2007) Solution NMR of supramolecular complexes: providing new insights into function. *Nature Methods* 4: 697-703.
124. Gross, J. D., Gelev, V. M., Wagner, G. (2003) A sensitive and robust method for obtaining intermolecular NOEs between side chains in large protein complexes. *J Biomol NMR* 25: 235-242.
125. Choy, W. Y., Shortle, D., Kay, L. E. (2003) Side chain dynamics in unfolded protein states: An NMR based ²H spin relaxation study of Δ 131 Δ . *Journal of the American Chemical Society* 125: 1748-1758.
126. Serber, Z., Straub, W., Corsini, L., Nomura, A. M., Shimba, N., Craik, C. S., Ortiz de Montellano, P., Dotsch, V. (2004) Methyl groups as probes for proteins and complexes in in-cell NMR experiments. *Journal of the American Chemical Society* 126: 7119-7125.
127. Tugarinov, V., Kanelis, V., Kay, L. E. (2006) Isotope labeling strategies for the study of high-molecular-weight proteins by solution NMR spectroscopy. *Nature Protocols* 1: 749-754.
128. Pervushin, K., Riek, R., Wider, G., Wuthrich, K. (1997) Attenuated T₂ relaxation by mutual cancellation of dipole-dipole coupling and chemical shift anisotropy indicates an avenue to NMR structures of very large biological macromolecules in solution. *Proc Natl Acad Sci U S A* 94: 12366-12371.
129. Pervushin, K. V., Wider, G., Riek, R., Wuthrich, K. (1999) The 3D NOESY-[(¹H),(¹⁵N),(¹H)]-ZQ-TROSY NMR experiment with diagonal peak suppression. *Proc Natl Acad Sci U S A* 96: 9607-9612.
130. Ollerenshaw, J. E., Tugarinov, V., Skrynnikov, N. R., Kay, L. E. (2005) Comparison of ¹³CH₃, ¹³CH₂D, and ¹³CHD₂ methyl labeling strategies in proteins. *J Biomol NMR* 33: 25-41.

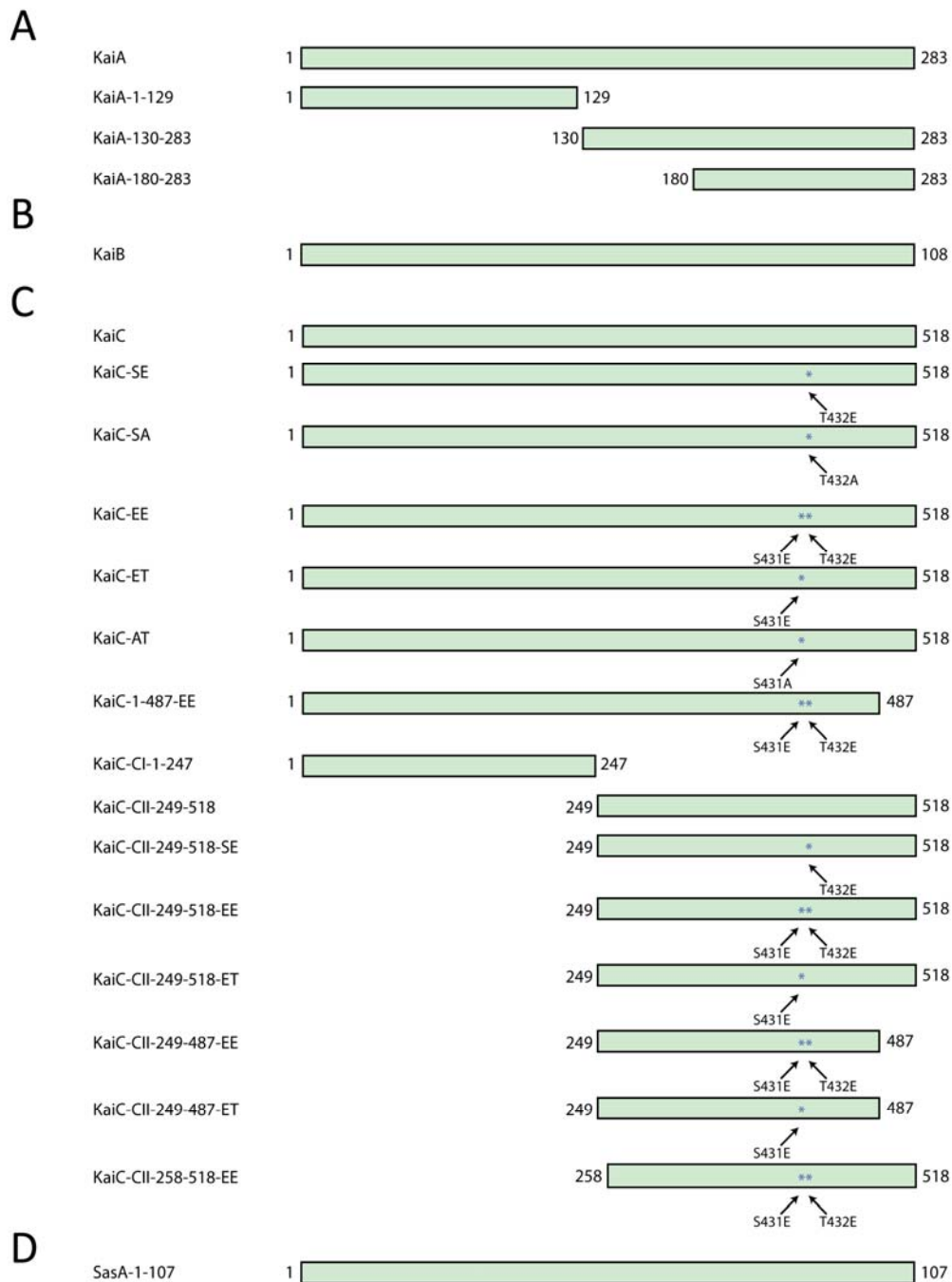
131. Sprangers, R., Gribun, A., Hwang, P. M., Houry, W. A., Kay, L. E. (2005) Quantitative NMR spectroscopy of supramolecular complexes: Dynamic side pores in ClpP are important for product release. *Proc Natl Acad Sci U S A* 102: 16678-16683.
132. Tzeng, S. R., Kalodimos, C. G. (2009) Dynamic activation of an allosteric regulatory protein. *Nature* 462: 368-372.
133. Wang, J., Lee, B., Cai, S., Fukui, L., Hu, W., Chen, Y. (2009) Conformational transition associated with E1-E2 interaction in small ubiquitin-like modifications. *J Biol Chem* 284: 20340-20348.
134. Niethammer, M., Valtschanoff, J. G., Kapoor, T. M., Allison, D. W., Weinberg, R. J., Craig, A. M., Sheng, M. (1998) CRIPT, a novel postsynaptic protein that binds to the third PDZ domain of PSD-95/SAP90. *Neuron* 20: 693-707.
135. Murayama, Y., Mukaiyama, A., Imai, K., Onoue, Y., Tsunoda, A., Nohara, A., Ishida, T., Maeda, Y., Terauchi, K., Kondo, T., *et al.* (2011) Tracking and visualizing the circadian ticking of the cyanobacterial clock protein KaiC in solution. *Embo J* 30 : 68-78
136. Kivimae, S., Saez, L., Young, M. W. (2008) Activating PER repressor through a DBT-directed phosphorylation switch. *PLoS Biol* 6: e183.
137. Gardner, K. H., Kay, L. E. (1998) The use of ²H, ¹³C, ¹⁵N multidimensional NMR to study the structure and dynamics of proteins. *Annual Review of Biophysics and Biomolecular Structure* 27: 357-406.
138. Ollerenshaw, J. E., Lidar, D. A., Kay, L. E. (2003) Magnetic resonance realization of decoherence-free quantum computation. *Physical Review Letters* 91: 217904.

139. Goto, N. K., Gardner, K. H., Mueller, G. A., Willis, R. C., Kay, L. E. (1999) A robust and cost-effective method for the production of Val, Leu, Ile (δ 1) methyl-protonated ^{15}N -, ^{13}C -, ^2H -labeled proteins. *J Biomol NMR* 13: 369-374.
140. Kitayama, Y., Iwasaki, H., Nishiwaki, T., Kondo, T. (2003) KaiB functions as an attenuator of KaiC phosphorylation in the cyanobacterial circadian clock system. *Embo J* 22: 2127-2134.
141. Xu, Y., Mori, T., Qin, X., Yan, H., Egli, M., Johnson, C. H. (2009) Intramolecular regulation of phosphorylation status of the circadian clock protein KaiC. *PLoS One* 4: e7509.
142. Iwasaki, H., Taniguchi, Y., Ishiura, M., Kondo, T. (1999) Physical interactions among circadian clock proteins KaiA, KaiB and KaiC in cyanobacteria. *Embo J* 18: 1137-1145.
143. Mutoh, R., Mino, H., Murakami, R., Uzumaki, T., Takabayashi, A., Ishii, K., Ishiura, M. (2010) Direct interaction between KaiA and KaiB revealed by a site-directed spin labeling electron spin resonance analysis. *Genes Cells* 15: 269-280
144. Iwase, R., Imada, K., Hayashi, F., Uzumaki, T., Namba, K., Ishiura, M. (2004) Crystallization and preliminary crystallographic analysis of the circadian clock protein KaiB from the thermophilic cyanobacterium *Thermosynechococcus elongatus* BP-1. *Acta Crystallogr D Biol Crystallogr* 60: 727-729.
145. Kageyama, H., Kondo, T., Iwasaki, H. (2003) Circadian formation of clock protein complexes by KaiA, KaiB, KaiC, and SasA in cyanobacteria. *J Biol Chem* 278: 2388-2395.
146. Vijayan, V., Zuzow, R., O'Shea, E. K. (2009) Oscillations in supercoiling drive circadian gene expression in cyanobacteria. *Proc Natl Acad Sci U S A* 106: 22564-22568.

147. Mori, T., Binder, B., Johnson, C. H. (1996) Circadian gating of cell division in cyanobacteria growing with average doubling times of less than 24 hours. *Proc Natl Acad Sci U S A* 93: 10183-10188.
148. Yang, Q., Pando, B. F., Dong, G., Golden, S. S., van Oudenaarden, A. (2010) Circadian gating of the cell cycle revealed in single cyanobacterial cells. *Science* 327: 1522-1526.
149. Taniguchi, Y., Takai, N., Katayama, M., Kondo, T., Oyama, T. (2010) Three major output pathways from the KaiABC-based oscillator cooperate to generate robust circadian kaiBC expression in cyanobacteria. *Proc Natl Acad Sci U S A* 107: 3263-3268.
150. Vakonakis, I., Klewer, D. A., Williams, S. B., Golden, S. S., LiWang, A. C. (2004) Structure of the N-terminal domain of the circadian clock-associated histidine kinase SasA. *J Mol Biol* 342: 9-17.
151. Dong, G., Kim, Y. I., Golden, S. S. (2010) Simplicity and complexity in the cyanobacterial circadian clock mechanism. *Current Opinion in Genetics & Development* 20: 619-625.
152. Rust, M. J., Golden, S. S., O'Shea, E. K. (2011) Light-driven changes in energy metabolism directly entrain the cyanobacterial circadian oscillator. *Science* 331: 220-223.

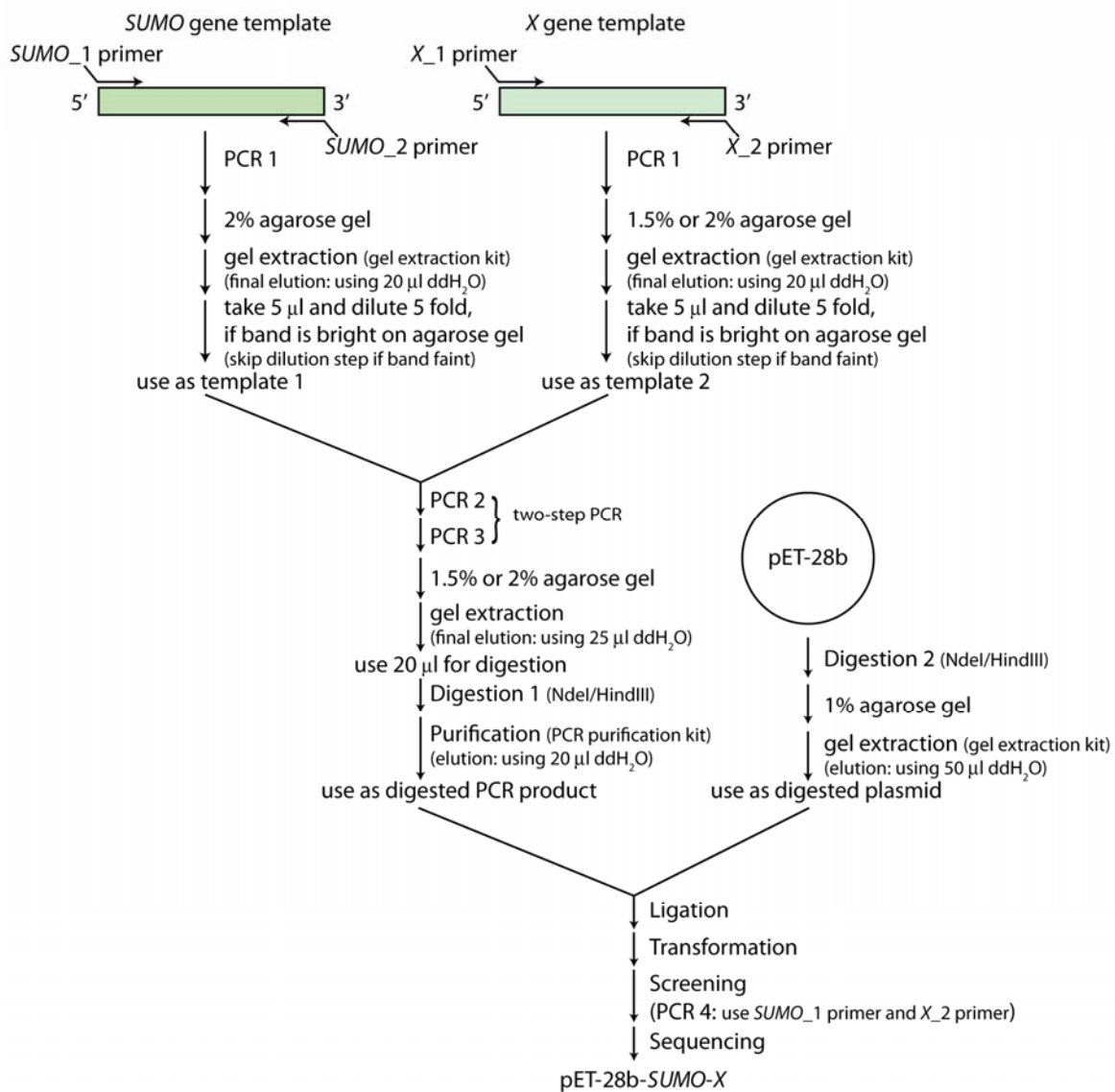
APPENDIX A

DIAGRAMS

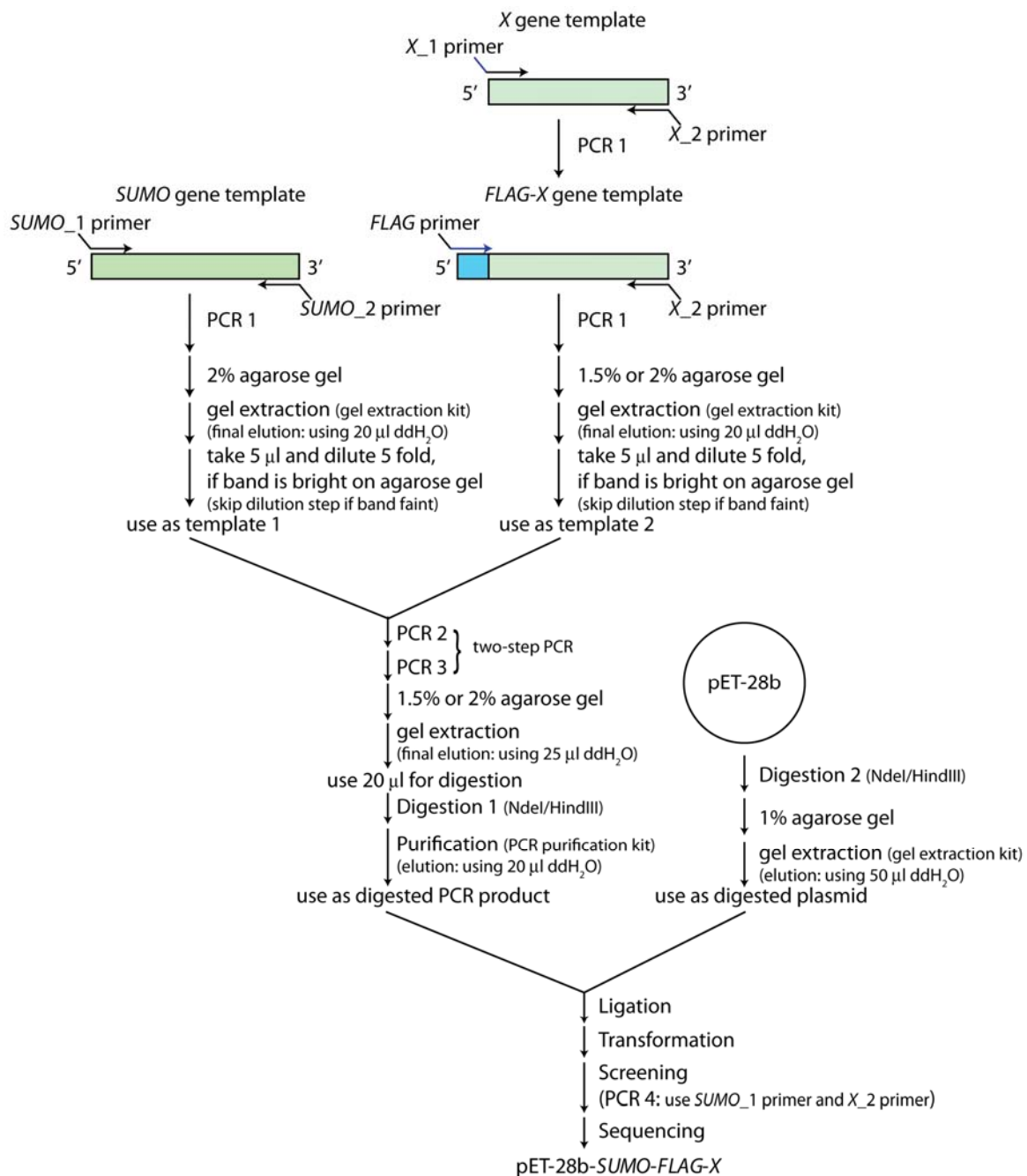


A-1. Schematic representation of full-length, fragments or mutants of A) KaiA, B) KaiB, C) KaiC, and D) SasA.

Cloning: pET-28b-SUMO-X

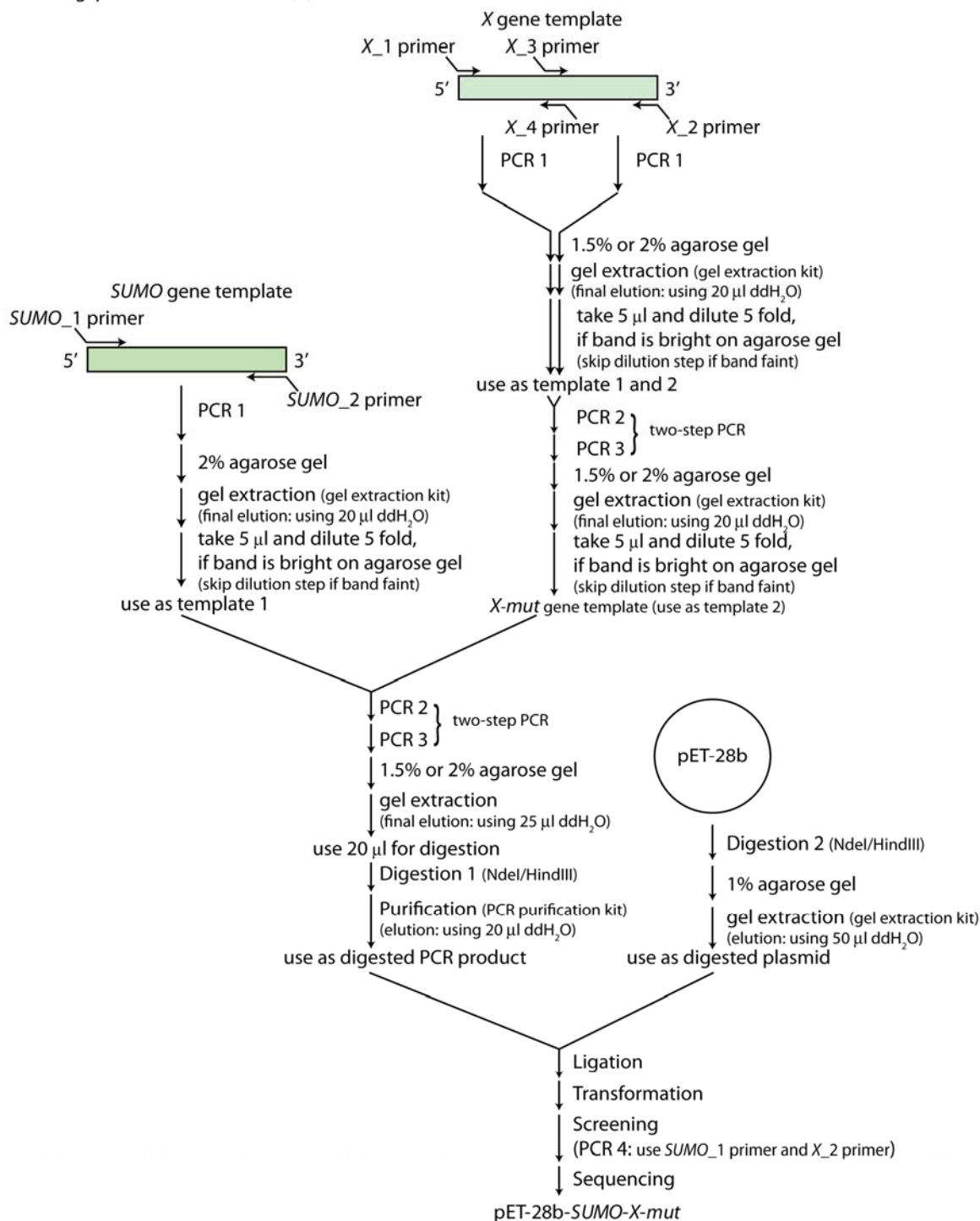


A-2. Diagram for cloning pET-28b-SUMO-X.



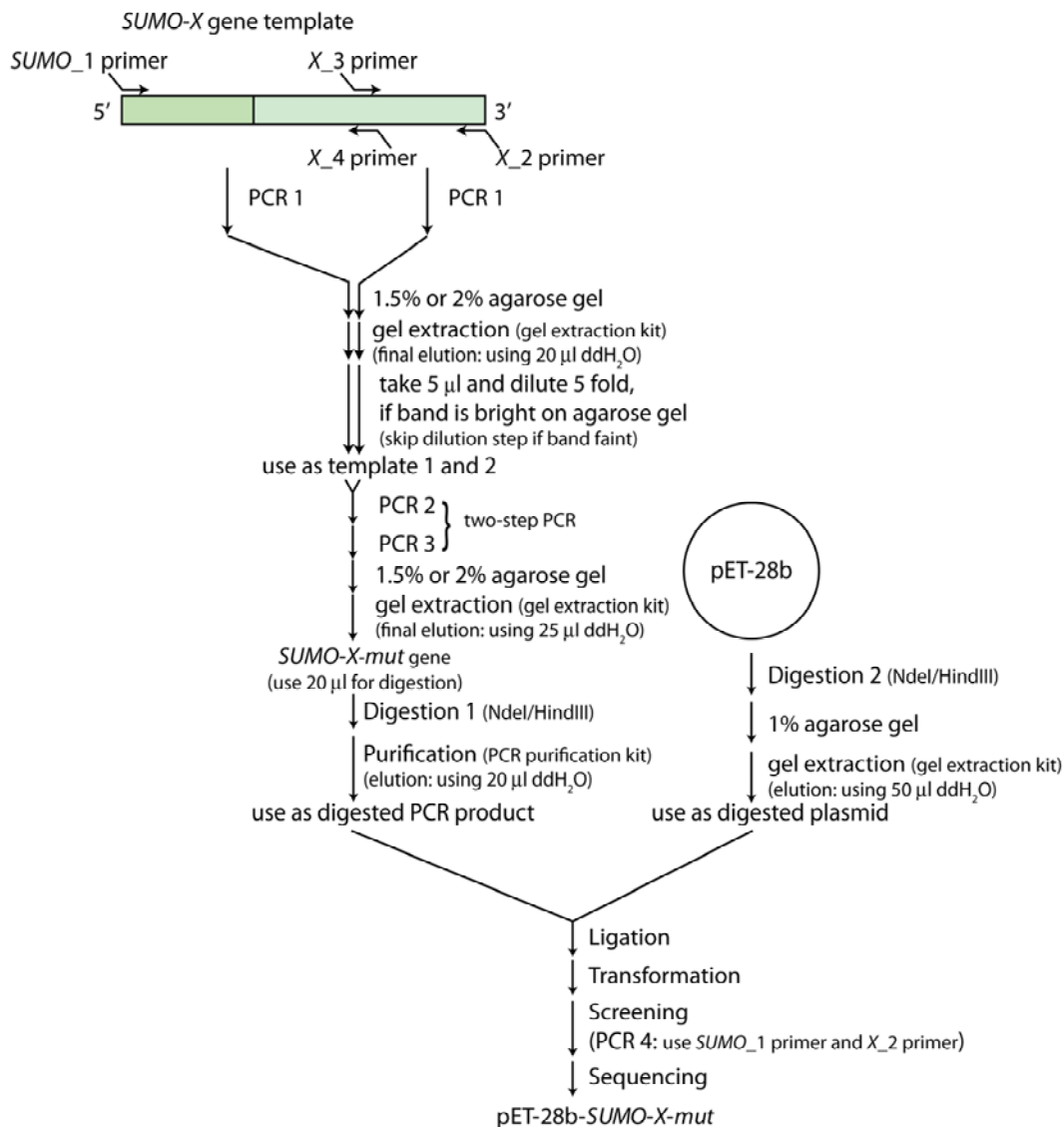
A-3. Diagram for cloning pET-28b-SUMO-FLAG-X.

Cloning: pET-28b-SUMO-X-mut (1)

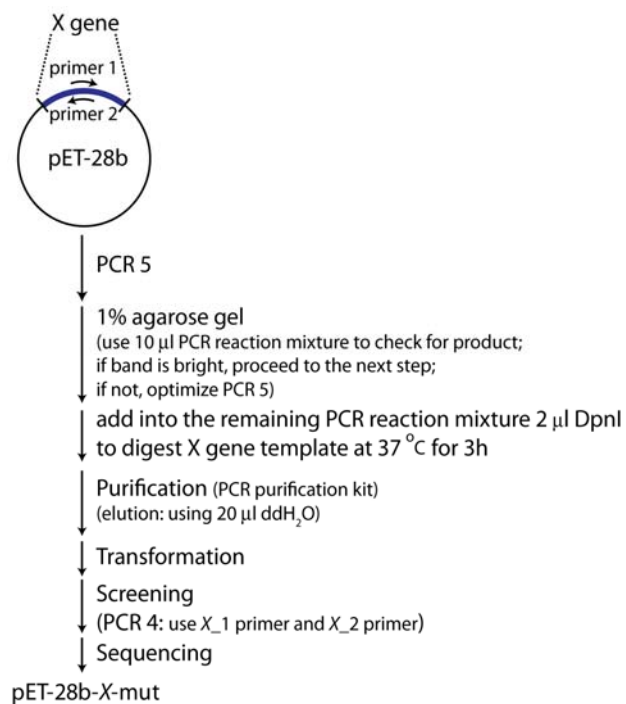


A-4. Diagram for cloning pET-28b-SUMO-X-mut by mutation X followed by splicing SUMO and X-mut. X-mut stands for mutation of X.

Cloning: pET-28b-SUMO-X-mut (2)

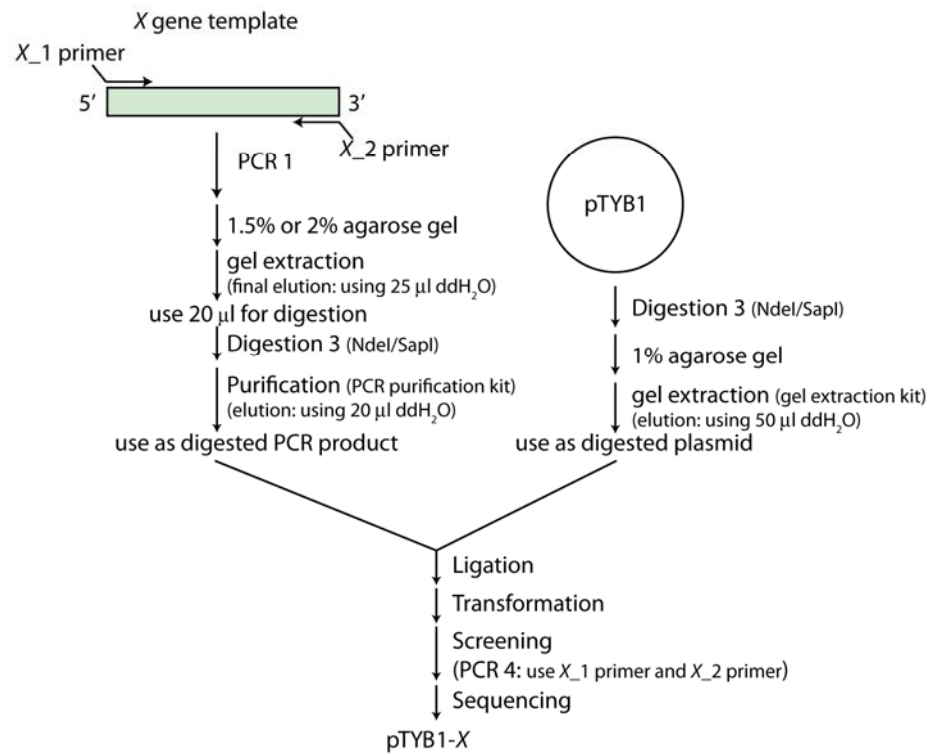


A-5. Diagram for cloning pET-28b-SUMO-X-mut by using SUMO-X as template.



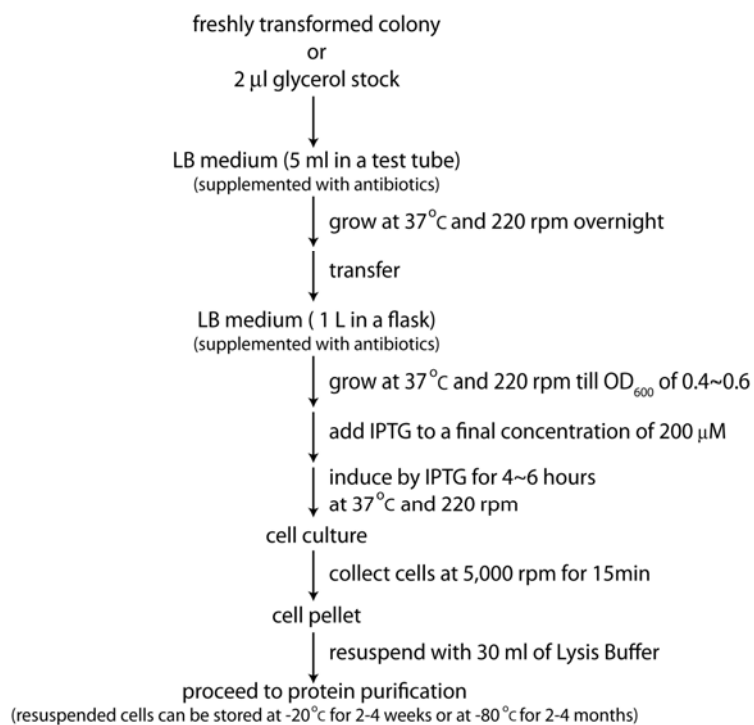
A-6. Diagram for cloning pET-28b-SUMO-X-mut by using QuickChange method.

Cloning: pTYB1-ThKaiA-1-129

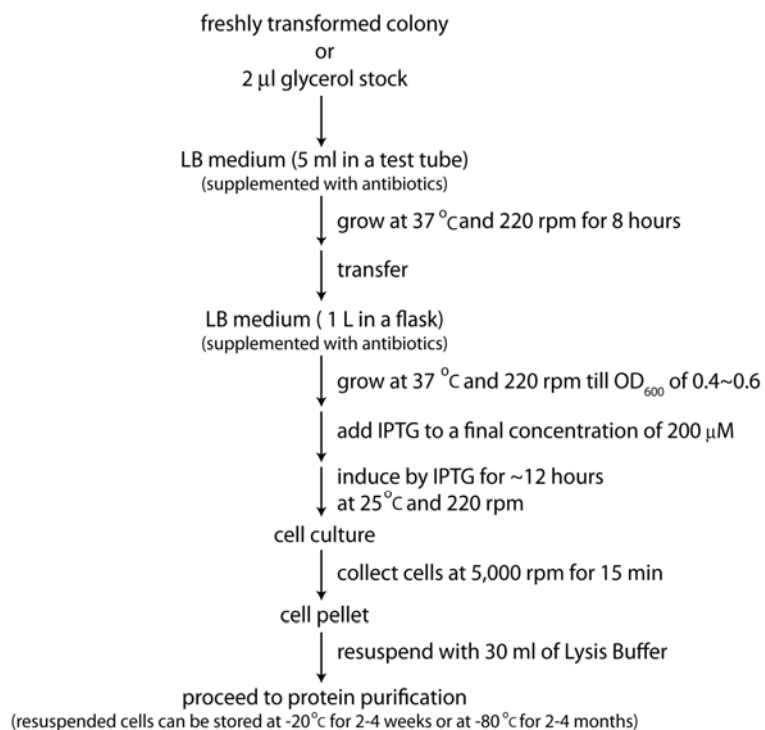


A-7. Diagram for cloning pTYB1-KaiA-1-129.

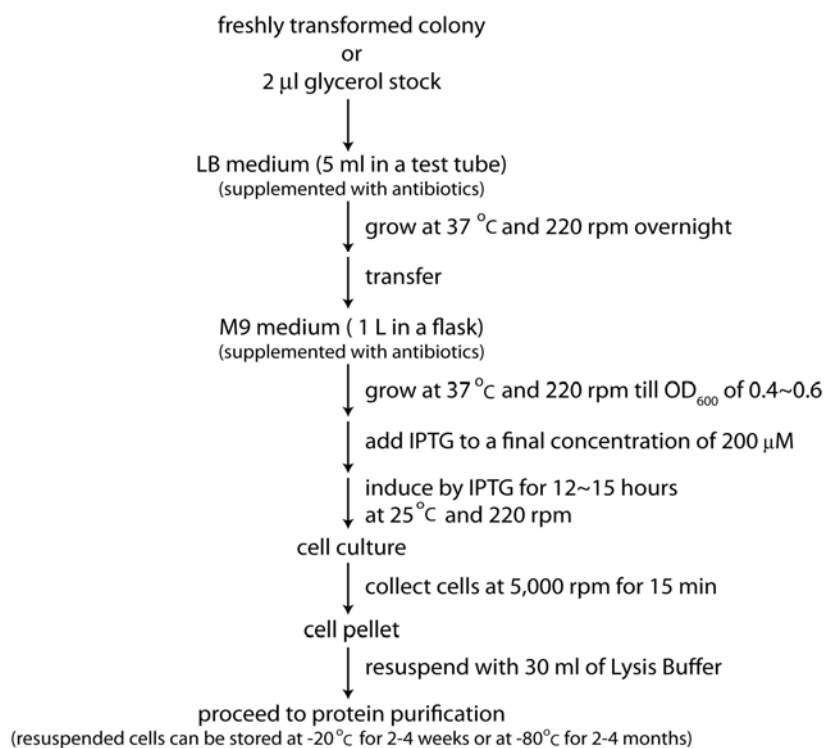
LB 1



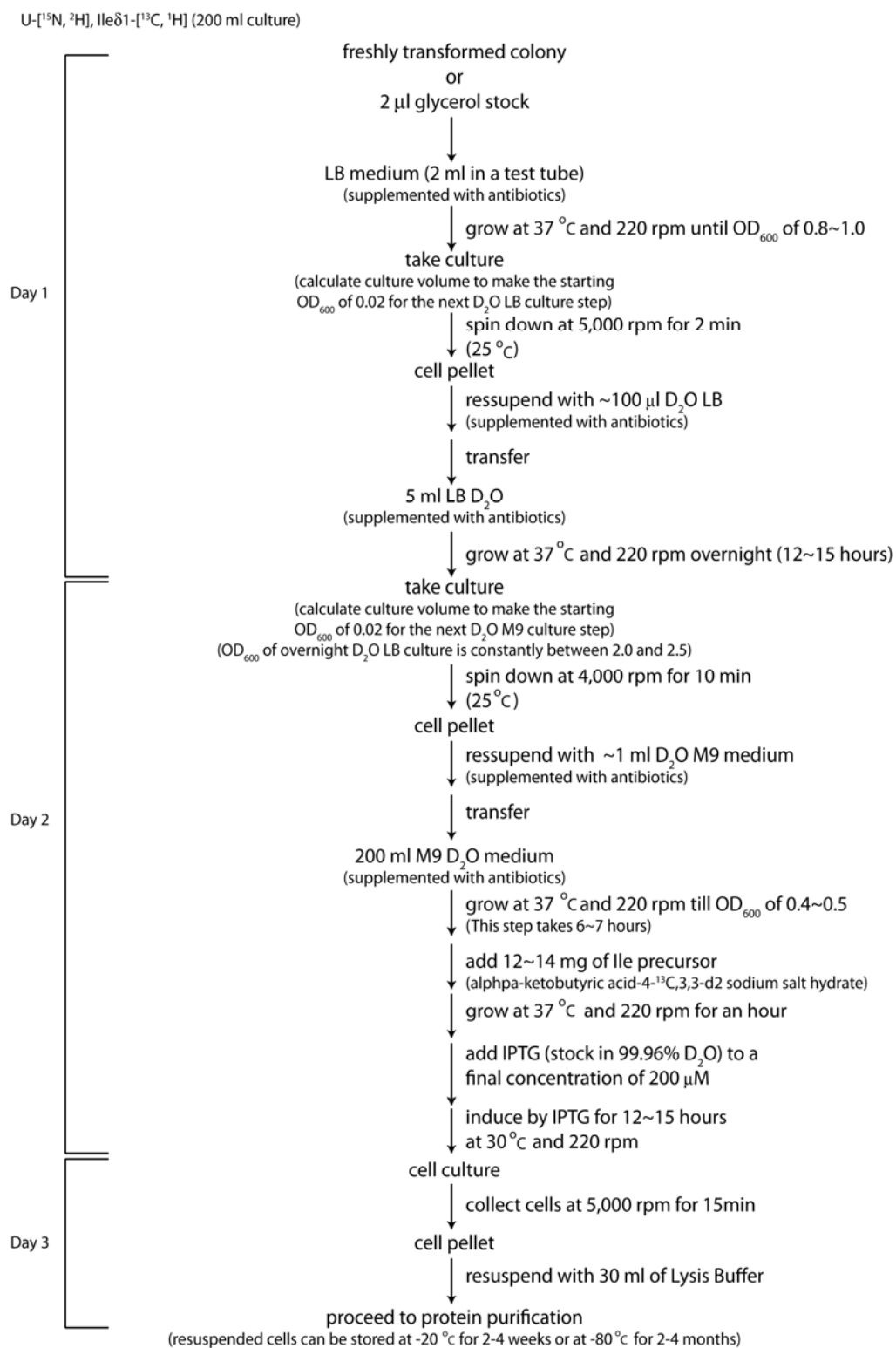
LB 2



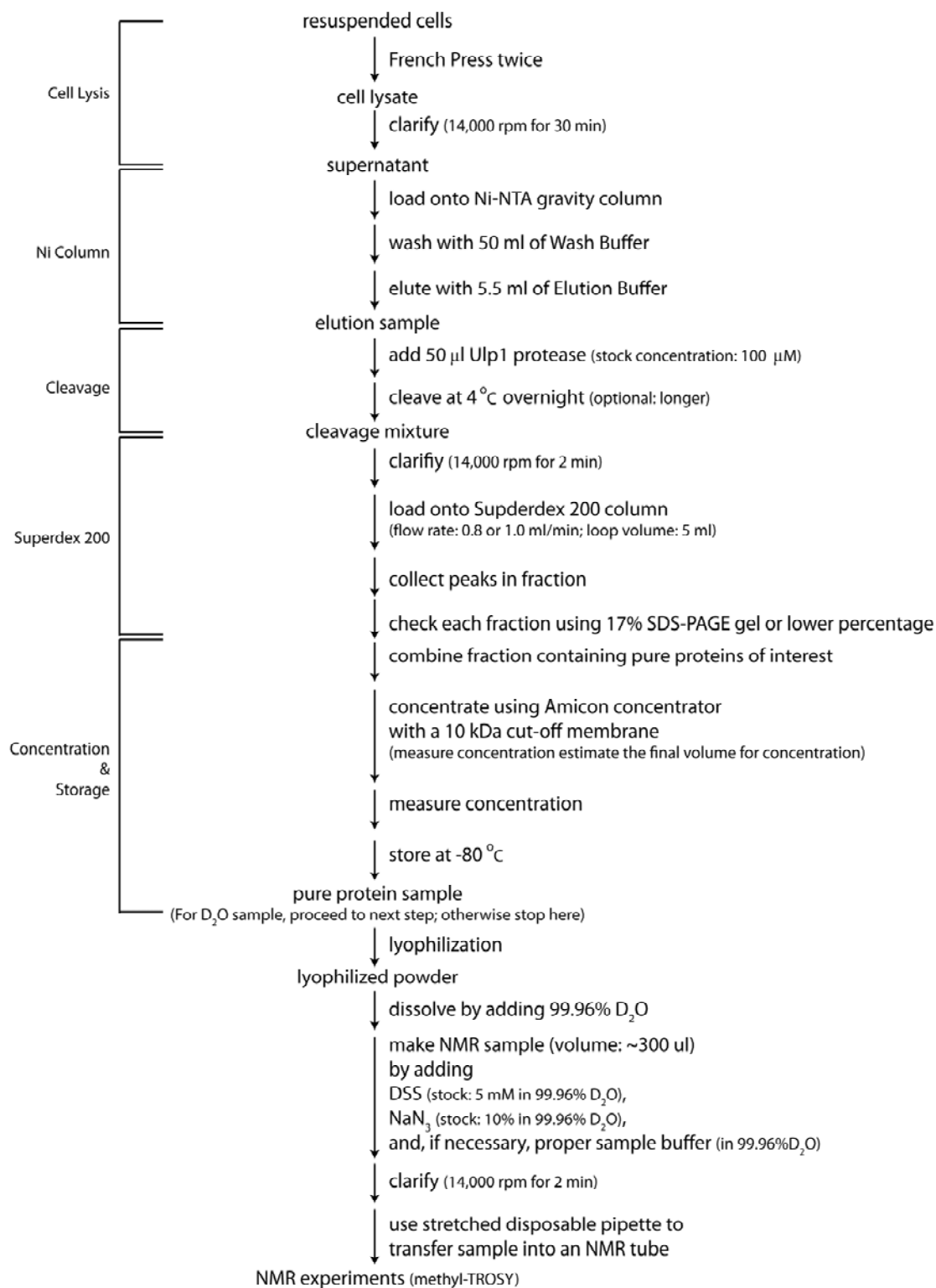
A-8. Diagram for expression of unlabeled proteins. LB1 and LB2 differ only in induction temperature and time.



A-9. Diagram for expression of ¹⁵N-labeled proteins.



A-10. Diagram for expression of U-[¹⁵N, ²H]-Ile-[δ1 ¹³CH₃]- proteins.



A-11. Diagram for protein purification with one-step Ni-NTA chromatography.



A-12. Diagram for protein purification with two-step Ni-NTA chromatography.

APPENDIX B

SUPPLEMENTARY TABLES

Table B1. Description of the plotting levels for spectra of KaiC variants for Figure 2.

U-[¹⁵ N, ² H]- Ile δ 1-[¹³ C, ¹ H]-labeled proteins	Concentration (μ M) (Conc.)	Number of Scan (NS)	Relative signal (Conc. x NS)	Normalized signal	Relative noise cut-off
KaiC-ST	15	128	1920	1.07	1.29E+006
KaiC-SE	8	256	2048	1.14	1.37E+006
KaiC-EE	16	128	2048	1.14	1.37E+006
KaiC-ET	14	128	1792	1.00	1.20E+006
KaiC-EE487	8	224	1792	1.00	1.20E+006

Table B2. Constructs of *Thermosynechococcus elongatus* *kaiA*, *kaiB*, *kaiC* and *sasA*

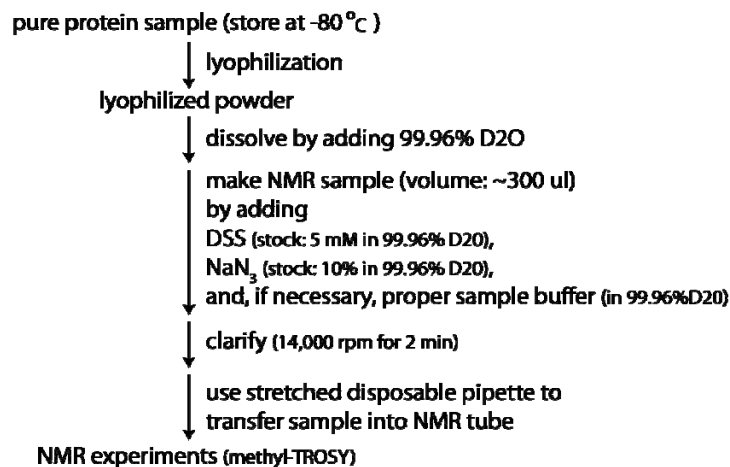
Construct	Cloning sites	Resistance	Cloning Strategy
<i>kaiA</i>			
pET-28b-SUMO- <i>kaiA</i>	NdeI/HindIII	Kanamycin	Figure S11
pTYB1- <i>kaiA</i> -1-129	NdeI/SapI	Ampicillin	Figure S16
pET-28b-SUMO- <i>kaiA</i> -130-283	NdeI/HindIII	Kanamycin	Figure S11
pET-32a- <i>kaiA</i> -180-283	NcoI/BamHI	Ampicillin	Figure S16
<i>kaiB</i>			
pET28b-SUMO-AMA- <i>kaiB</i>	NdeI/HindIII	Kanamycin	Figure S11
<i>kaiC</i>			
pET28b-SUMO-FLAG- <i>kaiC</i>	NdeI/HindIII	Kanamycin	Figure S12
pET28b-SUMO-FLAG- <i>kaiC</i> -SE	NdeI/HindIII	Kanamycin	Figure S14
pET28b-SUMO-FLAG- <i>kaiC</i> -EE	NdeI/HindIII	Kanamycin	Figure S14
pET28b-SUMO-FLAG- <i>kaiC</i> -ET	NdeI/HindIII	Kanamycin	Figure S15
pET28b-SUMO-FLAG- <i>kaiC</i> -1-487-EE	NdeI/HindIII	Kanamycin	Figure S11
pET28b-SUMO-FLAG- <i>kaiC</i> I-1-247	NdeI/HindIII	Kanamycin	Figure S12
pET28b-SUMO-FLAG- <i>kaiC</i> -CII-249-518	NdeI/HindIII	Kanamycin	Figure S12
pET28b-SUMO-FLAG- <i>kaiC</i> -CII-249-518-SE	NdeI/HindIII	Kanamycin	Figure S12
pET28b-SUMO-FLAG- <i>kaiC</i> -CII-249-518-EE	NdeI/HindIII	Kanamycin	Figure S12
pET28b-SUMO-FLAG- <i>kaiC</i> -CII-249-518-ET	NdeI/HindIII	Kanamycin	Figure S12
pET28b-SUMO-FLAG- <i>kaiC</i> -CII-249-487-EE	NdeI/HindIII	Kanamycin	Figure S11
pET28b-SUMO-FLAG- <i>kaiC</i> -CII-249-487-ET	NdeI/HindIII	Kanamycin	Figure S11
pET28b-SUMO- <i>kaiC</i> -CII-258-518-S258C-EE-FLAG (<i>short CII-EE</i>)	NdeI/HindIII	Kanamycin	Figure S11
<i>sasA</i>			
pET28b-SUMO- <i>sasA</i> -1-107	NdeI/HindIII	Kanamycin	Figure S11

APPENDIX C

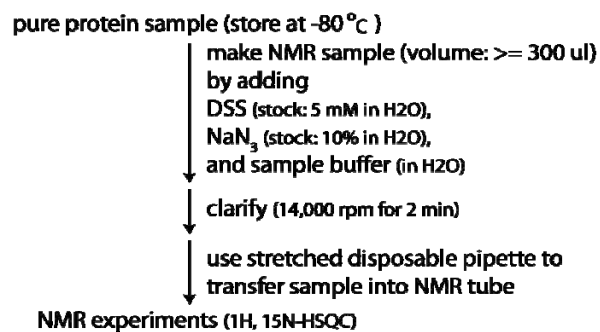
NMR SAMPLE PREPARATION AND SPECTROSCOPY

C-1. NMR sample preparation

NMR sample preparation: U- ^{15}N , ^2H], Ile δ 1- ^{13}C , ^1H] sample



NMR sample preparation: N15



C-2. NMR experiments

All NMR experiments were performed on a Bruker 600MHz AVANCE III spectrometer equipped with a TCI cryoprobe. ^1H , ^{15}N -HSQC and ^1H - ^{13}C methyl-TROSY experiments were performed with the following parameters:

^1H , ^{15}N -HSQC

^1H : carrier 4.75 ppm; sweep width of 16.0 ppm; acquisition time: 66.6 ms

^{15}N : carrier 119.5 ppm; sweep width of 26.5 ppm; acquisition time: 79.4 ms

^1H - ^{13}C methyl-TROSY

^1H : carrier -0.71 ppm; sweep width of 6.5 ppm; acquisition time: 63.9 ms

^{13}C : carrier 13.3 ppm; sweep width of 8.0 ppm; acquisition time: 82.7 ms

APPENDIX D

RECIPE FOR LB AND M9 MEDIA

LB (1 L)

10 g	Tryptone
5 g	Yeast extract
10 g	NaCl

Top up to 1 L with ddH₂O and autoclave.

D₂O LB (1L)

10 g	Tryptone
5 g	Yeast extract
10 g	NaCl

Top up to 1 L with 99.8% D₂O and filter sterilize using a 0.2 μm membrane (Millipore).

2xYT (1 L)

16 g	Tryptone
10 g	Yeast extract
5 g	NaCl

Top up to 1 L with ddH₂O and autoclave.

LB agar:

LB medium contains 15 g/L agar.

For example, add 1.5 g of agar to 100 ml of LB medium.

M9 (1L):

M9 salt solution (1L)

6.0 g	Na ₂ HPO ₄
3.0 g	KH ₂ PO ₄
0.5 g	NaCl
1.0 g	¹⁵ NH ₄ Cl

Top up to 1 L with ddH₂O and autoclave.

Other solutions:

20% D-glucose	(20 g/100 ml H ₂ O, filter sterilize)
1 M MgSO ₄	(autoclave)
1 M CaCl ₂	(autoclave)

Add the above solutions to 1 L of M9 salt solution to make M9 medium before culturing *E. coli* cells:

10 ml of 20% D-glucose	(final concentration: 2 g/L)
2 ml of 1 M MgSO ₄	(final concentration: 2 mM)
100 µl of 1 M CaCl ₂	(final concentration: 100 µM)
antibiotics	(Kanamycin final concentration: 50 µg/ml or Ampicillin final concentration 100 µg/ml)

D₂O M9 medium (200 ml)

We normally make 1L D₂O M9 salt solution and filter sterilize the medium using a 0.2 µm membrane (Millipore). The sterile D₂O M9 medium can be stored at room temperature for at least three months.

M9 salt solution (1L)

6.0 g	Na ₂ HPO ₄
3.0 g	KH ₂ PO ₄
0.5 g	NaCl
1.0 g	NH ₄ Cl

Top up to 1 L with 99.8% D₂O (Sigma) and filter sterilize the medium using a 0.2 µm membrane.

Other solutions:

1 M MgSO ₄ in 99.8% D ₂ O	(filter sterilize)
1 M CaCl ₂ in 99.8% D ₂ O	(filter sterilize)

Add the above solutions to 200 ml L of M9 salt solution to make M9 medium before culturing *E. coli* cells:

0.4 g [¹² C, ² H]-D-glucose	(final concentration: 2 g/L)
1.0 ml BioExpress (10X)	(final concentration: 0.5%)
0.4 ml of 1 M MgSO ₄ in 99.8% D ₂ O	(final concentration: 2 mM)
20 µl of 1 M CaCl ₂ in 99.8% D ₂ O	(final concentration: 100 µM)
200 µl of 50 mg/ml Kanamycin in 99.8% D ₂ O	(final concentration: 50 µg/ml)

Note that antibiotics vary depending on the resistance of the plasmid. The final concentration of Amp is 100 µg/ml, while that of Kanamycin is 50 µg/ml.

APPENDIX E

CLONING

Cloning of pET-28b-SUMO-X:

Strategy. PCR amplify SUMO and X gene with their respective sets of primers, SUMO_1 primer (5'...GGAGATATACATATGGCTAGCATGTCGGAC...3') and SUMO_2 primer (5'...TCCACCAATCTGTTCTCTGTGAG...3') for SUMO gene and X_1 and X_2 primers for X gene, using the PCR 1 reaction scheme (see section PCR reactions and cycles). Load PCR reaction mixtures onto 2% agarose gel and 1.5% (or 2%, depending on the size) agarose gel, respectively, which is followed by gel extraction using standard gel extract protocol provided by the manufacturer (Qiagen). If the band of interest is correct and bright on the agarose gels, dilute the purified PCR product by 5 fold and use as a template. Otherwise, use the purified PCR product as a template without dilution.

With the SUMO template and X gene template, carry out a two-step PCR reaction scheme (PCR 2 and PCR 3; see section PCR reactions and cycles) to produce the desired *SUMO-X* fragment. The desired fragment was obtained by loading the two-step PCR reaction mixture onto 1.5% (or 2%, depending on the size) agarose gel followed by the same gel extraction purification protocol mentioned above. *SUMO-X* fragment was digested using NdeI/HindIII endonucleases (New England Biolabs) and purified following the PCR purification protocol as described by the manufacturer. The digested *SUMO-X* fragment was ligated into pET-28b which was digested with the same endonucleases. Ligated product was used to transform competent BL21 (DE3) *E. coli* cells, which were then plated on LB agar plates supplemented with antibiotics and incubated at 37°C overnight. Transformed colonies were PCR screened using SUMO_1 and X_2 primers in the PCR 4 reaction scheme (see section PCR reactions and cycles). Plasmids from positive colonies were extracted using mini-prep plasmid extract kit (Qiagen) and submitted for sequencing.

See A-2 for protocol.

Cloning of pET-28b-SUMO-FLAG-X:

Strategy: introduce FLAG coding sequence to the 5' of X gene and then follow the protocol for cloning of pET-28b-SUMO-Y (here Y stands for FLAG-X)

Primer designs:

Two primers are used to introduce *FLAG* sequence. X_1 primer, which matches X and introduces *FLAG*, is used to amplify *FLAG-X*. FLAG primer, which matches *FLAG* and introduces partial *SUMO* sequence, is used to generate the *FLAG-X* fragment which will be used to generate *SUMO-FLAG-X*.

The coding sequence for the FLAG (DYKDDDDK) tag is: 5' ... GATTACAAGGATGACGAC GATAAG ...3'.

See A-3 for protocol.

Cloning of pET-28b-SUMO-X-mut

To make mutations on X gene, three strategies are used.

- (1) Use the two-step PCR reaction scheme (PCR 2 and PCR 3; see section PCR reactions and cycles) to produce X-mut and then follow the protocol for cloning pET-28b-SUMO-X For protocol, see A-4.
- (2) PCR amplify *SUMO-X1* (X1: the 5' end of X gene) using SUMO_1 and X_4 primers and X2 (X2: the 3' end of X gene) using X_3 and X_2 primers, and use the products as templates to obtain by following the two-step PCR reaction scheme (PCR 2 and PCR 3; see section PCR reactions and cycles) *SUMO-X-mut* fragment using SUMO_1 and X_2 primers. For protocol, see A-5.
- (3) QuickChange. For protocol, see A-6.

Cloning of pTYB1-X gene:

X gene was PCR amplified, and sequentially digested by NdeI and Sap I endonucleases (New England Biolabs). The digested mixture was then purified using PCR purification kit (Qiagen). The purified X gene was then ligated into pTYB1 which was also digested using Nde I/SapI endonucleases (New England Biolabs) sequentially. For protocol, see A-7.

Preparation of competent BL21 (DE3) *E. coli* cells

This method requires the following reagents:

200 ml LB medium (autoclaved)

0.1 M CaCl₂ (autoclaved)

50 ml centrifuge tubes (sterile)

80% glycerol (autoclaved)

1.5 ml tubes (autoclaved)

Make competent cells from 200 ml culture

- (01) inoculate 5 ml of LB medium with BL21(DE3) *E. coli* cells (Invitrogen)
- (02) grow at 37°C and 220 rpm overnight
- (03) transfer the overnight culture into 200 ml LB medium
- (04) grow at 37°C and 220 rpm until OD₆₀₀ reaches 0.8-1.0
- (05) put the culture on ice for at least 30 min
- (06) spin down the chilled cell culture at 4°C for 10 min
- (07) resuspend cell pellet with 10 ml pre-chilled 0.1 M CaCl₂ solution
- (08) leave on ice for at least 30 min
- (09) spin down at 4,000 rpm for 10 min
- (10) resuspend with 4 ml of 0.1 M CaCl₂, add 1 ml of 80% glycerol, and mix thoroughly
- (11) aliquot (100 µl each tube) and store at -80°C

PCR reactions and cycles

PCR 1

PCR reaction (each: 25 μ l)

16 μ l ddH₂O
 5 μ l 5X Herculase II reaction buffer
 2.5 μ l dNTP (stock: 2 mM each)
 0.5 μ l primer 1 (stock: 10 μ M)
 0.5 μ l primer 2 (stock: 10 μ M)
 0.5 μ l template (stock: 1 ng/ μ l)
 0.1 μ l Herculase II fusion DNA polymerase

PCR cycle

95^oC 2 min
 95^oC 30 s
 52^oC 30 s
 72^oC 1-3 min
 72^oC 5 min
 4^oC

← 28 cycles

PCR 2 (no primer)

PCR reaction (each: 25 μ l)

16 μ l ddH₂O
 5 μ l 5X Herculase II reaction buffer
 2.5 μ l dNTP (stock: 2 mM each)
 0.5 μ l template 1
 0.5 μ l template 2
 0.1 μ l Herculase II fusion DNA polymerase

PCR cycle

95^oC 2 min
 95^oC 30 s
 52^oC 30 s
 72^oC 1-3 min
 72^oC 5 min
 4^oC

← 5 cycles

PCR 3 (add primer and additional polymerase)

PCR reaction (each: 25 μ l)

Add into the 25 μ l reaction mixture of PCR 2 the following:
 0.5 μ l each primer (stock: 10 μ M)
 and 0.1 μ l additional Herculase II fusion DNA polymerase

PCR cycle

95^oC 2 min
 95^oC 30 s
 52^oC 30 s
 72^oC 1-3 min
 72^oC 5 min
 4^oC

← 28 cycles

PCR 4

PCR reaction (each: 20 μ l)

13 μ l ddH₂O
 4 μ l 5X Herculase II reaction buffer
 2 μ l dNTP (stock: 2 mM each)
 0.4 μ l primer 1 (stock: 10 μ M)
 0.4 μ l primer 2 (stock: 10 μ M)
 0.4 μ l template (stock: 1 ng/ μ l)
 0.1 μ l Herculase II fusion DNA polymerase

PCR cycle

95^oC 2 min
 95^oC 30 s
 52^oC 30 s
 72^oC 1-3 min
 72^oC 5 min
 4^oC

← 28 cycles

PCR 5

PCR reaction (each: 50 μ l)

32 μ l ddH₂O
 10 μ l 5X Herculase II reaction buffer
 5 μ l dNTP (stock: 2 mM each)
 1 μ l primer 1 (stock: 10 μ M)
 1 μ l primer 2 (stock: 10 μ M)
 1 μ l template (stock: 50 ng/ μ l)
 0.5 μ l Herculase II fusion DNA polymerase

PCR cycle

95^oC 2 min
 95^oC 30 s
 52^oC 30 s
 72^oC 8-10 min
 72^oC 5 min
 4^oC

← 28 cycles

Digestion

Digestion 1

Digestion reaction (each: 30 μ l) (37 °C 2 hours)

20 μ l PCR product (in ddH₂O)
 5 μ l ddH₂O
 3 μ l 10X NEBuffer 2
 1 μ l Nde I
 1 μ l Hind III

Digestion 2

Digestion reaction (each: 30 μ l) (37 °C 3 hours)

20 μ l pET-28b (in ddH₂O) (total amount: 0.5 μ g)
 5 μ l ddH₂O
 3 μ l 10X NEBuffer 2
 1 μ l Nde I
 1 μ l Hind III

Digestion 3

Step 1: Nde I digestion

Digestion reaction (each: 30 μ l) (37 °C 2 hours)

20 μ l PCR product (in ddH₂O)
 5 μ l ddH₂O
 3 μ l 10X NEBuffer 2
 1 μ l Nde I

Step 2: purify Step 1 reaction mixture

Step 3: Sap I digestion

Digestion reaction (each: 30 μ l) (37 °C 2 hours)

20 μ l PCR product (in ddH₂O)
 5 μ l ddH₂O
 3 μ l 10X NEBuffer 2
 1 μ l Sap I

Ligation

A typical ligation reaction is as follows:

ligation reaction (each: 10 μ l) (16 °C 3 hours)

7 μ l digested PCR product (in ddH₂O)
 1 μ l digested plasmid (in ddH₂O)
 1 μ l 10X T4 DNA ligase buffer
 1 μ l T4 DNA ligase

Transformation

- (1) take out a tube of competent cells (100 μ l) and thaw on ice for about 30 min
- (2) add ligation mixture (~10 μ l) into the above competent cells and incubate on ice for 30 min. [At this time, set the water bath to 42°C]
- (3) heat shock at 42°C for 45 s
- (4) incubate on ice for 3 min
- (5) add 600 μ l of 2xYT medium and shake at 220 rpm and 37 °C for 1 h
- (6) spin down at 5,000 rpm for 2 min
- (7) remove medium so that the remaining volume is about 100 μ l
- (8) resuspend cell pellet with the residual medium
- (9) plate on LB agar plate and incubate at 37°C overnight

PCR screening

- (1) pick up 2-4 colonies and inoculate 1 ml LB medium with appropriate antibiotics
- (2) grow at 37°C and 220 rpm for about 4 h (OD₆₀₀ about 0.4)
- (3) take 0.4 μ l as template for PCR screening using the PCR 4 reaction scheme (see section PCR reactions and cycles). Note the reaction volume is 20 μ l.
- (4) for positive colonies (two is enough in most cases), add additional 4 ml LB medium with appropriate antibiotics into the tubes
- (5) next morning, save 1 ml as glycerol stock and the rest is used for extraction of plasmid
- (6) extracted plasmids are submitted for sequencing

Construct of KaiA, KaiB, KaiC, and SasA

See Appendix B.

APPENDIX F

PROTEIN EXPRESSION

General Strategy

Expression of unlabeled proteins

The plasmid encoding the gene of interest was transformed into BL21 (DE3) *E. coli* cells. Cells harboring the plasmid (or such glycerol stocks) were grown in LB medium supplemented with appropriate antibiotics (Kanamycin final concentration: 50 µg/ml and Ampicillin final concentration: 100 µg/ml) at 37°C until an OD₆₀₀ of ~0.6. Protein expression was induced by adding IPTG to a final concentration of 0.2 mM. Protein induction period is about 4 h at 37°C or 12 h at 25°C. See appendix A-8 for detail.

Expression of ¹⁵N-labeled proteins

The plasmid encoding the gene of interest was transformed into BL21 (DE3) *E. coli* cells. Cells harboring the plasmid (or such glycerol stocks) were grown in M9 (H₂O) minimal medium supplemented with appropriate antibiotics (Kanamycin final concentration: 50 µg/ml and Ampicillin final concentration: 100 µg/ml) at 37°C until an OD₆₀₀ of ~0.6. Note that M9 minimal medium contains ¹⁵N-NH₄Cl and D-glucose as the sole nitrogen and carbon resource, respectively. Protein expression was induced by adding IPTG to a final concentration of 0.2 mM. Protein induction period is about 12 h at 25°C. See A-9 for detail. Note that M9 minimal medium contains ¹⁵N-NH₄Cl and fully deuterated D-glucose as the sole nitrogen and carbon resource, respectively, and BioExpress (Cambridge Isotope Laboratories) was used to increase the growth rate of *E. coli*.

Expression of U-[¹⁵N, ²H], Ileδ1-[¹³C, ¹H] proteins

The plasmid encoding the gene of interest was transformed into BL21 (DE3) *E. coli* cells. Cells harboring the plasmid (or such glycerol stocks) were grown in M9 (D₂O) minimal medium supplemented with Kanamycin at a final concentration of 50 µg/ml at 37°C and 220 rpm until an OD₆₀₀ of 0.4-0.5. Alpha-ketobutyric acid-4-¹³C,3,3-d₂ sodium salt hydrate (Sigma) was added and cultures continued to grow at 37°C and 220 rpm for an hour. Protein expression was induced by adding IPTG (stock in D₂O) to a final concentration of 0.2 mM. Protein induction period is about 12 h at 25°C. See appendix A-10 for detail. Note that M9 minimal medium contains ¹⁵N-NH₄Cl and fully deuterated D-glucose as the sole nitrogen and carbon resource, respectively, and BioExpress (Cambridge Isotope Laboratories) was used to increase the growth rate of *E. coli*.

Expression and Purification of Ulp1, KaiA, KaiB, KaiC, and Sasa

Ulp1

Unlabeled Ulp1

Expression: Follow protocol A-8.

Purification: Follow protocol A-12 but stops after the elution step of 1st Ni-NTA column.

Purification:

Lysis:

(Cell pellet from 1 L culture is resuspended in 30 ml of Lysis Buffer)

Lysis Buffer: 50 mM NaH₂PO₄, 500 mM NaCl, pH 8.0

Ni Column:

Wash Buffer: 50 mM NaH₂PO₄, 500 mM NaCl, 20 mM imidazole, pH 8.0

Elution Buffer: 50 mM NaH₂PO₄, 500 mM NaCl, 250 mM imidazole, pH 8.0

Note that Ulp1 is not stable in buffers where NaCl is at a concentration lower than 100 mM. For long-term storage, add equal volume of glycerol into the Ulp1 elution sample from Ni-NTA column and store at -80°C. Ulp1 elution sample can be diluted to a final

concentration of 200 μM before adding glycerol. Therefore, the final Ulp1 stock (stored at -80°C) will be 100 μM in the buffer of 25 mM NaH_2PO_4 , 250 mM NaCl , 125 mM imidazole, 50% glycerol, pH 8.0.

KaiA

Unlabeled KaiA

Expression: Follow protocol A-8

Purification: Follow protocol A-12

N15-labeled KaiA-130-283

Expression: Follow protocol A-9

Purification: Follow protocol A-12

Purification

Lysis:

(Cell pellet from 1 L culture is resuspended in 30 ml of Lysis Buffer)

Lysis Buffer: 50 mM NaH_2PO_4 , 500 mM NaCl , pH 8.0

1st Ni Column:

Wash Buffer: 50 mM NaH_2PO_4 , 500 mM NaCl , 20 mM imidazole, pH 8.0

Elution Buffer: 50 mM NaH_2PO_4 , 500 mM NaCl , 250 mM imidazole, pH 8.0

Desalting:

Desalting Buffer: 20 mM Tris, 50 mM NaCl , 20 mM imidazole, pH 8.0

2nd Ni Column:

Equilibration Buffer: the same as Desalting Buffer

Superdex 75:

Equilibration Buffer: 20 mM Tris, 50 mM NaCl , 1mM MgCl_2 , 5 mM DTT, 1mM ATP, pH 7.0

N15-labeled KaiA-1-129 (KaiA-N129)

Expression: Follow protocol A-9

Purification: protocol described as follows

Purification

Lysis:

(Cell pellet from 1 L culture is resuspended in 30 ml of Lysis Buffer)

Lysis Buffer: 20 mM Tris, 500 mM NaCl, 1 mM EDTA, pH 8.0

Chitin Column:

Wash Buffer: 20 mM Tris, 500 mM NaCl, 1 mM EDTA, pH 8.0

Cleavage Buffer: 20 mM Tris, 500 mM NaCl, 100 mM MENSA (sodium 2-mercaptoethanesulfonate; MP Biomedicals), 1 mM EDTA, pH 8.0

(The cleavage is carried out at 4°C for overnight.)

Elution Buffer: the same as Cleavage Buffer

Desalting:

Desalting Buffer: 20 mM Tris, 50 mM NaCl, 1mM MgCl₂, 5 mM DTT, 1mM ATP, pH 7.0

N15-labeled KaiA-180-283

Expression: Follow protocol A-9

Purification: protocol described as follows

(The Trx fusion protein Trx-KaiA-180-283 (KaiA-C180) is cleavage by enterokinase.)

Lysis:

(Cell pellet from 1 L culture is resuspended in 30 ml of Lysis Buffer)

Lysis Buffer: 50 mM Tris, 500 mM NaCl, pH 7.0

1st Ni Column:

Wash Buffer: 50 mM Tris, 500 mM NaCl, 20 mM imidazole, pH 7.0

Elution Buffer: 50 mM Tris, 500 mM NaCl, 250 mM imidazole, pH 7.0

1st Desalting:

Desalting Buffer: 20 mM Tris, 20 mM NaCl, pH 7.0

HP Q column:

Low Salt Buffer: 20 mM Tris, 20 mM NaCl, pH 7.0

High Salt Buffer: 20 mM Tris, 1 M NaCl, pH 7.0

2nd Desalting:

Cleavage Buffer: 20 mM Tris, 50 mM NaCl, 2 mM CaCl₂, pH 7.0

Enterokinase (EMD Chemicals) is added to a final concentration of 1 Unit/ml and NaN₃ is added to a final concentration of 0.02%. The cleavage is carried out at room temperature for overnight. If the cleavage is not complete, more protease will be added for extended cleavage.

2nd Ni Column:

Elution Buffer: 50 mM Tris, 500 mM NaCl, pH 7.0

2nd Desalting:

Desalting Buffer: 20 mM Tris, 50 mM NaCl, 1mM MgCl₂, 5 mM DTT, 1mM ATP, pH 7.0

KaiB

Unlabeled AMA-KaiB

Expression: Follow protocol A-8

Purification: Follow protocol A-12

U-[¹⁵N, ²H], Ile δ 1-[¹³C, ¹H]-KaiB

Expression: Follow protocol A-10

Purification: Follow protocol A-12

Purification:

Lysis:

(Cell pellet from 1 L culture is resuspended in 30 ml of Lysis Buffer)

Lysis Buffer: 50 mM NaH₂PO₄, 500 mM NaCl, pH 8.0

1st Ni Column:

Wash Buffer: 50 mM NaH₂PO₄, 500 mM NaCl, 20 mM imidazole, pH 8.0

Elution Buffer: 50 mM NaH₂PO₄, 500 mM NaCl, 250 mM imidazole, pH 8.0

Desalting:

Desalting Buffer: 20 mM Tris, 50 mM NaCl, 20 mM imidazole, pH 8.0

2nd Ni Column:

Equilibration Buffer: the same as Desalting Buffer

Superdex 75:

Equilibration Buffer: 20 mM Tris, 50 mM NaCl, 1mM MgCl₂, 5 mM DTT, 1mM ATP, pH 7.0

KaiC

Unlabeled KaiC KaiC, KaiC-SE, KaiC-EE, KaiC-ET, KaiC-EE487, and KaiC-EE497)

Expression: Follow protocol A-8

Purification: Follow protocol A-11

U-[¹⁵N, ²H], Ile^δ1-[¹³C, ¹H]-KaiC (KaiC, KaiC-SE, KaiC-EE, KaiC-ET, KaiC-EE487)

Expression: Follow protocol A-10

Purification: Follow protocol A-11

Purification:

Lysis:

(Cell pellet from 1 L culture is resuspended in 30 ml of Lysis Buffer)

Lysis Buffer: 50 mM NaH₂PO₄, 500 mM NaCl, 1 mM ATP, pH 8.0

1st Ni Column:

Wash Buffer: 50 mM NaH₂PO₄, 500 mM NaCl, 20 mM imidazole, 1 mM ATP, pH 8.0

Elution Buffer: 50 mM NaH₂PO₄, 500 mM NaCl, 250 mM imidazole, 1 mM ATP, pH 8.0

Desalting:

Desalting Buffer: 20 mM Tris, 50 mM NaCl, 20 mM imidazole, 1 mM ATP, pH 8.0

2nd Ni Column:

Equilibration Buffer: the same as Desalting Buffer

Superdex 200:

Equilibration Buffer: 20 mM Tris, 50 mM NaCl, 1mM MgCl₂, 5 mM DTT, 1mM ATP, pH 7.0

KaiC-CI

Unlabeled KaiC-CI

Expression: Follow protocol A-8

Purification: Follow protocol A-12

U-[¹⁵N, ²H], Ile δ 1-[¹³C, ¹H]-KaiC-CI

Expression: Follow protocol A-10

Purification: Follow protocol A-12

Purification:

Lysis:

(Cell pellet from 1 L culture is resuspended in 30 ml of Lysis Buffer)

Lysis Buffer: 50 mM NaH₂PO₄, 500 mM NaCl, pH 8.0

1st Ni Column:

Wash Buffer: 50 mM NaH₂PO₄, 500 mM NaCl, 20 mM imidazole, pH 8.0

Elution Buffer: 50 mM NaH₂PO₄, 500 mM NaCl, 250 mM imidazole, pH 8.0

Desalting:

Desalting Buffer: 20 mM Tris, 50 mM NaCl, 20 mM imidazole, pH 8.0

2nd Ni Column:

Equilibration Buffer: the same as Desalting Buffer

Superdex 75:

Equilibration Buffer: 20 mM Tris, 50 mM NaCl, 1mM MgCl₂, 5 mM DTT, pH 7.0

KaiC-CII

Unlabeled KaiC-CII (CII, CII-SE, CII-EE, CII-ET, CII-EE, CII-ET, short CII-EE)

Expression: Follow protocol A-8

Purification: Follow protocol A-12

U-[¹⁵N, ²H], Ile δ 1-[¹³C, ¹H]-KaiC-CII-249-518-EE:

Expression: Follow protocol on A-10

Purification: Follow protocol on A-12

Purification:

Lysis:

(Cell pellet from 1 L culture is resuspended in 30 ml of Lysis Buffer)

Lysis Buffer: 50 mM NaH₂PO₄, 500 mM NaCl, pH 8.0

1st Ni Column:

Wash Buffer: 50 mM NaH₂PO₄, 500 mM NaCl, 20 mM imidazole, pH 8.0

Elution Buffer: 50 mM NaH₂PO₄, 500 mM NaCl, 250 mM imidazole, pH 8.0

Desalting:

Desalting Buffer: 20 mM Tris, 50 mM NaCl, 20 mM imidazole, pH 8.0

2nd Ni Column:

Equilibration Buffer: the same as Desalting Buffer

Superdex 75:

Equilibration Buffer: 20 mM Tris, 50 mM NaCl, 1mM MgCl₂, 5 mM DTT, pH 7.0

SasA-N

N15-labeled SasA-N

Expression: Follow protocol on A-9

Purification: Follow protocol on A-12

Purification:

Lysis:

(Cell pellet from 1 L culture is resuspended in 30 ml of Lysis Buffer)

Lysis Buffer: 50 mM NaH₂PO₄, 500 mM NaCl, pH 8.0

1st Ni Column:

Wash Buffer: 50 mM NaH₂PO₄, 500 mM NaCl, 20 mM imidazole, pH 8.0

Elution Buffer: 50 mM NaH₂PO₄, 500 mM NaCl, 250 mM imidazole, pH 8.0

Desalting:

Desalting Buffer: 20 mM Tris, 50 mM NaCl, 20 mM imidazole, pH 8.0

2nd Ni Column:

Equilibration Buffer: the same as Desalting Buffer

Superdex 75:

Equilibration Buffer: 20 mM Tris, 50 mM NaCl, 1mM MgCl₂, 5 mM DTT, pH 7.0

VITA

Name: Nai-Wei Kuo

Address: Department of Biochemistry & Biophysics
103 Biochemistry/Biophysics Building
Texas A&M University
2128 TAMU
College Station, Texas 77843-2128

Email Address: nicolekuo@tamu.edu

Education: Ph.D. Biochemistry
May 2011
Texas A&M University
College Station, TX

M.S. Chemistry
June 2004
National Tsing Hua University
Hsinchu, Taiwan

B.S. Chemistry
June 2002
National Tsing Hua University
Hsinchu, Taiwan